Doctoral Dissertation (Shinshu University)

Study on static and dynamic mechanical behavior of woven fabric

織物の静・動的力学挙動に関する研究

September 2021

Interdisciplinary Graduate School of Science and Technology

HUANG CANYI

Contents

Contents

Abstract

Woven fabric is one of the most widely used materials in textile composites and structural applications. Some woven fabrics especially high-performance fabrics are viscoelastic in nature which exhibit a combination of both elastic and viscous behavior under different loading rate. Therefore, the characteristic of mechanical behavior of fabric material should include both static mechanical properties like tensile behavior and dynamic mechanical properties like impact behavior.

Nevertheless, there are still problems refer to the mechanism performance and behavior of woven fabric that have not been explored at present and they still require further study. For instance, there are few literature reports on the mechanism of the effect of crimp or inter-yarn friction on woven fabric's tensile properties, and research on low-velocity impacts on woven fabrics is almost nonexistent. It is crucial for engineering to develop woven fabrics especially high-performance fabrics with improved all-round being well understood performance.

Therefore, this dissertation carries out static and dynamic mechanical study by combing experimental and numerical methods to investigate in tensile and impact mechanical behavior of high-performance Twaron® woven fabric which have never been solved by other researchers up to present，and aiming to provide valuable application reference for body armer and composite materials industry.

In this dissertation, firstly, a physical-geometric-feature of continuous yarn in a plain-woven fabric is created and its FE model is analyzed by considering the two key

issues of woven fabric, the crimp and inter-yarn friction. The basic parameters of Young's modulus of single yarn and the inter-yarn friction coefficient are investigated for practical fabrics in tensile and pull-out tests. FE analysis indicated that the stress-strain curves of the FE model are effective in evaluating the equivalent modulus of a woven fabric by comparing with a tensile experiment on Twaron CT ® Plain Woven Fabric. In addition, a simplified three-dimensional model of the unit cell of plain-woven fabric (UCPW) is employed to quantitively investigate two important fabric characteristics – the crimp rate of the yarn and inter-yarn friction to determine their influence on the mechanical properties of the fabrics. Furthermore, we use FE analysis to evaluate how the crimp rate and inter-yarn friction affect the mechanical properties by determining the equivalent modulus of single yarn and UCPW in both uniaxial and biaxial tensile loading. The stresses at representative nodal points and the mechanical interaction between yarns are also investigated from a microscopic perspective, and their deformation mechanisms are also analyzed and discussed. Result showed that the equivalent modulus of plain-woven fabric dropped from 98.64% to 95.83% of the original modulus when the crimp increased from 1.167% to 4.658% when uniaxial tensile loading.

Secondly, low-velocity drop weight impact experiments of plain-woven Twaron CT® at an impact energy of 15, 20, 30 J are carried out on a 9250HV drop weight impact tester. Specially treated specimens are designed and used to deal with boundary conditions because the fabric is too flexible and cannot be fixed precisely. Experimental results reaffirm that Twaron® is an impact-rate-sensitive material and

that a greater initial impact energy resulted in a larger breaking load, greater failure strain, larger energy absorption and shorter contact duration to the fabric in the impact process. The mean energy absorption in the 30-J impact event is 1.71J, 18.8% and 39.0% greater than that achieved in the 20-J and 15-J impact events. Numerical impact model is created and the dynamic mechanical parameters of Twaron® is analyzed and applied to FE model to describe the rate-sensitive mechanical properties through a three-element spring-dashpot model. Standard earth gravity is applied to the impact model to reflect the impact process realistically as well. The results indicate that a remarkably close agreement is obtained between the simulation and experimental results in various impact scenarios. Thus, the energy absorption mechanisms and stress distributions during the impact process are clarified. The influence of specimen shape and size are also analyzed systemically. These results indicate that the present experimental set-up and the developed fabric geometry model are effective at investigating many additional mechanical problems in textile fabrics and/or flexible material structures.

Thirdly, as well known to all, defects, such as holes, appear in fabrics after long-term use or damage. Holes can weaken the mechanical properties of fabric-based soft body armor and fabric-reinforced composites to a certain degree. Hence, prediction the effect of hole defect in the mechanical properties of fabric is of great importance for material designers. In this dissertation, models of single- and multilayer panels of plain weave as well as different weaving architectures are designed and created with and without holes to compare impact properties. The influence of the size and location

of hole defect on the impact behavior of single-layer Twaron® fabric are investigated, the degree of influence of hole defects with different sizes on the impact behavior and the influence level by different location of the hole defects are well understood. The impact resistance ability was lower for larger hole defects than for the smaller hole defects. The fabric model with a hole size of 3 × 3 yarn interweaving points can only take11.9% of the energy absorption of the model without holes. In addition, the effect of hole defects on the impact behavior of multi-layer armor panel are also studied. Hole defects become less influential in terms of impact contact force and have less severe constraining effect on front layer of the panel when the number of multi-layer armor panels increased. Furthermore, the effect of hole defects on the impact behavior of different weaving architectures (i.e., plain, twill, basket, and satin weave) are analyzed. Plain weave fabric has the highest energy absorption capability in impact scenarios with and without holes among all the woven architectures. Plain weave fabric is the most affected and twill weave is the least affected by hole defects in terms of transverse wave velocity; the satin weave is the most affected and the twill weave is the least affected by hole defects in terms of energy absorption. These findings will provide guidance for engineering of soft body amour and composite materials.

Chapter 1

General Introduction

Chapter 1

Chapter 1: General Introduction

1.1 Woven fabric

1.1.1 Overall introduction

Woven fabric is one of the most widely used materials in textile composites and structural applications regardless of the clothing industry. They are produced principally by the multiple warp weaving method, and generally consist of two sets of interlaced yarn components, known as warp and weft (or fill) yarns according to the yarn orientation. Warp yarns run vertically or lengthwise in woven fabrics, while weft yarns run horizontally or crosswise. Each yarn is a bundle of filaments (or fibers) and its size is measured by the number of filaments in the yarn. Three-dimensional (3D) woven fabrics have additional yarns placed in through the thickness direction, 3D woven fabrics can be produced by using either conventional looms with multilayer constructions or entirely new equipment [1].

Woven fabric especially plain weave is the most commonly used basic reinforcement for woven composites. In a plain weaving structure, one warp yarn is repetitively woven over and under weft yarns. Other typically weave type such as twill weave, it has a looser interlacing, and the weave is characterized by a diagonal line. In a twill weaving structure, each warp yarn floats over two consecutive weft yarns, and under the following one weft yarn. And satin weave has a good drapability, with a smooth surface and minimum thickness. Currently, most of the pure and hybrid woven fabrics used in textile composites are simple 2D fundamental weaves as aforementioned plain,

twill and satin weaves, they are identified by the repeating patterns of the interlaced regions in warp and weft directions.

Woven fabrics generally exhibit good dimensional stability in the warp and weft directions, offer highest cover or yam packing density, and provide higher out of plane strength which can carry the secondary loads due to load path eccentricity, local bucking, etc. In addition, woven fabrics generally have a very low shear rigidity which gives a very good formability. As an important reinforcement material, woven fabric is commonly used in textile composites that are being widely used in advanced structures in aerospace, automobile, and marine industries. This brings great concern on studying the mechanical properties of woven fabric that made from high-performance fibers especially.

1.1.2 high-performance woven fabric Twaron®

High-performance fibers, which have high strength and high stiffness, including aramids, such as Kevlar® (DuPont) and Twaron® (by Teijin); PBO fibers, such as Zylon® (by Toyobo); and ultra-heavy molecular weight polyethylene (UHMWPE) fibers, such as Dyneema® (by DSM) and Spectra® (by Honeywell), are widely used in various industries especially protection use owing to their flexibility and high strength-to-weight ratio. High performance fiber Twaron®, similar to Kevlar®, is a kind of Para-aramid fiber. Para-aramid fiber is one of commonly used high-strength and high modulus fibers have good resistance to melt at high temperature. Extremely strong and heat resistant aramids fibers are a class of synthetic fibers which

introduced first by DuPont™ in the early 1960s. They are among the different polymeric fibers which is most recognized in the applications of protective systems. It is also constituted polyamides created from aromatic acids and amines.[2] Even though it is relatively expensive, fabrics made from such kind of fibers can provide high strength, high modulus, and good tenacity, which are desirable properties for the ballistic applications.

In general, aramid fibers are 43 percent lighter than fiber glass (at density of 1.44kg/m^3 compared to 2.55 kg/m^3 for fiber glass), twice as strong as E-Glass, ten times as strong as aluminum, same strength as of high strength carbon on a specific tensile strength basis. It is also display excellent dimensional stability with a slightly negative coefficient of thermal expansion (-2.4 $\times 10^{-6}$/°C) and could resist chemicals except for a few strong acids and alkalis. Moreover, the aramids fiber exhibited an excellent stability over a wide range of temperatures for prolonged periods with, no strength loss at temperatures as low as −320°F (−196°C) and do not melt but will start to carbonize at approximately 800 °F (427°C) [3].

Hundreds of Twaron® fibers are grouped together to make a yarn, and yarns are woven to produce a high-performance fabric. Twaron® fabric is one of the two commonly used para-aramid materials in the development of body armor industry. It is even five times stronger than steel but yet flexible. It is also heat resistant, cut resistant, chemical resistant, and can handle sever damage like high ballistic impacts.[4] Moreover, the most recently released version of Twaron® fabric could protects against knife and other weapon threats, and has led to the production of

multi-threat vests that can halt both bullet and stab attacks. Due to the excellent performance in mechanical performance, this dissertation as a result take Twaron® fabric as representative woven fabric for static and dynamic mechanical study.

1.2 Current research status of static mechanical behavior of woven fabric

The static mechanical properties of fabric materials include tension, compression and bending etc. Among these properties, tensile properties as the most basic properties of materials, have been widely studied. Through the tensile experiment of the material, the elastic modulus, strength, elongation, toughness, and other mechanical parameters of the material can be obtained. At the same time, the tensile properties also determine other properties of the material. For example, material with greater modulus, higher strength and greater elongation can always absorb more energy when failure, and show better resistance capacity to impact, deformation, and shear. As a result, this research mainly focuses on the static tensile behavior of woven fabric.

1.2.1 Current research status with experiment method

Research on quasi-static strength of yarns along with studies of dynamic strength has been reported in several studies. Schwartz et al. [5] carried out quasi-static tensile tests on single fibers of Kevlar 29 and 49 yarns taken from various locations within a spool and production lots. Variability in the failure load, tenacity, and linear density of single aramid filaments is studied experimentally. Data indicate that both the failure load and the tenacity of filaments, for a given gauge length and yarn cross section, can be fitted to a two parameter Weibull distribution. Farsi et al [6] studied the parameters

that affect the quasi-static and dynamic strength of five different yarns (Kevlar 129, Kevlar KM2, Kevlar LT, Twaron, and Zylon) using hydraulic and Hopkinson bar testing methods. The failure strengths of Kevlar products showed limited dependence on strain rate, while Twaron and Zylon products showed a more significant strain-rate dependency. Effect of specimen size on the failure stress of Kevlar 129 was studied by testing single fiber specimens at five (5, 16, 25, 50, and 100 mm) different gauge lengths and multifiber specimens tested at three different gauge lengths (24, 100, and 170 mm). Deju Zhu et al. [7] studied the multi-scale mechanical behaviors of Kevlar 49 in the forms of fiber, yarn and fabric subjected to uniaxial tension. The experimental results showed that the material mechanical properties are dependent on structural size scale and gage length of samples. The tensile strengths decrease with increasing gage length and structural size scale from fiber to yarn, and to fabric, and follow Weibull distribution by conducting statistical analysis, which is used to quantify the degree of variability in the tensile strengths of fiber and yarn with different gage lengths.

In addition, literatures indicate that many investigators have studied the deformation theory and mechanical properties of Kevlar woven fabrics. Zhu et al.[8] investigated the stress–strain response in warp and fill directions, the apparent Poisson's ratio, and the in-plane shear response of Kevlar 49 fabric including the possible effects of specimen size and pre-loading on the mechanical responses of the fabric. The experimental results showed that the fabric exhibits non-linear and orthogonal behavior in tension and has identical Young's modulus in warp and fill directions. The

apparent Poisson's ratio is a nonlinear function of strain and dependent upon the levels of pre-loading. The shear response is highly nonlinear and independent of specimen size after normalization. Naik et al. [9] characterized the behavior of Kevlar 49 dry fabric by means of tension tests, trellising shear tests, and friction tests. Results showed that Kevlar fabric has almost equal modulus of elasticity and tensile strength in both the warp and fill directions. The typical shear response displays an initial region with large increase in shear angle with minimal increase in the actuator load, during which the yarns begin to rotate offering a small resistance to the applied shear loading, and then the load tends to increase rapidly due to shear locking. The friction tests were carried out to obtain the coefficient of static and dynamic friction between two Kevlar fabric layers.

1.2.2 Current research status with numerical method

Over the past two decades, a great deal of work has been done on the computation-based engineering analyses and finite element simulations to tensile and related performance of high-performance fabrics. Shim et al. [10] Lim et al. [11] used pinjointed orthogonal bars to represent flexible–fabric yarns. While this method has the most notable advantages on the efficiency of approximating the mechanical behavior of woven fabrics, this oversimplified discrete yarn model immensely limited the predictive capability of the analyses without accounting for important contributions associated with weave architecture and friction governed yarn-to-yarn and layer-to-layer contacts (in multi-layer fabrics). Zhang et al.[12] and Duan et al.[13] carried out more detailed 3D continuum finite element analyses, which have proven to

be effective tools for capturing and elucidating the detailed mechanic response of single-layer fabrics with the disadvantages of demanding expense in computation when applied to practical armor systems which typically contain 30–50 fabric layers/plies. Nilakantan [14] established a reduced-resolution filament-level model to provide invaluable insight into the mechanical behavior of the yarn and demonstrated the sensitivity response to filament friction, material properties, and spreading and redistribution. Unit-cell-based approaches have received widespread use for the purpose to derive the equivalent (smeared) continuum-level (membrane/shell) material models in view of the knowledge of the meso-scale fiber and yarn properties, fabric architecture, and inter-yarn and inter-ply frictional characteristics.

Among the most remarkable studies based on these analyses are those carried out by Kawabata et al. [15] who introduced simple analytical models to capture the uniaxial, biaxial and shear behavior of fabrics. Ivanov and Tabiei [16] presented a computational material model of flexible woven fabric for finite element impact analysis utilizing the micro-mechanical approach and the homogenization technique and accounting for reorientation of the yarns and the fabric architecture. Based on the properties of the yarns and the weave architecture, Boisse et al. [17] and Peng et al. [18] came up with a new approach for deriving the continuum-level material model for fabrics, which involves the use of an energy minimization technique to establish the relationship between the configurations of the fabric structure and the microscopic deformation of fabric components. While the use of higher-order membrane elements was found to be indeed advantageous computationally, it was never fully validated by

comparing its results against either those obtained experimentally or those obtained using full 3D finite element analysis. Zhu et al. [8] tested to obtain the tensile mechanical behaviors and Weibull statistic parameters of Kevlar 49 single filaments and yarns with different gage lengths. The results of single filaments were then used to build a constitutive model for simulating the stress–strain response of single yarns and fabrics under quasi-static loading, and the experimental parameters of single yarns were used in finite element models with shell elements and solid elements to simulate the uniaxial tensile properties of fabrics.

1.3 Current research status of dynamic mechanical behavior of woven fabric

Some woven fabrics especially high-performance fabrics are viscoelastic in nature which exhibit a combination of both elastic and viscous behavior. Therefore, the characteristic of mechanical behavior of fabric material should include dynamic mechanical properties such as ballistic impact and drop weight impact. For many decades, many researchers have been applied various methods and approaches to derive and understand the constitute relation and simulate the overall impact resistant materials behavior in response of impact in order to use in various ballistic impact application. This section will discuss current research status in brief the different approaches used to investigate, analyzed, and understand the impact behaviors high-performance woven fabrics.

1.3.1 Current research status with experiment method

Experimental methods are one of the commonly used methods to investigate the

impact performances of high-performance fabrics, and it is effective to characterize and obtain relevant data to optimize applications of the ballistic material. [19-22] During experimental methods, the effect of different target configuration and target mechanical properties on ballistic performance of the material can be observed when struck by various standard bullet or FSP (Fragment simulating projectile) at the different velocities.[23] The experimental approach while ballistic impact test could also help to determine the energy absorbed by the target and transmitted beyond the target based on different parameters while using in body amours. [24] The different phenomenon including back face signature (BFS), damaged targets, residual velocity and caught bullets will be thoroughly examined using various techniques and equipment including optical microscope, SEM, and high-speed camera etc. for further analysis and interpretations.

Various researchers have used different approaches including high speed camera to capture and measured the values of the back face signatures on the standard backing clay (Roma Plastilina No.1- to preserves its shape after unloading) which is placed at the back of the target to support the packages.[25] Apart from back face signatures, the target perforation resistance [26] and surface damages [27] are also another variable which will be considered after the test to determine the ballistic impact performances of the final target. Some researchers are also tried to find out experimentally the damage modes, ballistic limit velocities, absorbed energies due to penetration, specific perforation energy capacity and some structural responses of the different target after impact test.

Different researchers also tried to analyze such failure mechanisms at the micro, meso and macro level by the help of optical microscope, digital camera, SEM etc. for investigation and interpretation. For example, an experimental investigation on multi-functional panels, which consist of two layers, one made of fiber-reinforced plastics (FRP), and the other of a self-healing ionomer, assembled in four different configurations with different surface density were carried out against under high velocity impact conditions. With a total of 16 impact experiments, different types of panel responses were observed. The panels with ionomer plate and carbon FRP laminate shows hole sealing and as the ionomer panels were placed at rear side the damages have also been reduced. [22]

Ying Wang et al. [28] presents a comprehensive experimental study of the effect of ply orientation on the ballistic performance of the multi-ply fabric panels. The fabric panels used in the experiments were constructed by laying plies of plain-woven fabrics in a selection of orientations. The results showed significant improvement in energy-absorbing capacity of the angled multi-ply panel over the conventional aligned panel where all fabric plies are laid in the same orientation. An experimental investigation into the responses of a woven fabric and a pliable laminate Twaron CT716 and Spectra Shield subjected to oblique projectile impact is undertaken by V.P.W. Shim et al. [29] With respect to energy absorption, results show that for both Twaron and Spectra Shield, the influence of impact obliquity on energy absorbed generally diminishes with an increase in impact velocity, and finally vanishes when the impact velocity is sufficiently high.

Even though this experimental method gives the real scenario, but due to its most costly task, destructive and very time-consuming nature, different methods were also available and have been used for better analysis and to minimize comprehensive experimental impact tests.

1.3.2 Current research status with numerical method

Enormous researchers have also preferred and used a numerical modelling approach which relies on techniques, such as finite element and finite difference methods by the help of commercial packages, such as ABAQUS, DYNA3D, LSDYNA, ANSYS etc. to establish projectile-fabric simulation model and conduct the ballistic impact performances of the materials.[30-31] This method is generally an effective approach in terms of time and cost as compared to the experimental approach due to it reduces the work of experimental test. However, it still required high computing power and resources for simulating the process. Generally, three main numerical methods are commonly used, namely pin-jointed model, [32] full 3D continuum model [33] and mesoscale unit-cell based model [34] to model the fabric structure. Regarding fabric modelling, both 3D continuum and pin-joint model considers the woven fabrics construction methods using warp and weft yarns, whereas unit-cell based model bases woven fabric as an assembly of crossovers. Moreover, the unit-cell model has shown better efficiency to predict the ballistic impact responses of multi-ply fabric panels compared to both pin-jointed and 3D continuum model. [35]

However, even till now, simulation of the impact responses of fabrics that constructed

from continuous filament yarns remains a challenging task due to their complex multi-scale structures and the material interactions from fiber to filament, yarn and fabric-levels. Fiber-level numerical approach [36] have been also developed and utilized to model the ballistic resistance of Kevlar® KM2. Such model could be, however, computationally intensive to simulate the multilayer systems. Several analytical, numerical and hybrid approaches [37-38] have been explored to model the ballistic impacts of woven fabrics. Numerical models at different scales were developed, including the macro-scale that simulates fabric layer as homogenized membranes, the mesoscale that constructs the fabrics from anisotropic continuum yarn, and the microscale focusing on the fiber level. Ha-Minh et al. [39] have implemented a multi-scale model, which is a combination between macroscopic and mesoscopic finite element models to investigate the ballistic impact on 2D KM2® plain weave fabrics. Mesoscale fabric model is based on modelling individual continuum yarn at millimeter length-scale [40]. By this way, detailed mechanisms of the yarn interactions, such as friction and failures, could be captured enabling the model to provide in depth understandings of damage evolution and energy transfer during ballistic impact [41]. The above computational studies focus mostly on the impact of single layer plain-woven fabric systems, while similar studies on other weaving structures and the associated multilayer systems have not been performed.

Over the past several decades there has been a lot of work carried out to understand the ballistic impact behavior of single yarns and fabrics using numerical techniques. [42-43] The use of finite element analysis (FEA) facilitates a description of the

contact between the yarns, fabric plies, and projectile. The fabric yarns can be modelled explicitly, which leads to the capturing of certain phenomena that are not fully possible in other approaches, such as yarn pullout and the effect of inter-yarn friction. [44] With this method, Zeng et al. [45], Gogineni et al. [46], Zhou et al. [47] and Sun et al. [48] in their simulations observed that the energy absorption increases with the coefficient of friction in certain range, whereas the energy absorption begins to decrease at much higher frictional levels. Finite element models were built up by Yi Zhou et al. [49] and was used to predict the response of woven fabrics with different structural parameters, including fabric structure, thread density of the fabric and yarn linear density. The same method was used by Xiaogang Chen et al. [50] to predict the response of different layers of fabric in a twelve-layer fabric model upon impact. It was found that the front layers of fabric are more likely to be broken in shear, and the rear layers of fabric tend to fail in tension.

However, the method also has drawbacks due to its costly nature, time-consuming, and most importantly lack of necessary data mining systems to generate and involve sufficient data for better analysis and getting genuine results.

1.4 Purpose and significance of this research

Judging from the current research status of static mechanical behavior of woven fabric, it is clearly that numerous papers have been published on the experimental and numerical simulation that show physical parameters of woven fabrics will affect the mechanical properties. Fabric's physical parameter such as crimp rate and inter-yarn

friction are two key issue of woven fabric which were widely studied and proved to influence fabric's mechanical properties to a certain degree. However, there are few literature reports on the mechanism of the effect of crimp or inter-yarn friction on fabric's tensile properties. The main reason for this is, unlike physical parameters such as linear density and thread density of yarn, crimp rate and friction coefficient of fabrics are difficult to qualitatively compare, control and analyze from an experimental point of view. Therefore, although numerical simulations can facilitate qualitative comparisons, it is difficult to verify them through experiment results.

In addition, according to the current research status of dynamic behavior of woven fabric, we noted that most existing impact research on soft body fabric armor was focused on medium to high velocity (30 m/s–1000 m/s) low-mass projectiles. Research on low-velocity impacts on high-performance fabrics is almost nonexistent. From an experimental perspective, in experiments using projectiles with low mass and low velocity (e.g., Hopkinson pressure bar or air gun tests), the impact energy is too slight to puncture the fabric, thus the fabric's failure point cannot be ascertained, which greatly diminishes the value of the research. In addition, experiments using projectiles with high mass and low velocity (e.g., drop weight impact tests), the specimen is always difficult to fix precisely because of the fabric's flexibility, which results in inaccurate results. From a numerical analysis perspective, the CPU calculation time of low-velocity impacts may be as much as a dozen times longer than that for high-velocity impacts because the low-velocity impactor takes much longer to penetrate the fabric (which happens only if the impact energy is high enough) and the

time step in the explicit schema is always much lower to ensure the calculation precision. Thus, compared with studying high-velocity impacts, studying low-velocity impacts on soft body armor is more challenging.

In summary, this research aims to combine experiment method and numerical simulation to study the influence mechanism of physical parameters crimp rate and inter-yarn friction on Twaron® fabric's tensile performance, as well as the reflection mechanism and behavior of Twaron® fabric under low-velocity impact and the effect of hole defects on the low-velocity impact resistance of Twaron® woven fabric, those problems have still never solved by existed literatures.

1.5 Outline of the dissertation

This dissertation is structured to provide a summary of "study on static and dynamic mechanical behavior of woven fabric".

In Chapter 1, an overview of characteristic of woven fabric and high-performance Twaron® fiber, current research status of static as well as dynamic mechanical behavior in terms of experiment and numerical methods have been presented.

In Chapter 2, existed modelling techniques are compared and discussed, 3D solid element yarn-level method is implemented and geometric fabric model which is physically based on Twaron® fabric is introduced and the woven fabric model is created.

In Chapter 3, tensile and pull-out tests are carried out or practical fabrics and basic parameters of Young's modulus of single yarn and the inter-yarn friction coefficient

are investigated. In addition, The commercial code ANSYS® is employed, and a simplified three-dimensional model of the unit cell of plain woven fabric (UCPW) is employed to quantitively investigate the influence on the mechanical properties of the fabrics by crimp rate and inter-yarn friction of the yarn.

In Chapter 4, Low-velocity drop weight impact experiments of plain-woven Twaron® is carried out on a 9250HV drop weight impact tester. The commercial code ANSYS®-AUTODYN is employed for impact FE analysis, and the dynamic mechanical property of Twaron® is analyzed with a semi-empirical approach of a three-element spring-dashpot model. The results indicate that a remarkably close agreement is obtained between the simulation and experimental results in various impact scenarios. Thus, the energy absorption mechanisms and stress distributions during the impact process are clarified. The influence of specimen shape and size are also analyzed systemically.

In Chapter 5, Based on FE impact model which was validated by experiment, the influence of the size and location of hole defect on the impact behavior of single-layer Twaron® woven fabric are investigated, the degree of influence of hole defects with different sizes on the impact behavior and the influence level by different location of the hole defects are well understood. In addition, the effect of hole defects on the impact behavior of multi-layer armor panel are studied. Furthermore, the effect of hole defects on the impact behavior of different weaving architectures (i.e., plain, twill, basket, and satin weave) are also analyzed.

In Chapter 6, summary and conclusions of this dissertation are presented.

References

[1] P. Tan, L. Tong and G. P. Steven. Modelling for predicting the mechanical properties of textile composites -A review. Composites PartA. 28A (1997) 903-922.

[2] Wanger L. Military and law enforcement applications. In: Bhatnagar A, editor. Lightweight Ballistic Composites. 1st ed. Abington Hall, Abington, Cambridge CB16AH, England: Woodhead Publishing; 2006. p. 1–25.

[3] Mulat Alubel Abtew, François Boussu, Pascal Bruniaux, Carmen Loghin c, Irina Cristian. Ballistic impact mechanisms – A review on textiles and fibre-reinforced composites impact responses. Composite Structures 223(2019)110966.

[4] Finckernor MM. Comparison of high-performance fiber materials properties in simulated and actual space environments. NASA Tech. Rep. 2017.

[5] Schwartz, P., Wagner, H. D., and Phoenix, S. L. "A study of statistical variability in the strength of single aramid filaments." J. Compos. Mater., 18(4), 312–338.

[6] Farsi, D. B., Nemes, J. A., and Bolduc, M. "Study of parameters affecting the strength of yarns." J. Phys. IV, 134, 1183–1188.

[7] Deju Zhu, Xiaotong Zhang, Yunfu Ou and Mengying Huang. Experimental and numerical study of multi-scale tensile behaviors of Kevlar 49 fabric. Journal of Composite Materials 0(0) 1–17.

[8] Zhu D, Mobasher B, Vaidya A, et al. Mechanical behaviors of Kevlar 49 fabric subjected to uniaxial, biaxial tension and in-plane large shear deformation. Compos Sci Technol 2013; 74: 121–130.

[9] Naik D, Sankaran S, Mobasher B, et al. Development of reliable modeling methodologies for fan blade out containment analysis–Part I: Experimental studies. Int J Impact Eng 2009; 36: 1–11.

[10] Shim V, Lim C and Foo K. Dynamic mechanical properties of fabric armour. Int J Impact Eng 2001; 25: 1–15.

[11] Lim C, Shim V and Ng Y. Finite-element modeling of the ballistic impact of fabric armor. Int J Impact Eng 2003; 28: 13–31.

[12] Zhang GM, Batra RC and Zheng J. Effect of frame size frame type and clamping pressure on the ballistic performance of soft body armor. Compos Part B: Eng 2008; 39: 476–489.

[13] Duan Y, Keefe M, Bogetti TA, et al. Finite element modeling of transverse impact on a ballistic fabric. Int J Mech Sci 2006; 48: 33–43.

[14] Nilakantan G. Filament-level modeling of Kevlar KM2 yarns for ballistic impact studies. Compos Struct 2013; 104: 1–13.

[15] Kawabata S, Niwa M and Kawai H. The finite-deformation theory of plain-weave fabrics. Part I: The shear deformation theory. J Text Inst 1973; 64: 62–85.

[16] Tabiei A and Ivanov I. Computational micro-mechanical model of flexible woven fabric for finite element impact simulation. Int J Numer Meth Eng 2002; 53: 1259–1276.

[17] Boisse P, Zouari B and Gasser A. A mesoscopic approach for the simulation of woven fibre composite forming. Compos Sci Technol 2005; 65: 429–436.

[18] Peng X and Cao J. A dual homogenization and finite element approach for

material characterization of textile composites. Compos Part B: Eng 2002; 33: 45–56.

[19] Cunniff PM. An analysis of the system effects in woven fabrics under ballistic impact. Text Res J 1992,62(9):495–509.

[20] Song B, Park H, Lu W-Y, Chen W. Transverse impact response of a linear elastic ballistic fiber yarn. J Appl Mech 2011;78(5):051023.

[21] Hassanpour Roudbeneh F, Liaghat G, Sabouri H, Hadavinia H. Experimental investigation of impact loading on honeycomb sandwich panels filled with foam. Int J Crashworthiness 2018,8265:1–12.

[22] Mudric T, Giacomuzzo C, Francesconi A, Galvanetto U. Experimental investigation of the ballistic response of composite panels coupled with a self-healing polymeric layer. J Aerosp Eng 2016;29(6):04016047.

[23] Almohandes AA, Abdel-Kader MS, Eleiche AM. Experimental investigation of the ballistic resistance of steel-fiberglass reinforced polyester laminated plates. Compos Part B Eng 1996;27(5):447–58.

[24] Karahan M, Kuş A, Eren R. An investigation into ballistic performance and energy absorption capabilities of woven aramid fabrics. Int J Impact Eng2008;35(6):499–510.

[25] Cork CR, Foster PW. The ballistic performance of narrow fabrics. Int J Impact Eng 2007,34:495–508.

[26] Ke P, Gieleta R, Morka A, Niezgoda T, Surma Z. Experimental study of hybrid soft ballistic structures. Compos Struct 2016; 153:204–11.

[27] Mudric T, Giacomuzzo C, Francesconi A, Galvanetto U. Experimental

investigation of the ballistic response of composite panels coupled with a self-healing polymeric layer. J Aerosp Eng 2016;29(6):04016047.

[28] Ying Wang, Xiaogang Chen, Robert Young, Ian Kinloch, Wells Garry. An experimental study of the effect of ply orientation on ballistic impact performance of multi-ply fabric panels. Textile Research Journal.2016, Vol. 86(1) 34–43.

[29] V.P.W. Shim, Y.B. Guo, V.B.C. Tan. Response of woven and laminated high-strength fabric to oblique impact. International Journal of Impact Engineering 48 (2012) 87-97.

[30] Teng JG, Chen SF, Hu JL. A finite-volume method for deformation analysis of woven fabrics. Int J Numer Methods Eng 1999;46(12):2061–98.

[31] Lim CT, Shim VPW, Ng YH. Finite-element modeling of the ballistic impact of fabric armor. Int J Impact Eng 2003;28(1):13–31.

[32] Termonia Y. Impact resistance of woven fabrics. Text Res J 2004;74(8):723–9.

[33] Nilakantan G, Keefe M, Wetzel ED, Bogetti TA, Gillespie JW. Effect of statistical yarn tensile strength on the probabilistic impact response of woven fabrics. Compos Sci Technol 2012;72(2):320–9.

[34] King MJ, Jearanaisilawong P, Socrate S. A continuum constitutive model for the mechanical behavior of woven fabrics. Int J Solids Struct 2005;42(13):3867–96.

[35] Shahkarami A, Vaziri R. A continuum shell finite element model for impact simulation of woven fabrics. Int J Impact Eng 2007;34(1):104–19.

[36] M. Grujicic, et al., Fiber-level modeling of dynamic strength of Kevlar® KM2 ballistic fabric, J. Mater. Eng. Perform. 21 (7) (2012) 1107–1119.

[37] C. Yang, P. Tran, T. Ngo, P. Mendis, W. Humphries, Effect of textile architecture on energy absorption of woven fabrics subjected to ballistic impact, Appl. Mech. Mater. 553 (2014) 757–762.

[38] E. Yang, T. Ngo, D. Ruan, P. Tran, Impact resistance and failure analysis of plain woven curtains Int. J. Protective Struct. 6 (1) (2015) 113–136.

[39] C. Ha-Minh, T. Kanit, F. Boussu, A. Imad, Numerical multi-scale modeling for textile woven fabric against ballistic impact, Comput. Mater. Sci. 50 (7) (2011) 2172–2184.

[40] M. Grujicic, W.C. Bell, G. Arakere, T. He, B.A. Cheeseman, A meso-scale unit-cell based material model for the single-ply flexible-fabric armor, Mater. Des. 30 (9)(2009) 3690–3704.

[41] G. Nilakantan, M. Keefe, E.D. Wetzel, T.A. Bogetti, J.W. Gillespie, Computational modeling of the probabilistic impact response of flexible fabrics, Compos. Struct.93 (12) (2011) 3163–3174.

[42] D'Amato E. Nonlinearities in mechanical behavior of textile composites. Compos Struct 2005,71:61–7.

[43] Lim CT, Tan VBC, Cheong CH. Perforation of high-strength double-ply fabric system by varying shaped projectiles. Int J Impact Eng 2002;27(6):577–91.

[44] Tabiei A, Nilakantan G. Ballistic impact of dry woven fabric composites: a review. Appl Mech Rev 2008;61(1–6):0108011–01080113.

[45] X. Zeng, V. Tan, V. Shim, Modelling inter-yarn friction in woven fabric armour, Int. J. Numer. Methods Eng. 66 (8) (2006) 1309–1330.

[46] S. Gogineni, X.-L. Gao, N. David, J. Zheng, Ballistic impact of Twaron CT709® plain weave fabrics, Mech. Adv. Mater. Struct. 19 (6) (2012) 441–452.

[47] Y. Zhou, X. Chen, G. Wells, Influence of yarn gripping on the ballistic performance of woven fabrics from ultra-high molecular weight polyethylene fiber, Compos. Part B.62 (2014) 198–204.

[48] D. Sun, X. Chen, Plasma modification of Kevlar fabrics for ballistic applications, Text.Res. J. 82 (18) (2012) 1928–1934.

[49] Yi Zhou, Xiaogang Chen. A numerical investigation into the influence of fabric construction on ballistic performance. Composites Part B.76 (2015) 209-217.

[50] Xiaogang Chen, Yi Zhou, Garry Wells. Numerical and experimental investigations into ballistic performance of hybrid fabric panels. Composites: Part B 58 (2014) 35–42.

Chapter 2

Preparation of FE model of Twaron® woven fabric

Chapter 2

Chapter 2: Preparation of FE geometric model of Twaron® woven fabric

2.1 Introduction

In recent years, numerical methods, such as finite element analysis, have been identified as effective techniques for mechanical behavior investigation of woven fabric [1,2]. Commercial packages, such as ANSYS®, ABAQUS®, and LS-DYNA®, have frequently been used to develop simulation models and analyze the mechanical performance of fabric materials. Although numerical methods have high requirements in terms of computing power and resources for simulating the process, there are clear advantages to these methods: they are fairly accurate, inexpensive, easy, and consume no materials [3]. Thus, these methods have become widely used tools for quickly and efficiently exploring new materials, weaves, and architectures through parametric studies and for identifying and understanding various mechanisms of deformation, failure, and energy dissipation that cannot be easily elucidated through experimental means [4].

In the process of numerical analysis, geometric model modeling is an essential foundation for numerical analysis. The accuracy of the model will determine the validity of the analysis results greatly. Looking at the current research, different modeling techniques are implemented in finite element method to study the fabric mechanical behavior. Fig.2-1 shows the existed modelling techniques. Single-scale macro-level modeling techniques include representing the entire fabric as

homogenized membranes [5,6,7], shell elements method[8,9], meso-level explicitly capturing yarn level architecture [10,11,12] and micro-level capturing filament level architecture [13,14]. Modeling the mechanical response of fabrics woven from continuous filament yarns is very challenging because of their intricate multi-hierarchical fabric-yarn-filament type architectures and complex material behavior, furthermore, the filament-level model will bring extremely computation cost and as a result this model technique is not an efficient and favorable method.

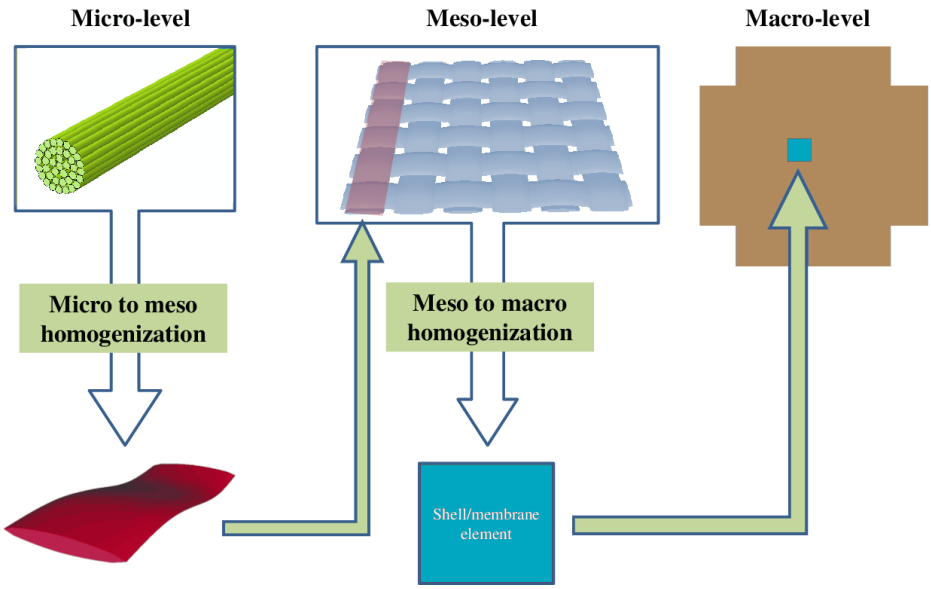

Fig.2-1 Modeling techniques of woven fabric

Among the model techniques, the homogenized membranes modeling is relatively simple, requires low computing hardware conditions, and is faster. Due to the computational efficiency, the use of homogenized membranes allows one to model multi-layer fabrics of realistic in-plane dimensions. However, many important and complex interactions that govern the impact and penetration of a fabric cannot be studied with this approach since the entire fabric architecture has been homogenized

without explicitly accounting for the yarn-level architecture. As a consequence, many of the important interaction like yarn–yarn interactions, yarn transverse compression and shearing, yarn frictional sliding, yarn decrimping, and yarn reorientation cannot be modeled accurately with homogenized membranes [15].

Another popular approach is to use woven shell elements of constant element thicknesses to model the woven yarns. This approach is effective in regions that are tension dominated. But is not accurate for regions where transverse compression, shear, and friction between tows are important and need to be considered. This is because shell elements cannot handle thickness changes or yarn cross-sectional shape changes. This in turn affects the estimation of normal contact forces between two yarns which in turn affects the mechanisms of frictional sliding interactions. Frictional sliding interactions have been shown to have an important effect on the fabric energy dissipating capabilities.

These limitations of using homogenized membranes and shell elements to model a fabric can be overcome by using 3D solid elements to accurately model the yarns throughout each layer of woven fabric. Although such an approach is associated with large computational requirements in terms of both processing power and memory requirements because of the large number of degrees of freedom of the model and number of computations to process each element. While these analyses have proved to be powerful technique for capturing and elucidating the detailed static and dynamic response of single-layer fabrics as well as multilayer fabrics. In present study, due to the advantage of the yarn-level model, the 3D solid element technique is applied for

the fabric model creation.

2.2 FE geometric model of Twaron® woven fabric

The plain-woven Twaron CT®, a high-performance fabric with light weight and high protection application, made by TEIJIN was employed in this study. This fabric is manufactured using a plain weave of 11 × 11 yarns (per cm^2), each yarns consisting of 500 filaments. The bulk density and linear density are 1.44 g/cm^3 and 550dtex, respectively. The cross-sectional area of each yarn was calculated as $3.82\times10^{-4}cm^2$ by dividing the linear density of the material by its bulk density. We created the fabric model in SolidWorks®. The fabric model was created at the yarn level. We implemented the plain weave fabric model in the present study—which considers two geometrical aspects, i.e., the cross-sectional shape and the path of the yarn—to describe the yarn geometry. Based on the photo of micro-structural cross-section of Twaron CT® taken by Yashima® digital microscope YDU-3S shown in the upper part of Fig.2-2(b), we assumed that the cross-section the warp and weft yarns of the fabric was lenticular in shape and consisted of two identical arcs facing each other. In the geometrical model, the cross-section of the yarn remains constant along its length, and the path of the yarn is the curve that represents the yarn waviness through the yarns in the other direction. Cross-sectional views of the yarn and fabric model are provided in Fig. 2-2(a) and(b). All geometrical parameters can be calculated using the following expressions [16]:

$$L = 2/\text{thread density}, \quad (1)$$

b=fabric thickness/4, (2)

$a=(2bR_1 - b^2)^{1/2} = L/4$, (3)

$R_2=(a^2+b^2)/2b$, (4)

$R_1=R_2-b$, (5)

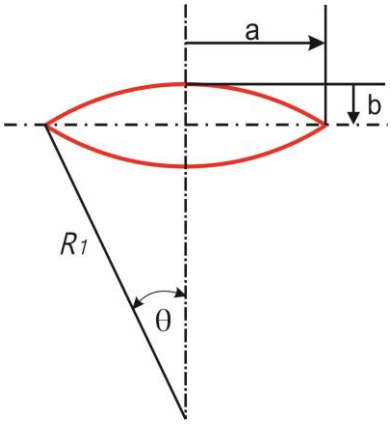

(a)

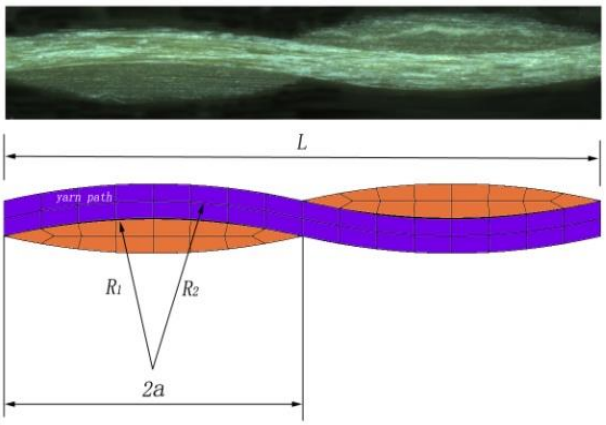

(b)

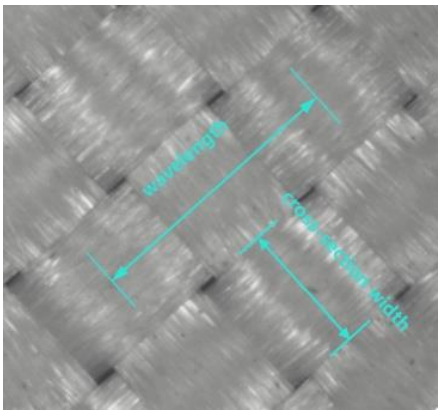

(c)

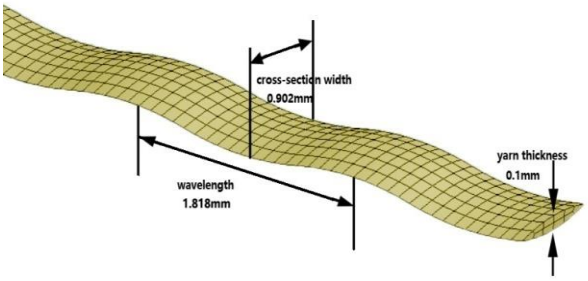

(d)

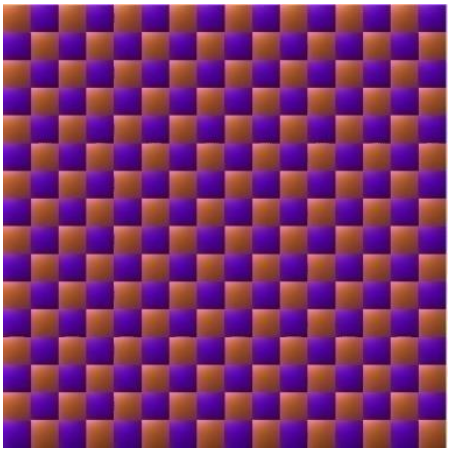

(e)

Fig. 2-2 (a) Cross-sectional view of the yarn; (b) Comparison of cross-sectional view of the Twaron CT® fabric and geometry model (c) Microscopic appearance of Twaron® fabric; (d) Dimensions of the yarn model (e) model of Twaron CT® woven fabric

Table 2-1. Physical parameters of Twaron CT®

Fabric type	Thread density (per cm)	Areal density(g/m^2)	Cross-sectional area of yarn(cm^2)	Thickness(mm)
Twaron CT	11	120	3.82×10^{-4}	0.2

where L is the wavelength of the yarn path, R_1 is the radius of the arc for the yarn cross-section, R_2 is the radius of the arc for the yarn path, and a and b are half of the width and half of the height of the yarn cross-section, respectively.

Photo of the fabric geometry is taken, and geometrical parameters are also measured from the digital microscope, as shown in Fig. 2-2(c) and (d). The average width of the yarn cross-section and wavelength of the yarn are 0.902 mm and 1.818 mm, respectively. The average thickness of the fabric is 0.2 mm, based on measurements using a digital Vernier caliper. Fig. 2-2(c) shows the final geometry model of Twaron CT® woven fabric, Table 2-1 shows the physical parameters.

2.3 Conclusions

In present study, due to the advantage of the yarn-level model, the 3D solid element technique is applied for the fabric model creation. Based on real physical parameters of Twaron® fabric, the geometry model was constructed in Solid works and the model will be used for further analysis of fabric's mechanical properties.

References

[1] Tarfaoui M, Akesbi S. A finite element model of mechanical properties of plain weave. Colloids Surf A Physicochem Eng Asp 2001;187–188.

[2] Lim CT, Shim VPW, Ng YH. Finite-element modeling of the ballistic impact of fabric armor. Int J Impact Eng 2003;28(1):13–31.

[3] Mulat Alubel Abtew, François Boussu, Pascal Bruniaux, Carmen Loghin, Irina Cristian. Ballistic impact mechanisms – A review on textiles and fibre-reinforced composites impact responses. Composite Structures.223 (2019) 110966.

[4] Gaurav Nilakantan, Steven Nutt. Effects of ply orientation and material on the ballistic impact behavior of multilayer plain-weave aramid fabric targets. Defence Technology 14 (2018) 165-178.

[5] I. Ivanov, A. Tabiei.Loosely woven fabric model with viscoelastic crimped fibers for ballistic impact simulations.International Journal for Numerical Methods in Engineering, 61 (2004), pp. 1565-1583.

[6] C.T. Lim, V.P.W. Shim, Y.H. Ng. Finite-element modeling of the ballistic impact of fabric armor.International Journal of Impact Engineering, 28 (2003), pp. 13-31.

[7] Nilakantan, G,Keefe, M, Bogetti, T.A, Gillespie Jr, Multiscale modeling of the impact of textile fabrics based on hybrid element analysis. International Journal of Impact Engineering.37(2010),1056-1071.

[8] Barauskas, R., 2007. Multi-scale modeling of textile structures in terminal ballistics. In: Proceedings of the 6th European LS-DYNA Users' Conference, Gothenburg, Sweden.

[9] R. Barauskas, A. Abraitiene. Computational analysis of impact of a bullet against the multilayer fabrics in LS-DYNA.International Journal of Impact Engineering, 34 (2007), pp. 1286-1305.

[10] B. Gu. Ballistic penetration of conically cylindrical steel projectile into plain-woven fabric target – a finite element simulation. Journal of Composite Materials, 38 (22) (2003), pp. 2049-2074.

[11] Y. Duan, M. Keefe, T.A. Bogetti. Finite element modeling of transverse impact on a ballistic fabric. International Journal of Mechanical Sciences, 48 (2006), pp. 33-43.

[12] M. Grujicic, G. Arakere, T. He, M. Gogulapati, B.A. Cheeseman. A numerical investigation of the influence of yarn-level finite-element model on energy absorption by a flexible-fabric armour during ballistic impact. Proceedings of the Institution of Mechanical Engineers, Part L: Journal of Materials: Design and Applications, 222 (4) (2008), pp. 259-276.

[13] Wang, Y., Sun, X., 2000. Determining the geometry of textile preforms using finite element analysis. In: Proceedings of the American Society for Composites, vol. 9. pp. 25–27.

[14] GauravNilakantan.Filament-level modeling of Kevlar KM2 yarns for ballistic impact studies. Composite Structures.104(2013), pp.1-13.

[15] GauravNilakantan, MichaelKeefe, Travis A.Bogetti, RobAdkinson, John W.Gillespie Jr. On the finite element analysis of woven fabric impact using multiscale modeling techniques. International Journal of Solids and Structures. 47(2010), pp.2300-2315.

[16] Ying Wang, Xiaogang Chen, Robert Young, Ian Kinloch. A numerical and experimental analysis of the influence of crimp on ballistic impact response of woven fabrics. Composite Structures 140 (2016) 44–52.

Chapter 2

Chapter 3

Yarn crimp and inter-yarn friction effect on the tensile performance of woven fabric

Chapter 3

Chapter 3: Yarn crimp and inter-yarn friction effect on the tensile performance of woven fabric

3.1 Introduction

Woven fabrics are currently most often used in clothing, industrial textiles, and even composite manufacture. Therefore, there is a great deal of interest in prediction of their behavior [1]. The elastic modulus is one of the most important mechanical properties and is a measure of a material's resistance to elastic deformation. Besides, the finite element analysis (FEA) has frequently been used to simulate and simplify engineering problems. As a result, several researchers have used this technique to study woven fabric's static tensile properties. Tehrami et al. [2] investigated the tensile behavior of woven fabrics with various weave patterns using the FEA. Lin [3] attempted to predict elastic properties to determine the tensile damage behavior of a woven fabric. Chen et al. [4] investigated the static tensile behavior of PVC-coated woven membrane materials under uniaxial and biaxial loads. Lin et al. [5] used a modeling approach to study the mechanical behavior of textile reinforcements; the model simulated combinations of compaction and in-plane shear loading to represent important interactions. Kollegal and Sridharan [6] investigated the mechanical behavior of plain weave fabric composites under in-plane loading using 3-D finite element analysis in conjunction with a micro-mechanical model. Other related published works [7-12] are also concerned with the various static tensile behaviors of woven fabric under different kinds of loading.

Furthermore, the physical properties of woven fabrics—including crimp rate and inter-yarn or even inter-fiber friction—have a significant influence on their mechanical performance. Tan et al. [13] and Wang et al. [14] have demonstrated the influence of crimp rate on the ballistic properties of woven fabrics. Broughton et al. [15] investigated the effect of inter-fiber friction on the tensile properties of yarns and demonstrated that inter-fiber friction can be the dominant factor in determining the tensile properties of a ring-spun staple yarn. Wang et al. [16] studied the effect of inter-fiber friction on fiber damage propagation and the ballistic limit of 2-D woven fabrics. Chu et al. [17] showed that greater inter-yarn friction leads to less slippage of the primary yarns at the center of impact and prolongs the failure of primary yarns.

Numerous papers have been published on the experimental and numerical simulation of the tensile or other mechanical properties of fabrics, as well as on the influence of the physical properties of woven fabrics such as crimp rate and inter-yarn friction. However, there are few reports on the determination of the equivalent modulus (note: equivalent modulus in present study refers to the real performed tensile modulus of fabric differentiated from material's original modulus) of woven fabric during tensile loading to investigate how the crimp or inter-yarn friction affects their mechanical properties. Therefore, in this chapter, a physical-geometric-feature-based continuous yarn in a plain-woven fabric is implemented, and its FE model is analyzed by considering the two key issues of a woven fabric, the crimp and inter-yarn friction. The basic parameters of Young's modulus of single yarn and the inter-yarn friction coefficient are investigated by the experimental of the practical fabrics in tensile and

pull-out tests. The FE analysis indicates that the stress-strain curves of FE model are effective in evaluating the equivalent modulus of a woven fabric by compared with the tensile experiment of Twaron CT® Plain Woven Fabric. Furthermore, we use the FE analysis to evaluate how the crimp rate and inter-yarn friction affected the mechanical properties by determining the equivalent modulus of single yarn and the unit cell of plain-woven fabric (UCPW) in both uniaxial and biaxial tensile loading.

3.2 FE model and experimental verification

3.2.1 Basic mechanical parameters of woven fabric model

In this research, an orthotropic linear-elastic material model is employed, and the mechanical properties of Twaron CT® are shown in Table 3-1. The material constants are dominated by the longitudinal tensile modulus E_{11}, according to existing studies [18,19]. $E_{11}$was obtained by tensile test of single yarn of Twaron CT®, tensile result can be seen in Fig .3-1. The tensile strength (TS) is also calculated as 2.764Gpa. E_{22}, E_{33}, G_{12}, G_{13} and G_{23} were calibrated by taking suggestions from the model by S. Gogineni et al. [20] and C.T. Lim et al. [21]. Many study have been proved that Poisson's ratios (V_{12}, V_{23}, V_{13}) should be zero and the transverse Young's modulus (E_{22}, E_{33}) and shear modulus (G_{12}, G_{13}, G_{23}) should be very small with respect to the longitudinal Young's modulus E_{11} to reproduce a thread behavior for the yarn [22].

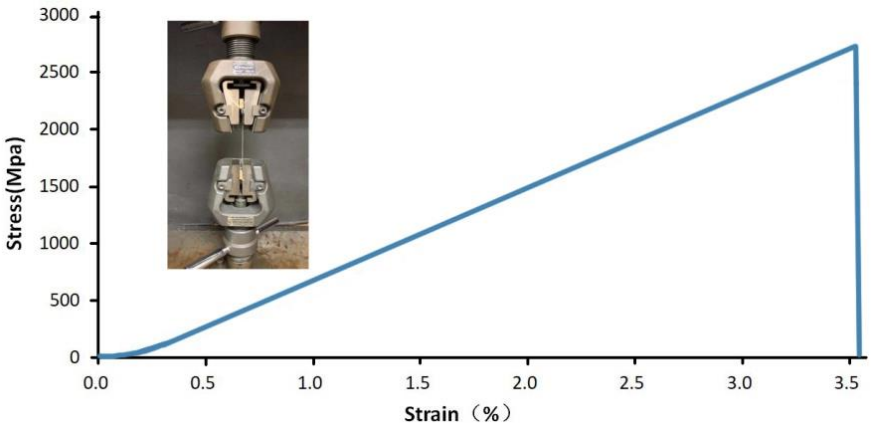

Fig. 3-1. Tensile experiment results of single yarn of Twaron CT®

Table 3-1. Orthotropic linear-elastic material parameters of single yarn of Twaron CT® (GPa)

E_{11}	E_{22}	E_{33}	G_{12}	G_{13}	G_{23}	V_1	V_2	V_3	TS
72.63	1.13	1.13	1.04	1.04	1.04	0	0	0	2.764

3.2.2 Inter-yarn friction coefficient of Twaron CT® woven fabric

Inter-yarn friction has shown to have a significant effect in determining fabric's mechanical properties; it is also an indispensable parameter in mechanical behavior simulation. An inter-yarn friction coefficient obtaining method of comparing experiment and simulation result was used in this research [23].

Firstly, yarn pull-out test is carried out using a uniaxial tensile test machine (TENSILON®RTF-2350), an individual yarn from the Twaron CT® is pulled out with velocity of 0.1mm/min and repeated eight times. The effective dimension of the fabric is 70 mm length and 50 mm width. The shear deformation and transverse tension are minimized using a special grip consisted of two U-shaped metallic plates, shown in Fig.3-2(a).

In addition, simulation is also carried out. Considering the computing cost, a smaller fabric model of Twaron CT® woven fabric with 3yarns*11yarns, is created and used to simulate pull-out process. The displacement of the two short-yarn side is constrained in all the edges but allowing the spin. The contact between the warp and weft yarns is defined as frictional. Fig.3-2(b) shows the simulation process. In order to examine the effects of the friction, 4 different frictional coefficient (FC) cases are modeled respectively in the test (FC = 0.1; 0.2; 0.3; 0.4). Numerical simulation results are compared to experimental yarn pull-out curves. Linear regression relation equations for 1^{st}-4^{th} peak force (totally five peaks，more detail in Fig.3-3) and FC is concluded (the 5^{th} peak was neglected because the error is positive when the experiment test reach fabric's edge), the inter-yarn friction coefficient μ is concluded to be 0.3 by averaging the results of in each peak. Table.3-2 shows linear regression relation equations of peak force and frictional coefficient.

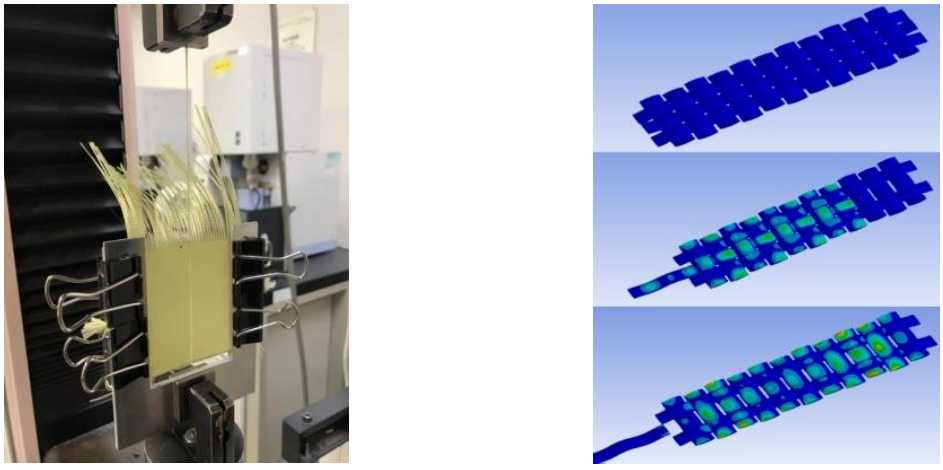

(a) (b)

Fig.3-2. Pull-out of Twaron CT® woven fabric (a) Experiment process (b) Simulation process

Table 3-2. Linear regression relation equations of peak force and frictional coefficient for 1st -4th peak

	Linear regression relation equation	R^2	Peak Force(N)	μ
1st peak	F= 0.542 μ + 0.0705	0.9955	0.291	0.275
2nd peak	F = 0.432 μ + 0.05	0.9918	0.226	0.289
3rd peak	F = 0.32 μ + 0.0355	0.9905	0.177	0.318
4th peak	F = 0.256 μ + 0.012	0.9893	0.123	0.334

-

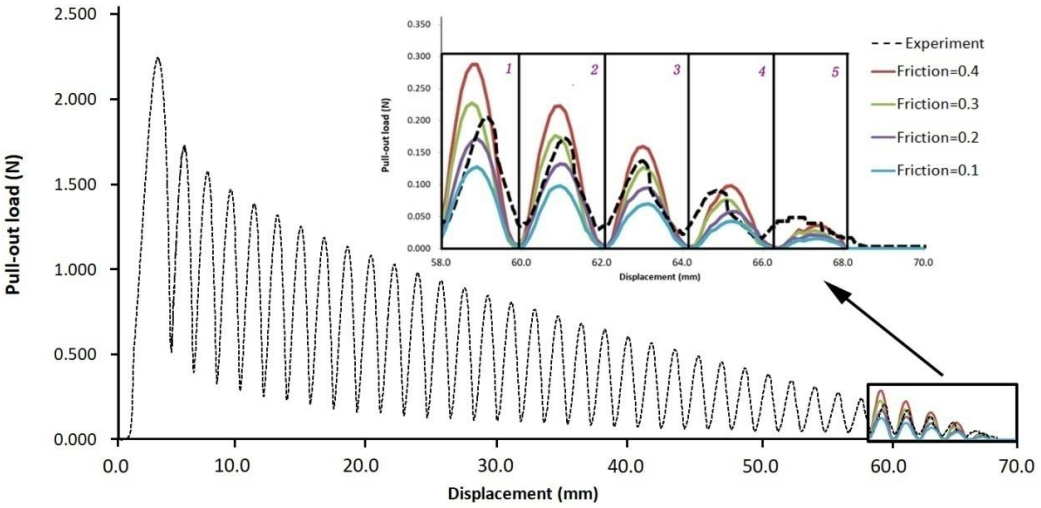

Fig.3-3. Comparison of simulation results and experimental result of single yarn pull-out from Twaron CT®

3.2.3 Tensile simulation and experimental verification

Tensile simulation of Twaron CT® is carried out accordingly. Mechanical parameters and inter-yarn frictional coefficient obtained above are applied to the model. The Stress-strain curve during tensile process is depicted as red dash line in Fig.3-4, and the Young's modulus of the fabric Es is calculated to be 71.35GPa when the frictional coefficient is designated to be 0.3. Moreover, a friction coefficient of 0 is also taken into consideration, stress-strain curve is depicted as grey dash line in Fig.3-4. It can be

obviously found out that the frictional coefficients have influence on the tensile result. We will discuss it deeply in the following content.

In order to validating the effectiveness of the model and simulation process, experiment of tensile test of practical Twaron CT® is carried out. A quasi-static tensile test is done in a 20KN INSTRON machine with a cross-head speed of 1 mm/min. The effective zone of the samples are designated to 2cm×10cm（22yarns×110yarns, the samples are firstly cut into oversized ones using a special aramid-use scissor, 8 replicates are cut with the length along the warp direction, then extra yarns along the samples length were removed from both sides in order to ensure that the edge defects are minimized and no slip of loaded yarns during the test. Besides, High-strength epoxy is glued to the ends of the test specimen in order to prevent slippage. Thin aluminum clamp is used for the fixture of the test samples. High resolution photos taken from camera shows negligible slip between the samples and grips, and no pullout of yarns.

The typical stress-strain curve under uniaxial tension is also depicted. As what we concerned is the tensile property before fabric's failure, so we stop the tensile experiment before fabric's complete failure. The curve can be divided into 3 regions, crimp region, linear pre-peak region and post-peak region. In the crimp region, the stress increases lowly due to the straightening of the undulated yarns in loading direction with limited yarn stretching. The maximum strain in crimp region is only 0.0078. This is negligible when compared with the strain at failure. As the strain increases, the fabric exhibits a linear response before failure. The Young's modulus of

the fabric is defined by the slope of the stress–strain curve in this region. And the average Young's modulus of the Twaron CT® is calculated to be Ee=73.18GPa.

The comparison of tensile stress-strain curve between experiment and simulation can been seen at Fig.3-4, the estimated results with a frictional coefficient of 0.3 show great similarity with the experiment result, the Young's modulus estimated by simulation shows approximately 2.5% smaller than the experiment result. As a result, we can conclude that the model used in the simulation can generally reflect the tensile property of real fabric; the model and simulation can be proved to be effective.

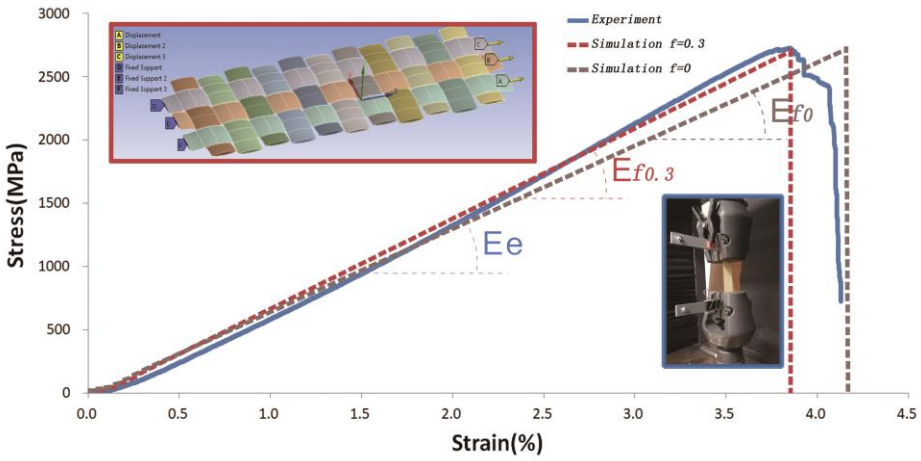

Fig.3-4. Comparison of tensile stress-strain curve between experiment and simulation of Twaron CT® fabric

3.3 Yarn crimp effect on the tensile performance of woven fabric

As we know, different types of fabrics have different crimp and inter-yarn friction coefficients even the fabrics are made of the same material. It is difficult to qualitatively judge their influence effect respectively on mechanical properties through real material experiments, whereas FEA can help dealing these problems due to its powerful parameterization solution ability. Firstly, five fabric models with the

same thickness (0.2mm) and different crimp rates were created for FEM analysis. The crimp rate of a woven fabric can be calculated using Eq. (1):

$$\text{Crimp}=\left(8\pi R_2 \frac{\theta}{360} - L\right)/L \times 100\%, \quad (1)$$

where θ is half of the central angle (in degrees) of the arc forming the shape of the yarn cross-section. $R_2$and L can be seen Fig.2-2 in chapter 2. The structural details of these models are listed in Table 3-3.

Table 3-3. Structural details of fabrics used in finite element (FE) analysis

Model	Thread density (1/cm)	crimp (%)
1	8.6	1.167
2	10.2	1.986
3	11	2.329
4	11.7	3.341
5	12.5	4.658

In addition, the present model employed in test still cost a lot of calculation time. As a result, a unit cell of plain woven (UCPW) was proposed (see Fig.3-5) for improve the calculation effectiveness. Tensile simulation results showed there was no different in results of fabric's Young's modulus between the model employed above and the unit cell model which was applied an extra circulated boundary condition in simulation process [24]. This kind of UCPW model was employed in all following cases of tests.

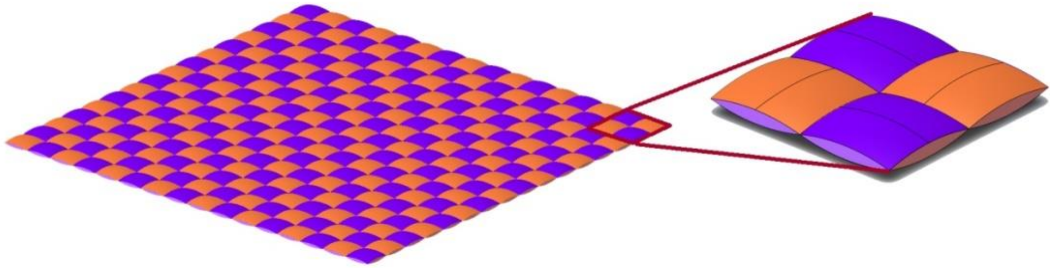

Fig.3-5. Schematics of the unit cell of plain woven (UCPW)

3.3.1 Yarn crimp effect on tensile performance of a single yarn

Firstly, before tensile test on fabric, we try to investigate how the crimp impacts the mechanical behavior of single yarn. Five types of yarns with different crimps rate are employed in the tensile simulation. An elongation rate of 1% is set in the tensile direction in all the tensile tests as during linear elastic processes the level of elongation rate does not affect the results.

Equivalent tensile modulus, as one of important indexes of material's mechanical property, is calculated from simulation results by obtaining normal stresses and strains in the tensile direction (the z direction in Ansys) during the tensile load is applied. The stresses and strains of all nodal points when tensile load is applied to the cross-section of the tensile end—denoted by $\sigma_1, \sigma_2 \cdots \sigma_n, \varepsilon_1, \varepsilon_2 \cdots \varepsilon_n$—are excluded from the analysis results. Therefore, the equivalent tensile modulus (Ee) of the yarns during tensile loading can be calculated using the following equation:

$$Ee=\sum_1^n \sigma/\sum_1^n \varepsilon. \quad (2)$$

The tensile deformation of a single yarn with a crimp of 3.341% is represented in Fig. 3-6(a). The crimped yarn straightened during the tensile process, and the movement of

the yarn reveals that both tensile and bending phenomena occurred during the tensile process. The normal stress distribution in the tensile direction is represented in Fig. 3-6(b). The results of the analysis are acceptable because there was no stress concentration. Conspicuously, the maximum normal stress was located at both sides of the areas of greatest curvature, as represented by the red and blue areas.

The equivalent modulus for each degree of crimp was calculated, and the reducing trend in the equivalent modulus was also obtained, as shown in Fig. 3-7. The equivalent tensile moduli of the single yarns were obviously smaller than those of the original material (72.63 GPa) over all crimp rates, and they were inversely proportional to the crimp rate. The equivalent moduli of the yarns dropped from 98.35% to 94.78% of the original modulus when the crimp increased from 1.167 % to 4.658%. This means that for the same material with the same original tensile modulus, the degree of crimp resulting from the production process affects the equivalent modulus of the yarn during mechanical loading; the more curved the yarn, the smaller its tensile modulus.

We then carried out a microscopic examination of the stress at the FE nodal points. Fig. 3-8 shows the normal stress distribution in the tensile direction (z) of nodal points through the upper surface of a yarn with a crimp of 3.341%. The selected nodal points are highlighted in violet in the side view of the single yarn model. The schematic of the results represents an approximate trigonometric function curve. The normal stresses at representative nodal points (C1-C5) in three yarns with different crimp rates are listed in Table 3-4. The results illustrate that each nodal stress in the tensile

direction (in absolute terms) was greater when the degree of crimp was smaller. This result also means that under the same tensile elongation, the yarn with the greatest crimp rate experienced less stress in the tensile direction. We also investigated the deformations of the same nodal points in the perpendicular Y direction (see Table 3-5). The results illustrate that the deformation of each nodal point in the Y direction is greater when the degree of crimp is larger. Because displacement reduces stress to some extent, during tension, the greater the degree of deformation perpendicular to the direction of tension, the smaller the stress in the direction of tension inside the material. This means that, under the same elongation rate, yarns with a greater crimp rate experience greater bending deformation, and unstable dynamic action reduces the tensile stress and strain in the tensile direction, making the yarn easier to stretch than a yarn with a lower crimp rate. Such yarns also have a lower equivalent modulus.

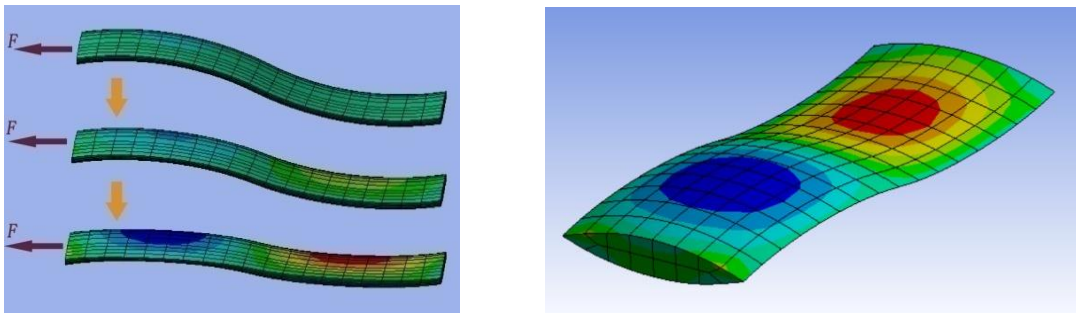

(a) (b)

Fig. 3-6. Schematics of FE tensile characteristics of a single yarn with a crimp of 3.341%. (a) Tensile deformation process; and (b) normal stress distribution in the tensile direction

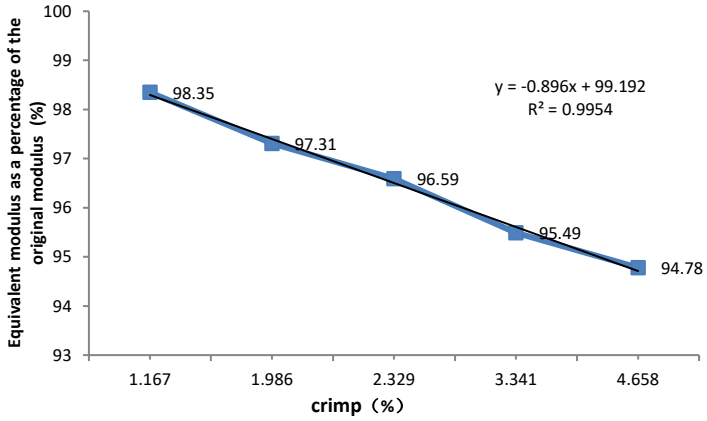

Fig. 3-7. Equivalent modulus as a percentage of the original modulus versus the crimp rate in a tensile test on a single yarn

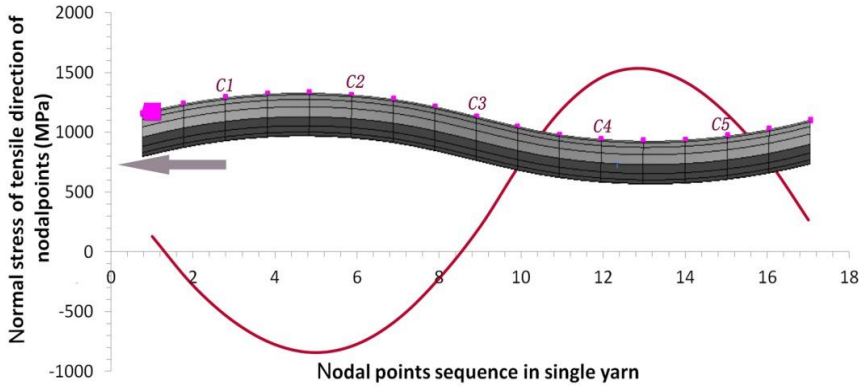

Fig. 3-8. Normal stress distribution of nodal points in the tensile direction through the upper surface of a yarn with a crimp of 3.341%

Table 3-4. Comparison of normal stresses (MPa) in the tensile direction at representative nodal points C1-C5 for yarns with various crimp rates

Nodal point	Normal stress (MPa)		
	Crimp1.167%	Crimp2.329%	Crimp4.658%
C1	592.3	589.1	585.4
C2	790.2	783.9	771.2
C3	288.9	258.3	211.6
C4	1488.9	1477.5	1465.8
C5	1195.3	1178.6	1156.7

Table 3-5. Comparison of deformation (mm) of nodal points C1-C5 in the perpendicular Y direction for yarns with various crimp rates

Nodal point	Crimp1.167%	Crimp2.329%	Crimp4.658%
C1	0.137	0.158	0.169
C2	0.118	0.134	0.143
C3	0.064	0.078	0.086
C4	0.019	0.026	0.032
C5	0.006	0.009	0.0011

3.3.2 Yarn crimp effect on the tensile performance of woven fabric

3.3.2.1 Uniaxial tensile

A unit cell of plain woven (UCPW) comprises four contact regions because it is composed of two warp yarns and two weft yarns. These contact regions are responsible for inter-yarn friction, which cannot be negligible in the tensile simulation process. Therefore, a constant frictional coefficient between the contact regions of 0.3 is applied in tests at all crimp levels. A model UCPW comprising yarns with a crimp of 3.341% and applied boundary conditions are represented in Fig.3-9. Cross-sections A and B represent fixed ends, whereas cross-sections C and D are tensile ends. The cyclic symmetry of the normal stress distribution in the tensile direction owing to the symmetry of the UCPW can also be seen in the lower right schematic surrounded by the red border in Fig.3-9. The maximum normal stress area is located around the outside rim of the cross-section in the load-bearing yarn. The stress distribution of the cross-section of the UCPW can be seen in the upper right schematic surrounded by the red border. The stress in the load-bearing yarns is greater than in the non-loaded

yarns.

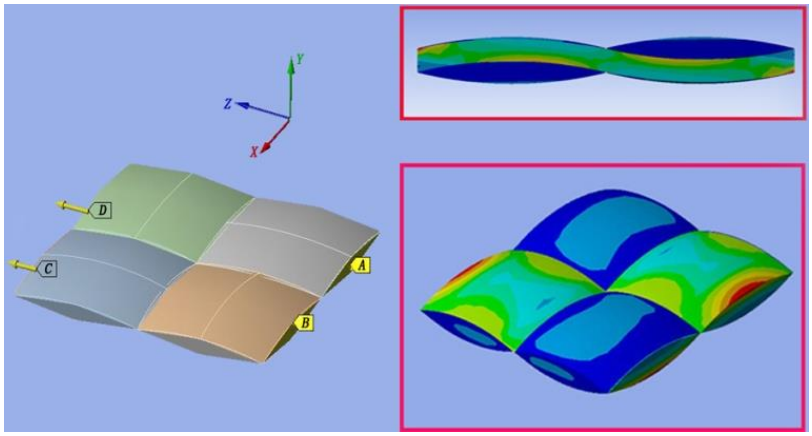

Fig. 3-9. Schematics of boundary conditions and normal stress distribution in the tensile direction in a uniaxial tensile test on a unit cell of plain woven (UCPW)

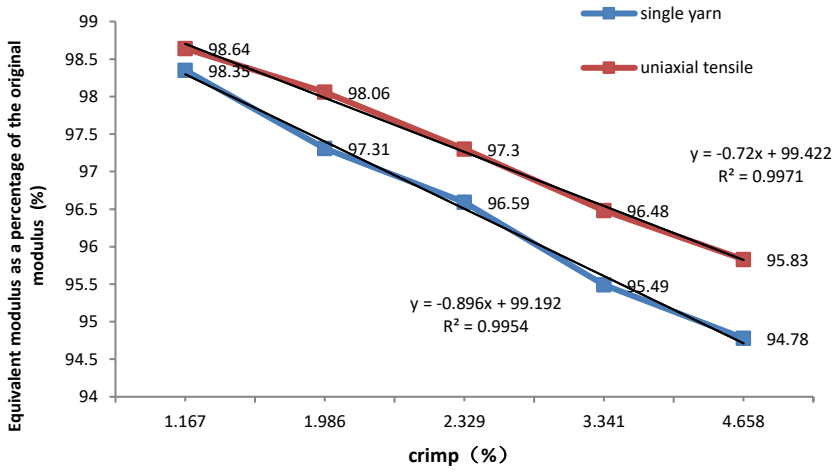

Fig. 3-10. Comparison of equivalent modulus as a percentage of the original modulus of a single yarn and a UCPW versus the crimp rate in a uniaxial tensile test

The equivalent tensile modulus of the UCPW under uniaxial tensile loading demonstrated the same trend as the single yarn test: a greater crimp resulted in a lower equivalent modulus (Fig. 3-10). The equivalent modulus of the UCPW dropped from 98.64% to 95.83% of the original modulus when the crimp increased from 1.167% to 4.658%. It is also clear that the moduli at all levels of crimp are smaller than the modulus of the original material. A comparison of the uniaxial tensile tests on the

single yarn and on the UCPW reveals that the equivalent modulus is greater in the UCPW at all levels of crimp than in the single yarn, this result is accordance with above tensile experiments. In addition, the linearly fitted results from the uniaxial tensile tests reveal that crimp has a slightly greater influence on the single yarn than on the UCPW. Furthermore, the difference in the equivalent modulus between the single yarn and the uniaxial tensile case increased from 0.2% to 1.1% as the crimp increased.

We also investigate the stress between the yarns in the cross-section of the UCPW under uniaxial tensile loading. When tensile loading was applied, tensile elongation in yarn A resulted in friction stress on the contact surface (indicated by the red line in the side view in Fig. 3-11) caused by the hindrance of yarns B and C; simultaneously, bending in yarn A resulted in extrusion stress normal to the fabric plane on the contact surface, also due to the hindrance of yarns B and C. Fig. 12 shows the stress condition at the central contact nodal point of yarn A. In contrast, in the single yarn test there is no hindering yarn to prevent the elongation and bending of the tensile yarn, so compared with the UCPW, the single yarn is easier to stretch. This explains the difference in the equivalent moduli between the UCPW and the single yarn.

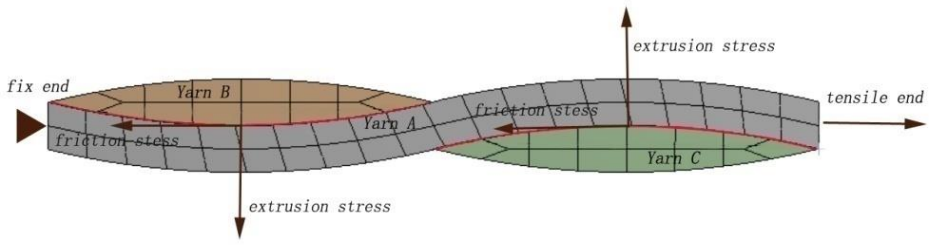

Fig. 3-11. Stress between yarns in cross-section of UCPW at the central contact nodal point during uniaxial tensile loading

3.3.2.2 Biaxial tensile test

We also take biaxial tensile tests into consideration. Compared with the uniaxial tensile tests, in the biaxial test we applied tensile loading to yarns in both the warp and weft directions while maintaining an inter-yarn frictional coefficient of 0.3. Cross-sections A, B, C, and D are the fixed ends, and cross-sections E, F, G, and H are the tensile ends (Fig. 3-12). In the biaxial test we apply tensile loads to the warp and weft yarns simultaneously at a rate of 1% elongation in both directions. Considering the symmetry of the UCPW, the results for the two directions should be the same. Therefore, the results for either direction are acceptable. The schematic surrounded by the red border in the lower right of Fig.3-12 also shows the normal stress distribution in a single tensile direction (the schematic represents a view magnified by five times). The cyclic symmetry results also reveal that the maximum stress occurred both around the rim of the cross-section and around the cross-contact area between the two groups of yarns. Furthermore, the stress is quite evenly distributed between the weft and warp yarns, as shown in the schematic surrounded by the red border in the upper right of Fig.3-12.

Fig. 3-13 reveals that the equivalent tensile moduli in UCPWs with different crimps are closer to the modulus of the original material in the biaxial tensile test than in the uniaxial test. As in the uniaxial case, the distribution of the moduli has the same downward trend. The equivalent modulus of the UCPW dropped from 99.79% to 97.08% of the original modulus when the crimp increased from 1.167% to 4.658%. Therefore, at the same crimp and inter-yarn friction coefficient, the equivalent

modulus is greater in the biaxial tensile test than in the uniaxial test. The linear fitting results also reveal that the crimp has slightly less influence in the case of the biaxial tensile test than in the uniaxial test.

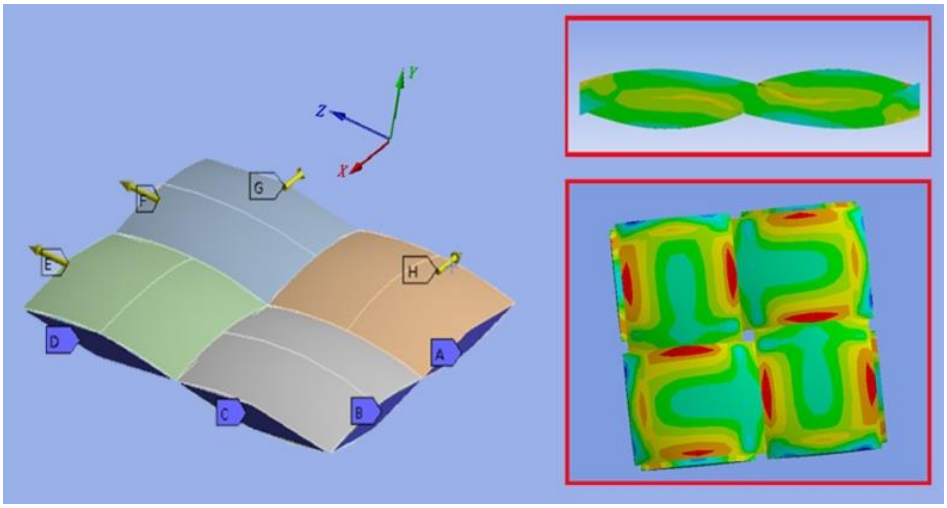

Fig. 3-12. Schematic of boundary condition and normal stress distribution in the single tensile direction in UCPW during the biaxial tensile test

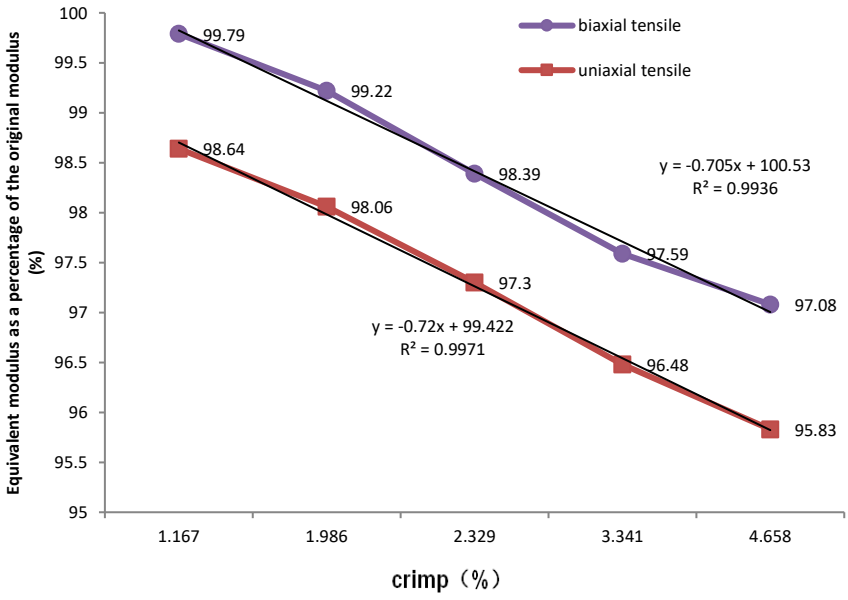

Fig. 3-13. Comparison of equivalent modulus as a percentage of the original modulus versus crimp in UCPW in the uniaxial and biaxial tensile tests

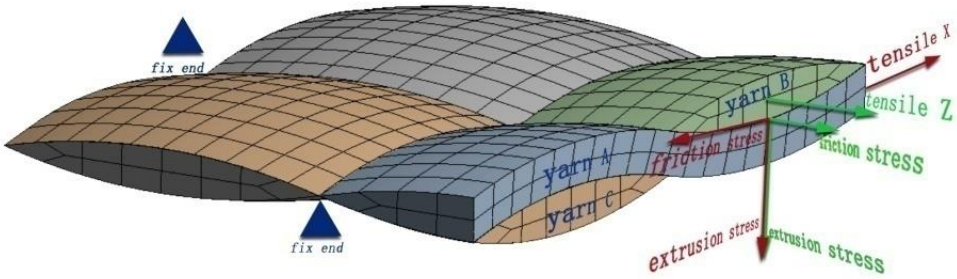

Fig. 3-14. Stress between yarns in the cross-section of UCPW at the central contact nodal point of yarn A under biaxial tensile loading

From a microscopic perspective, as tensile loading is applied to the yarns in the warp and weft directions, the stress situation is much more complicated in the biaxial test than in the uniaxial case, as shown in Fig. 3-14. For example, in the central contact nodal point of yarn A, the tensile load in the x direction (tensile x in the schematic) is applied directly to yarn A. As in the uniaxial case, tensile elongation resulted in friction stress at the contact surface caused by the hindrance of yarns B and C; simultaneously, the bending of yarn A also resulted in extrusion stress normal to the fabric plane on the contact surface due to the hindrance of yarns B and C. In addition, another tensile load is applied to yarns B and C in the z direction. Owing to symmetry, only yarn B was taken into consideration. The tensile elongation of yarn B resulted in friction stress on the contact surface of A, and the bending of yarn B also resulted in extrusion stress on yarn A. Therefore, it is obvious that both friction stress and extrusion stress in the nodal points of the contact area are greater compared with the uniaxial case. In the following analysis, we will discuss the quantification of inter–yarn friction.

Generally, regardless of the type of tensile test (single yarn, uniaxial, or biaxial), the

equivalent modulus gradually decreases as the crimp of the yarn increases. Furthermore, at the same level of crimp, the equivalent modulus of the UCPW decreases in the order: biaxial test; uniaxial test; single yarn test.

3.4 Inter-yarn friction effect on the tensile performance of woven fabric

Typically, the compressive stress generated on the contact surface and the contact friction coefficient are the two main factors affecting friction force, and under the same objective condition, the friction force between yarns in the fabric is supposed to have an influence on the fabric's tensile properties. Therefore, in the present study we attempted to determine the effect of inter-yarn friction on a fabric's tensile properties from the perspective of both contact stress and friction coefficient, and to elucidate the underlying mechanism.

3.4.1 Investigation of contact stress

The inter-yarn friction force is very difficult to calculate in fabrics [25]. However, the greater the pressure between the contact surfaces, the greater the friction force generated. Therefore, the variation in the friction force can be determined by measuring the change in the contact pressure. From a microscopic perspective, the frictional force of each affected FE nodal point is determined by the normal contact stress. In the present study, we chose the cyclic contact area highlighted by the surrounding red line in the UCPW shown in Fig.3-15. We select seven representative nodal points on the surface of a certain yarn and designated them N_1 to N_7, then examined and compared the stresses at these seven nodal points. Because the model is

symmetrical, the stresses at these representative nodal points basically represent those of the whole yarn or UCPW. We examine perpendicular stresses (in the y direction, perpendicular to the fabric plane) to determine the extrusion pressure between the contact area of the yarn. At the same crimp of 3.341%, and an inter-yarn frictional coefficient of 0.3, we investigate the three tests (single yarn, uniaxial, and biaxial tensile) at the same representative nodal points. The perpendicular stresses at N_1 to N_7 in the different tests are given in Fig.3-16.

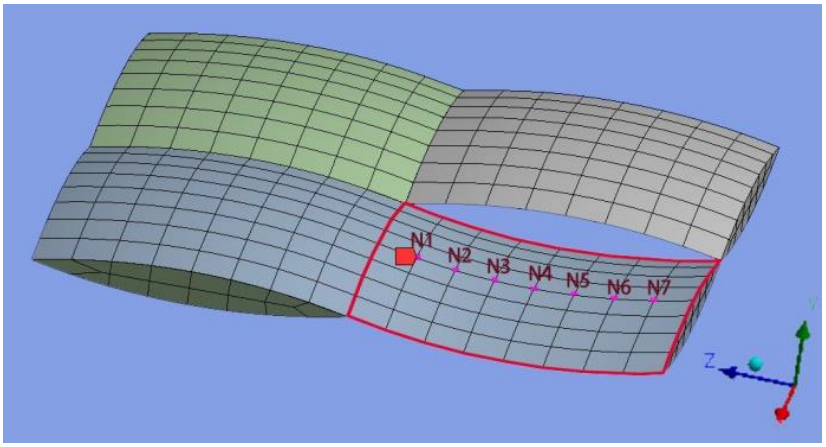

Fig. 3-15. The positions of N1 to N7 in the UCPW and the single yarn at a crimp rate of 3.341%

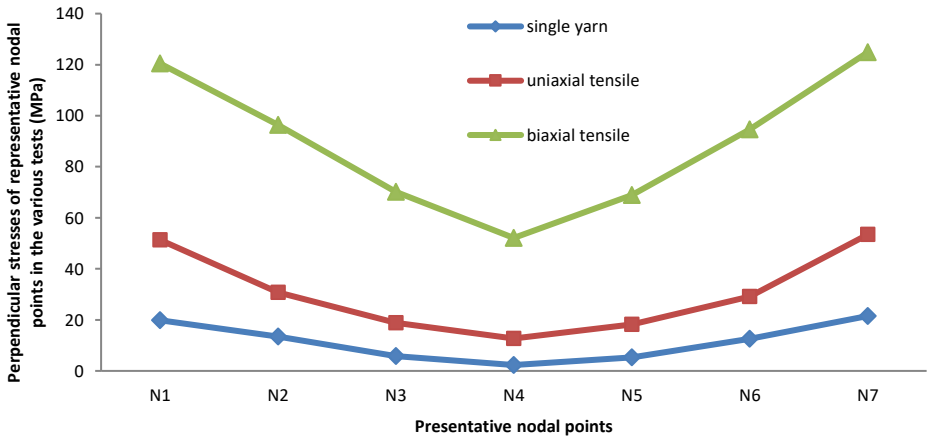

Fig. 3-16. Perpendicular stresses (MPa) at representative nodal points in the various tests at the same crimp 3.341%and inter-yarn frictional coefficient 0.3

In a tensile process involving a single yarn, the perpendicular stress is caused by the bending of the yarn, as mentioned above, whereas in uniaxial or biaxial tensile processes, in addition to bending, the mutual extrusion interaction at the contact area of the yarn caused by tensile loading also contributes to perpendicular stress. Fig.3-16 demonstrates that during tensile processes, the perpendicular stresses at the representative points in a single yarn, which are mostly caused by bending, are quite small compared with those in the UCPW (approximately 12.5% of the perpendicular stress in the biaxial case and 36.8% in the uniaxial case). In other words, bending only accounts for a small part of the stress compared with mutual extrusion between yarns. In the UCPW tensile test, the mutual extrusion between contact yarns is responsible for most of the perpendicular stress. In the single yarn tensile case, the perpendicular stress is quite small because there is no inter-yarn contact; whereas in the UCPW case, the yarn protrudes from the deformation as a result of tensile loading and the deformation in the biaxial case is greater than in the uniaxial case because multiple loading is applied. This led to greater mutual extrusion stress in the biaxial test than in the uniaxial test. Under the same friction coefficient, the greater the interaction pressure between yarns, the greater the friction produced during a tensile process. Therefore, under biaxial tension, more protruding deformation causes more contact stress resulting in greater friction. According to the statistical analysis of the representative nodal points, the perpendicular stress in the biaxial case is on average 2.86 times greater than in the uniaxial case, and 7.93 times greater than in the single yarn. At the same crimp, a larger friction force leads to larger internal stress in the

yarns, which makes them more difficult to stretch, resulting in a larger equivalent modulus than during uniaxial tension. This provides a good explanation for why the equivalent modulus of the UCPW differed between the single yarn, uniaxial, and biaxial tensile processes.

3.4.2 Inter-yarn friction effect on the tensile performance of woven fabric

Inter-yarn friction is another important factor that influences the mechanical properties of a fabric. At the same crimp rate and the same tensile elongation, a larger friction coefficient results in a greater friction force between two contact yarns during tensile loading. A greater friction force contributes to greater internal stress in the yarn during loading, as mentioned above, which further influences the tensile properties. We are most concerned with how, and to what extent, the inter-yarn friction coefficient affects the equivalent modulus during tensile processes. Therefore, we use the same UCPW at the same crimp rate of 3.341% in both the uniaxial and biaxial tensile tests. We apply five friction coefficients (0.1, 0.2, 0.3, 0.4, and 0.5) to the contact boundary condition. The results are shown below.

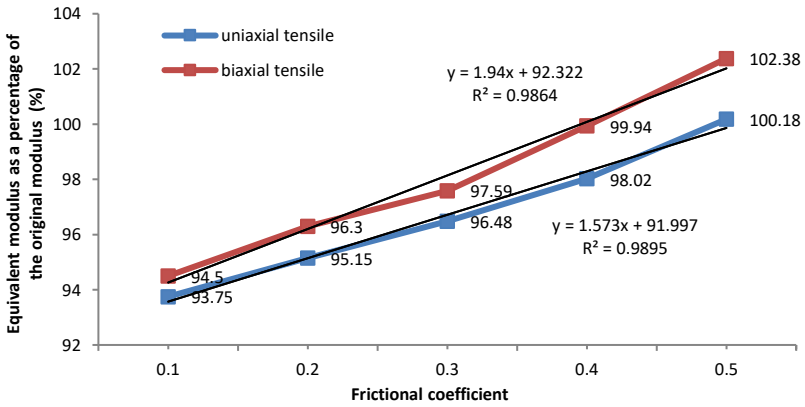

Fig. 17. Equivalent modulus as a percentage of the original modulus versus inter-yarn frictional coefficient in UCPW under tensile loading

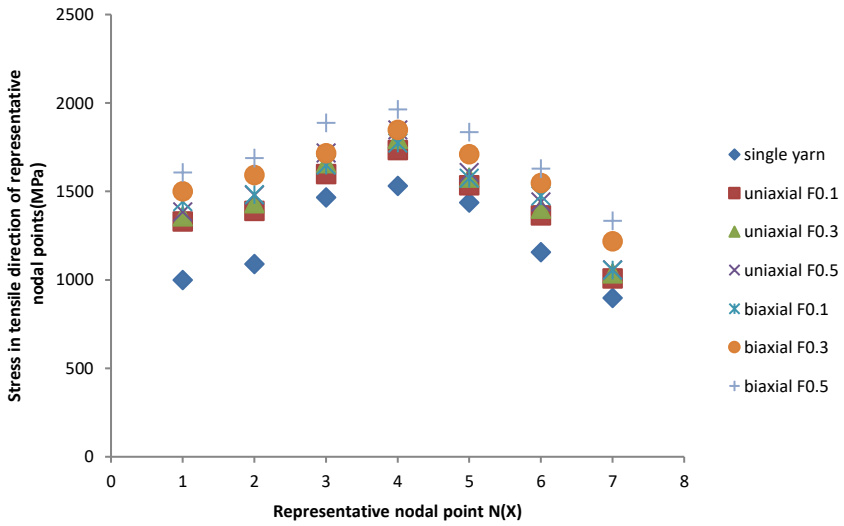

Fig. 3-18. Comparison of stress at representative nodal points in the tensile direction for the various tests

Fig. 3-17 shows that the equivalent modulus increased as the frictional coefficient increased. Increasing the inter-yarn friction raises the friction force during the tensile process, and this leads to stronger resistance, resulting in an increase in the equivalent modulus. Furthermore, the results show that the equivalent modulus was greater than the original modulus when the friction coefficient reached 0.5 both tensile cases. Therefore, the equivalent modulus may be larger than the original modulus when the inter-yarn friction is large enough. Moreover, under certain mechanical conditions, and at a certain inter-yarn friction, it is possible for the equivalent modulus of a fabric to be the same as the original modulus.

Fig.3-18 shows the stresses in the tensile direction (z) at the representative nodal points at a crimp of 3.341% in the single yarn, biaxial, and uniaxial tensile cases at friction coefficients of 0.1, 0.3, and 0.5. The results reveal the following. First, the stress in the single yarn case is lowest at all points because there is no inter-yarn

friction. Second, in both the biaxial and uniaxial tests, the stress in the tensile direction became noticeably higher when the friction coefficient increased, owing to the higher friction force between the yarns. According to the statistical analysis of the representative nodal points, the stress in the tensile direction in the biaxial and uniaxial tests increased by 19.3% and 8.8% on average, respectively, when the frictional coefficient varied from 0.1 to 0.5. Third, at the same friction coefficient, the stress is higher in the biaxial case than in the uniaxial case. According to the statistical analysis of the representative nodal points, the stress in the tensile direction is 24.2% larger on average in the biaxial test than in the uniaxial test; this also explains why the equivalent modulus in the biaxial case is higher than in the uniaxial case at the same crimp and friction coefficient.

3.5 Conclusions

In this chapter, we investigated how, and to what extent, the physical characteristics of a fabric influence its mechanical properties during tensile processes. Firstly, FE model of Plain Weave was created and proved to be effective by compared with the tensile experiment with Twaron CT® Plain Weave Fabric. Secondly, tensile simulations representing a single yarn, and uniaxial and biaxial UCPWs were carried out by considering different yarn crimp rates. Regardless of the tensile test (single yarn, uniaxial, or biaxial), the equivalent modulus gradually decreases as the crimp of the yarn increases. Furthermore, at the same level of crimp, the equivalent modulus decreases in the following order: biaxial test; uniaxial test; single yarn test. We chose representative nodal points and investigated and analyzed the deformation and normal

stress. The results revealed that, in the case of a single yarn, a yarn with a greater crimp will have greater displacement caused by bending during the tensile process, and unstable dynamic action reduces the tensile stress in the tensile direction. In other words, the bigger the crimp, the easier it is to stretch the yarn, which has a smaller equivalent modulus. Moreover, we determined why there was a difference in the equivalent modulus between the single yarn, uniaxial, and biaxial tensile tests by investigating the stress at the representative inner nodal points. Thirdly, we considered the influence of inter-yarn friction. We analyzed the contact stresses in a group of nodal points chosen in the model, and the results showed that under biaxial tension, more protruding deformation causes more contact pressure, producing a larger friction force. At the same crimp, a larger friction force leads to larger internal stress in the yarns, which makes them more difficult to stretch, resulting in a larger equivalent modulus than during uniaxial tension. We then carried out tensile tests on UCPWs with different inter-yarn frictional coefficients at the same crimp rate. The stresses in the tensile direction at the representative nodal points were also investigated. There was an obvious tendency for the equivalent moduli of the UCPWs to increase as the frictional coefficient increased in both the uniaxial and biaxial tensile tests.

References

[1] Y. Mahadik *, S.R. Hallett, Finite element modeling of tow geometry in 3D woven fabrics, Composites: Part A 41 (2010) 1192–1200.

[2] Tehrami-Dehkordi M, Nostray H. Tensile behavior simulation of woven fabric with different weave pattern based on finite element method. Journal of Textiles and

Polymers, 2015,3.

[3] J. J. Lin, “Applying GM to predicting elastic property and FEM to analyzing tensile damage behavior for woven fabric” J. Text. Inst., vol.105, pp. 1029-1041, 2014.

[4] Chen S, Ding X, Fangueiro R, Yi H, Ni J. Tensile behavior of PVC-coated woven membrane materials under uni- and bi-axial loads. J Appl Polym Sci2008,107:2038–44.

[5] H. Lin, A.C. Long, M. Sherburn, M. J. Clifford. Modelling of mechanical behaviour for woven fabrics under combined loading, International Journal of Material Forming, 2008.4:899–902.

[6]Manohar G. Kollegal, Srinivasan Sridharan.Strength prediction of plain woven fabrics, Journal of composite materials.2000,34(3):240-257.

[7] Wu J, Pan N. Grab and strip tensile strengths for woven fabrics: an experimental verification. Text Res J 2005,75:789-96.

[8] G. A. V. Leaf and K. H. Kandil, “The initial load-extension behaviour of plain woven fabrics”, J. Text. Inst., vol. 71, pp. 1-7,1980.

[9] Reinhardt HW. On the biaxial testing and strength of coated fabrics. Exp Mech 1976;16(2):71–4.

[10[Chen S, Ding X, Yi H. On the anisotropic tensile behaviors of flexible polyvinyl chloride-coated fabrics. Text Res J 2007;77(6):369–74.

[11] Zhang Y, Zhang Q, Ke L, Bei-lei K. Experimental analysis of tensile behaviours of polytrafluoroethylene-coated fabrics subjected to monotonous and cyclic loading.

Text Res J 2014;84(3):231–45.

[12] Majid Tehrani-Dehkordi and Hooshang Nosraty. Tensile behavior simulation of woven fabric with different weave Pattern based on finite element method. Journal of textiles and polymers, 3(1)2015.1,34-39.

[13] Tan VBC, Shim VPW, Zeng X. Modelling crimp in woven fabrics subjected to ballistic impact. Int J Impact Eng 2005,32:561–74.

[14] Ying Wang, Xiaogang Chen, Robert Young, Ian Kinloch. Finite element analysis of effect of inter-yarn friction on ballistic impact response of woven fabrics. Composite Structures 135 (2016) 8–16.

[15] Roy M. Broughton, Yehia El Mogahzy, D. M. Hall. Mechanism of Yarn Failure, textile research journal,1992, 62(3): 131-134.

[16] Youqi Wang , Yuyang Miao , Lejian Huang , Daniel Swenson , Chian-Fong Yen , Jian Yu , James . Zheng. Effect of the inter-fiber friction on fiber damage propagation and ballistic limit of 2-D woven fabrics under a fully confined boundary condition. International Journal of Impact Engineering 97 (2016) 66–78.

[17] Yanyan Chu, Shengnan Min, Xiaogang Chen. Numerical study of inter-yarn friction on the failure of fabrics upon ballistic impacts. Materials and Design 115 (2017) 299–316.

[18] A. Gasser, P. Boisse, S. Hanklar, Mechanical behavior of dry fabric reinforcement. 3D simulations versus biaxial tests, Comput. Mater. Sci. 17(1999) 7–20.

[19] Duan Y, Keefe M, Bogetti T, Cheeseman B. Modeling friction effects on the

ballistic impact behavior of a single-ply high-strength fabric. Int J Impact Eng 2005;31(8):996–1012.

[20] S. Gogineni , X. -L. Gao , N. V. David ,J. Q. Zheng, Ballistic Impact of Twaron CT709® Plain Weave Fabrics, Mechanics of Advanced Materials and Structures, 19:6, 441-452.

[21] C.T. Lim*, V.P.W. Shim, Y.H. Ng, Finite-element modeling of the ballistic impact of fabric armor, International Journal of Impact Engineering 28 (2003) 13–31.

[22] A. Gasser, P. Boisse, S. Hanklar, Mechanical behavior of dry fabric reinforcement. 3D simulations versus biaxial tests, Comput. Mater. Sci. 17(1999) 7–20.

[23] Hector López-Gálvez, Marcos Rodriguez-Millán ∗, Norberto Feito, Henar Miguelez . A method for inter-yarn friction coefficient calculation for plain wave of aramid fibers. Mechanics Research Communications 74 (2016) 52–56.

[24] Carvelli. V, Poggi. C. A homogenization procedure for the numerical analysis of woven fabric composites.Composites Part A: Applied Science and Manufacturing, 2001(32), 1425–1432.

[25] Łukasz Frącczak, Małgorzata Matusiak, Piotr Zgórniak. Investigation of the Friction Coefficient of Seersucker Woven Fabrics. FIBRES & TEXTILES in Eastern Europe 2019; 27, 3(135): 36-42.

Chapter 3

Chapter 4

Low-velocity impact behavior of Twaron® woven fabric

Chapter 4

Chapter 4: Low-velocity impact behavior of Twaron® woven fabric

4.1 Introduction

Woven fabrics comprising high-strength continuous filament yarns such as Twaron® are frequently used in protective items such as protective clothing for special industries, turbine engines for aircraft and spall liners in certain vehicles. For such applications, these textile structures are required to provide penetration resistance against incident high kinetic energy projectiles [1]. The penetration and perforation of targets by projectiles involve highly complex processes, which have been investigated experimentally for more than two centuries, and analytically largely during the last few decades [2-8].

By overviewing these related areas of research, different research approaches were used to investigate, analyze, and understand the ballistic impact behaviors and mechanisms of the different materials. Experimental approaches are a commonly used method to investigate the ballistic impact performance of different materials, and to characterize and obtain relevant data to optimize applications of the ballistic material [9-10]. Several researchers [11-14] have conducted studies to determine the damage modes, ballistic limit velocities, absorbed energies experimentally for penetration, specific perforation energy capacity and some structural responses of different targets after impact tests. In addition, analytical methods are one approach used to investigate and understand the ballistic impact mechanisms of different materials. Parga-Landa et al. [15] considered the fiber as a linear elastic fracture and the projectile as rigid. In

addition, the impact behavior of soft body amours, including the ballistic curve, impact force, tension of each target layer, and stress and strains of yarn and surface damage, could also be understood using analytical models. Recently, the ballistic impact behavior of two-dimensional woven fabric composites was investigated through an analytical formulation [16]. The empirical approach is another method, which mainly focuses on data from experimental work to investigate ballistic material impact responses and different failure mechanisms [17]. Empirical studies may be the most straightforward method but are often not sufficient in obtaining data due to a lack of necessary experimental means. Moreover, numerical modeling approaches, such as finite element analysis, are preferred and have been frequently implemented by researchers. Commercial packages, such as ABAQUS®, LSDYNA® and ANSYS® are effective at establishing projectile fabric simulation models and conduct the ballistic impact performance tests of the materials. Several researchers [18-23] determined such properties as energy absorption; failure modes; the influence of ply orientation, weave type, yarn mechanical and physical properties and boundary conditions on the penetration mechanism using numerical modeling methods. However, it must be noted that most existing impact research on soft body armor was focused on medium to high velocity (30 m/s–1000 m/s) low-mass projectiles. Research on low-velocity impacts on high-performance fabrics is almost nonexistent.

From an experimental perspective, in experiments using projectiles with low mass and low velocity (e.g., Hopkinson pressure bar or air gun tests), the impact energy is too slight to puncture the fabric, thus the fabric's failure point cannot be ascertained,

which greatly diminishes the value of the research. In addition, experiments using projectiles with high mass and low velocity (e.g., drop weight impact tests), the specimen is always difficult to fix precisely because of the fabric's flexibility, which results in inaccurate results. From a numerical analysis perspective, the CPU calculation time of low-velocity impacts may be as much as a dozen times longer than that for high-velocity impacts because the low-velocity impactor takes much longer to penetrate the fabric (which happens only if the impact energy is high enough) and the time step in the explicit schema is always much lower to ensure the calculation precision. Thus compared with studying high-velocity impacts, studying low-velocity impacts on soft body armor is more challenging. Nevertheless, the impact failure mechanism of ballistic fabrics under low-velocity impacts still requires study; it is crucial for engineering and developing ballistic fabrics with improved all-round impact resistance performance.

Therefore, the study of low-velocity drop weight impacts on high-performance fabric is carried out in this chapter. Of note, because it is very difficult to fully understand and describe the impact phenomenon in low-velocity impact situations, experimental and numerical approaches are simultaneously implemented. Specially treated specimens are designed to solve the boundary fixing problem in the experiments. Furthermore, in the numerical simulation, a physically based fabric model is designed according to fabric's geometry parameters, and the experimental set-up and dynamic mechanical properties are taken into consideration to clarify the rate-sensitive character of Twaron®. A huge calculation time is the cost of attempting to make a

breakthrough in the study of low-velocity impacts on soft body armor.

4.2 Low-velocity drop weight impact test

4.2.1 Experiment equipment

A 9250HV drop weight impact tester provided by INSTRON® is used in this research. It is a free-fall drop dart machine with changeable load cells allowing for a large measurement capacity. The impactor's height and weight are adjustable to facilitate obtaining different initial impact energies. The impactor head is hemispherical with a diameter of 12.7 mm. The impactor is made from 4340 steel for high rigidity. Fig.4-1(a) shows a general schematic of the drop weight machine. A data acquisition system, acceleration transducer and load cell connected to the impactor are applied to simultaneously record the force and deflection as they form the force–deflection (F–d) curve during the impact process. Velocity curves versus deflection are also obtained from the force–acceleration diagram. The minimum impactor height is 100 mm and minimum weight is 7.07 kg, including the tup and screw mass. The pneumatic brake system is monitored by a position sensor to prevent the impactor from making multiple impacts following the first impact with the test specimen. When impact experiment starts, the specimen is fixed by two metallic plates with a circular hole (70-mm diameter) in the center of each, and the device is driven by pneumatic system. Fig.4-1(b) shows the overhead view of the impactor and pneumatic clamp.

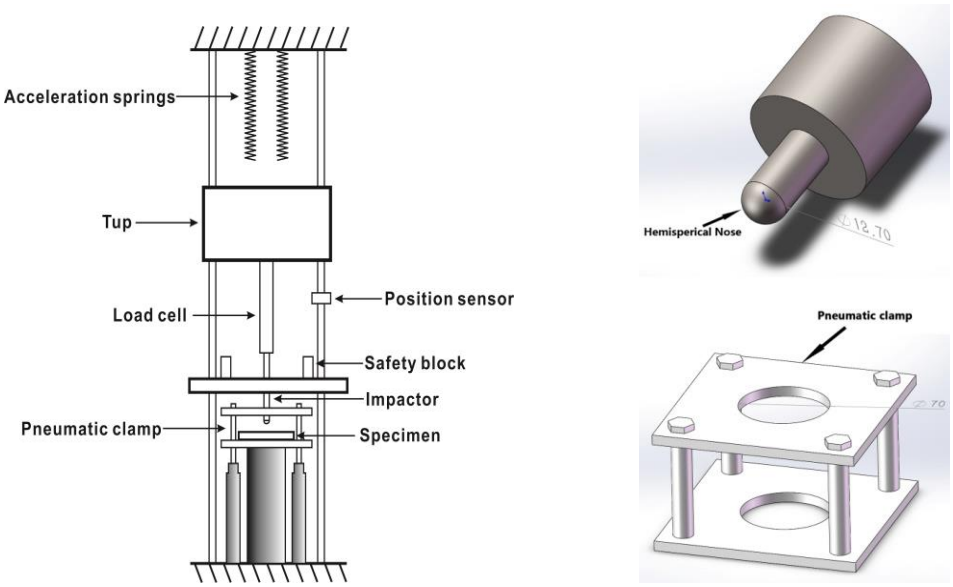

Fig. 4-1. Schematic of the 9250HV drop weight impact tester. (a) General view of the equipment (b) Overhead view of the impactor and pneumatic clamp

4.2.2 Experiment specimen preparation

The plain-woven fabric Twaron CT® made by TENJIN® is employed in this study. This fabric is manufactured using a plain weave of 110×110 yarns (per mm^2), with each yarn consisting of 500 filaments. The bulk density and linear density are 1.44 g/cm^3 and 550 dtex, respectively.

As mentioned in the Introduction, fabrics, unlike hard materials such as steel and composites, are too flexible and cannot be fixed precisely by pneumatic clamp during drop weight impact events. Hence, the specimens have to be specially treated before an impact experiment. In this work, the fabric was first cut to a small size with 100 mm × 100 mm, then sandwiched between two treated acrylic plates and bonded by super glue. The acrylic plate structure was cut by laser cutting machine to a size of 100 mm × 100 mm × 5 mm with a 70-mm diameter hole cut into the middle. The 70-mm diameter was selected because that is the same size as the circular hole of

pneumatic clamp. The surface of each acrylic plate was sanded to increasing adhesion before being bonded with the selected fabric. Specimens were rested for 24 h at room temperature before the experiments to ensure complete bonding. Fig.4- 2 shows a schematic of a specimen.

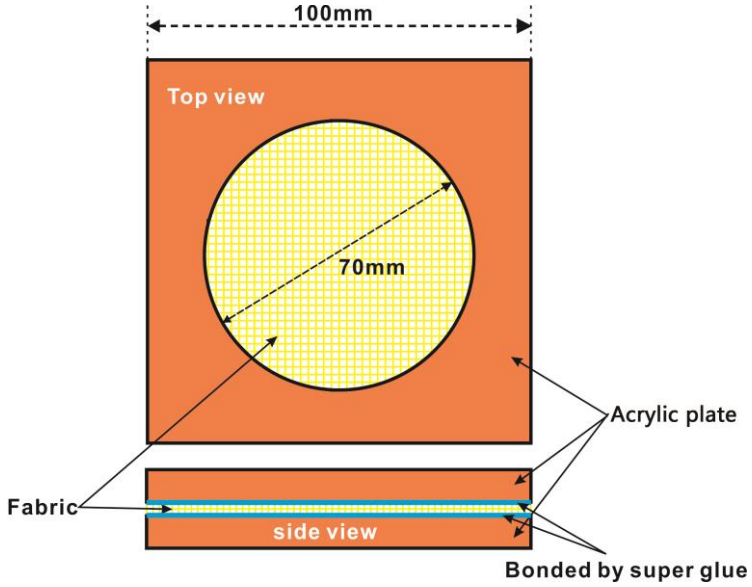

Fig. 4-2. Top and side view of a specially treated specimen

4.2.3 Low-velocity impact testing

First, the specimen is fixed to the tester by aligning the circular holes between specimen and the pneumatic clamp. The impactor weight is kept constant at the minimum value of 7.07 kg for all tests. Impact energies of 15, 20 and 30J is applied sequentially by adjusting the drop height. To avoid random errors and ensure repeatability, at least five specimens were tested repeatedly for each impact energy. Typical impact process proceeds as follows. The impactor drops freely from a certain height and its velocity increases to the intended impact velocity as it reaches the fabric. At that point, the fabric begins to deform, and it exerts an impact resistance force to the impactor. The impact resistance force increases before eventually reaching its

peak when the yarns in the fabric begin to break. Then, the fabric rapidly reaches complete failure, and at the moment of failure, the resistance force drops dramatically. Afterwards, only a small amount of friction force remains to prevent the impactor from reaching its residual velocity, then impact process ends.

4.3 Experiment results and discussion

4.3.1 Fabric failure mode

All three impact energies resulted in perforation of the respective specimens. Fig.4-3 shows photographs (front and back) of the sample at the 30-J impact energy. No pull-out phenomenon appeared in the fixed boundary area, which proved the successful design of the specimen. A roughly square impact hole is seen from front of the specimen, and the fractured yarn within the square area is at the back. Severe perforation failure is also obvious in the primary yarns (yarns in direct contact with the impactor during the impact process), although the secondary yarn (yarns not directly in contact with the impactor) hardly changes. Different impact energies result from different impact speeds and cause different degrees of strain rate impact tension. After impact, the ends of the fibers are fractured and are pulled apart. To further investigate the mechanical properties of the yarn, the fracture morphology of the fibers is observed under a digital microscope. Fig.4-4 shows the damage of the fiber tows under different impact energies. It is clear from the images that the fiber tows fibrillate around the region of failure, fibrils separate from one another before they break, and the fibers are no longer single strands. Fig.4-4 also shows the fiber

becoming thinner toward the tip, where it breaks. The fibers under lower impact energy (low strain-rate) result in more lengthy fibrils splitting axially, and fibers under higher impact energy (high strain-rate) exhibit fewer and shorter fibrils. In other words, the stain-rate has an obvious influence in fabric's failure mode. Thus, Twaron CT® yarns under high strain-rate impact show a more fragile character and yarns under lower stain-rate show a more viscous character.

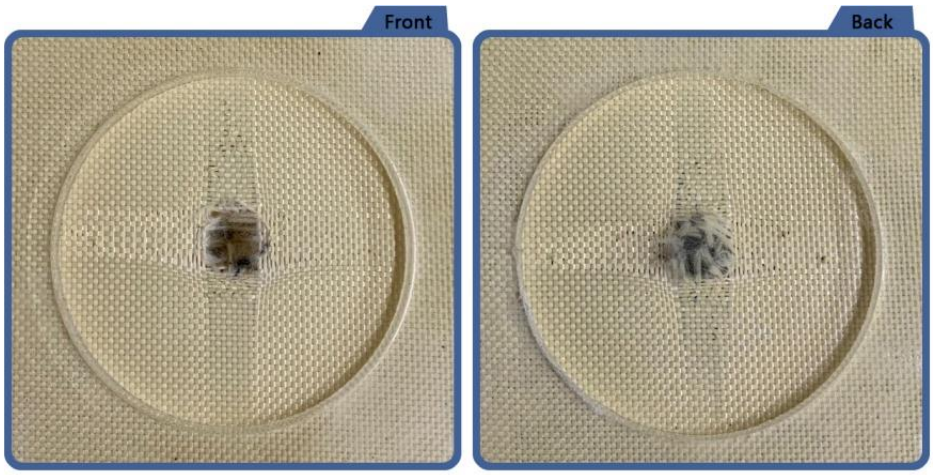

Fig.4-3. Photographs of impacted specimens (front and back)

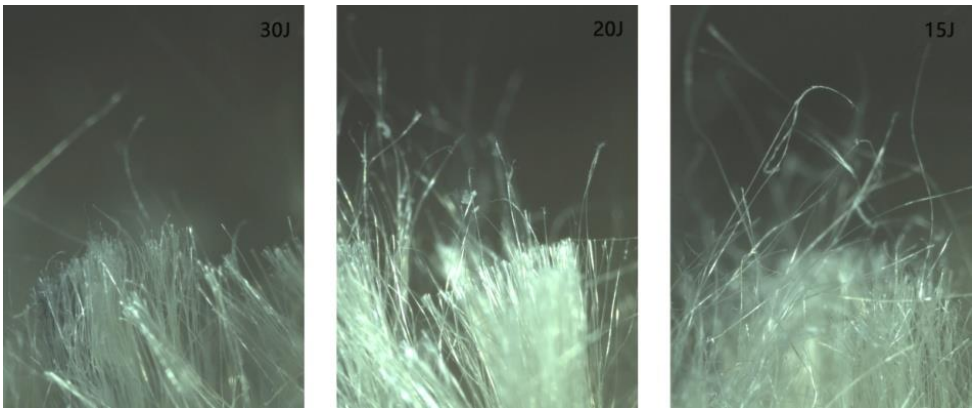

Fig. 4-4. Fractographs of Twaron fiber tow under different impact energies

4.3.2 Force-deflection and Force-time diagrams

Contact force is an important parameter in impact problems and is generally defined as the reaction force applied by specimen to the impactor. Commonly, contact force is

one index that reflects the material's ability to resist impact. Contact force is never measurable in high-velocity impact experiments because the sensor is difficult to attach to the impactor; however, it is able to be recorded in drop weight experiments because the sensor can be attached to the load cell. In addition, deflection is obtained from recording the vertical displacement of the impactor nose. Fig.4-5(a) shows a contact force–deflection (*F–d*) diagram under various impact energies. Similar curves are found as contact force increases until a certain deflection, at which time, a drastic fall in contact force is observed. The maximum force value increases with greater initial impact energy. Thus, the mean maximum contact force of the impactor during the 30-J impact event was as much as 1020 N, which is 9.4% and 25.1% greater than what is achieved during the 20-J and 15-J impact events, respectively. In addition, larger deflection at failure is discovered in greater initial impact energy scenarios. The mean deflection during the 30-J impact event is as much as 4.88 mm, which is 3.0% and 6.6% greater than what is achieved during the 20-J and 15-J impact events, respectively. This means that a greater initial impact energy results in a larger failure strain of the fabric. Furthermore, slightly greater stiffness is also found during a greater initial impact energy scenario, although the difference is not extreme. Fig.4-5(b) shows that the contact force exhibits the same trend as for the *F–d* plots, while a longer contact duration of fabric is found in lower energy impact scenarios. The mean contact duration is 1.67 ms, 1.99 ms and 2.21 ms in the 30-J, 20-J and 15-J impact events, respectively. The experimental results proved that strain rate obviously influences the mechanical properties of Twaron® fabric.

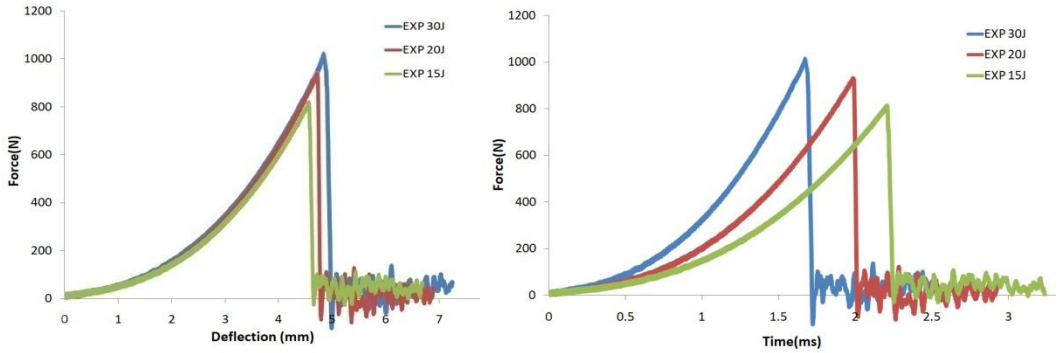

(a) (b)

Fig. 4-5. Variation in contact force during impact processes under different impact energies (a) *F-d* diagram (b) *F-t* diagram

4.3.3 Velocity-time and Deflection-time diagrams

Fig.4-6(a) shows velocity versus time at the 30-J impact energy level. Different from a typical high-speed impact, the maximum velocity during the impact process is not at the beginning of the impact event. When the impact event begins, the impactor still accelerates until the specimen's resistance force reaches the same level of the gravity as that of the impactor. The mean time consumed reaching maximum velocity for the 30-J, 20-J and 15-J impact events is 0.41 ms, 0.52 ms, and 0.63 ms, and results in deflections of 1.19 mm, 1.24 mm and 1.31 mm, respectively. After reaching the maximum velocity, owing to the extreme increase in the contact force, the velocity of the impactor drops obviously before the failure of the specimen. Afterwards, the velocity of impactor gradually increases again under the effect of gravity. Fig.4-6(b) shows the deflection with respect to time at various impact energies; the greater impact energy always results in a larger deflection at every second of the impact event; the curve of the lower impact energy event shows a greater degree of bending.

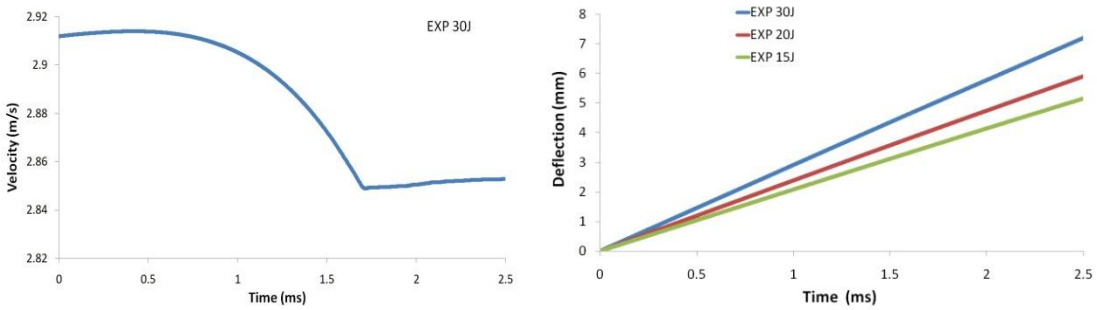

(a) (b)

Fig. 4-6 (a) *V-t* at a 30-J impact; (b) *D-t* at various impact energies

4.3.4 Energy absorption diagram

Fig.4-7 shows the energy absorption diagram for the *E–d* curve. The energy absorption curve is very similar to the contact force curve, showing a parabolic upward trend. At the fabric's moment of failure, the energy absorption value reaches the inflection point. The capacity remains almost stable except for a slight increase due to the effect of friction. Greater impact energy results in increased energy absorption with longer deflection of the projector within a shorter contact endurance time. The mean energy absorption in the 30-J impact event is 1.71 J, 18.8% and 39.0% greater than that achieved in the 20-J and 15-J impact events, respectively.

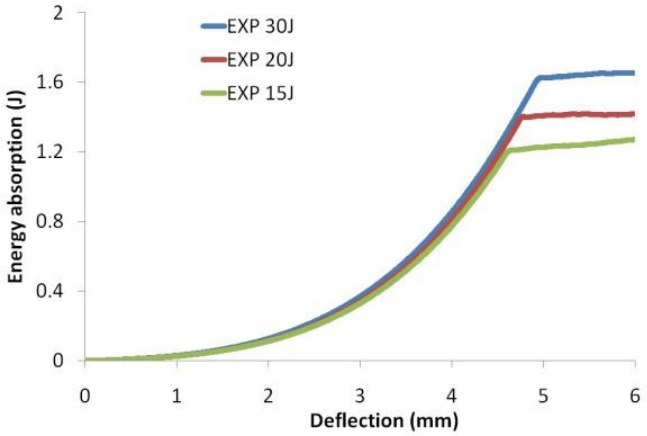

Fig. 4-7. Energy absorption diagram at various impact energies

As a reference, Table 4-1 presents the statistics results from 5 repeated impact experiments of mean values and standard deviations of maximum contact force(F_M),

contact duration time(T)and deflection(D)when the impactor reaches maximum contact force, as well as energy absorption(E) at different impact energy events, standard deviations are shown in brackets.

Table 4-1. Mean values and standard deviations of impact results at different impact energy events

	F_M (N)	T (ms)	D (mm)	E (J)
30J	1020(24.2)	1.67(0.02)	4.88(0.05)	1.71(0.5)
20J	932.4(18.9)	1.99(0.02)	4.74(0.04)	1.44(0.4)
15J	815.3(19.7)	2.21(0.03)	4.58(0.05)	1.23(0.4)

4.4 Simulating a low-velocity drop weight impact on a Twaron® fabric

4.4.1Modeling and boundary condition

A commercial explicit nonlinear FEA code, ANSYS®-AUTODYN, is employed for FE modeling of low-velocity drop weight impacts on a Twaron® fabric. In the present investigation, based on the fabric model created in chapter 2 and according to the nature of clamping employed in the experimental tests, the fabric target is clamped with a circular test field at the center, as shown in Fig.4-2. Therefore, the circumference of the fabric has to be fixed so the fabric model is designed and created to be circular with a diameter of 70 mm. Fig.4-8 shows the impact assembly model.

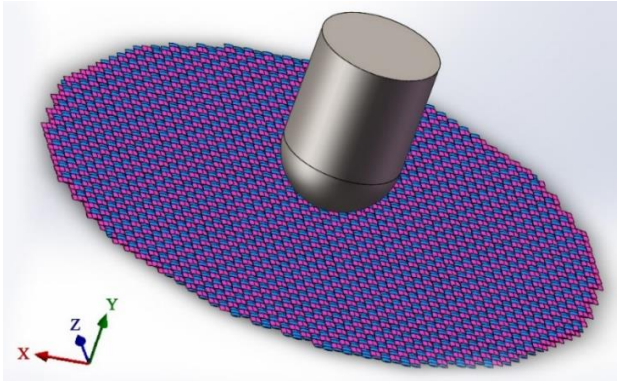

Fig. 4-8 Impact assembly model

To validate the model, in addition to geometrical parameters, the configuration of the material parameters for the simulation should also be consistent with the actual yarn properties. During the impact process, the impactor is regarded as a rigid body and impacts from the Y direction to the fabric, which is placed in the X–Z plane. All degrees of freedom of the impactor are restricted but it is allowed to move in the direction normal to the X–Z plane. The impact weight is 7.07 kg. The standard earth gravity is applied to the model, which is unlike a ballistic impact where the impactor's gravity can be neglected. A fixed boundary condition around the fabric circumference is employed to reflect the specimen clamping. A surface to surface contact algorithm is applied on the impactor/yarn and yarn/yarn contact in the FE model. Simple Coulomb friction is introduced between yarns and between the impactor and the fabric. A friction coefficient of 0.3, which is obtained from experiments on Twaron® fabrics in our former study [24], is used for yarn/yarn contact. The friction coefficient of impactor/yarn is set at 0.2 by following the model of Yanfei Yang et al. [25]. The density of the Twaron® yarn is set as 1440 kg/m ^{3}.

Mesh density has a significant effect on the impact results obtained in present study. Mesh sensitivity studies for various element sizes have suggested that it is appropriate that the cross-section of a primary yarn is meshed using 10 elements and 20 elements through the yarn wavelength as shown in Fig. 2-2(d) in chapter 2. Simulation result of impact on a straight single yarn indicated that the chosen mesh density was able to capture transverse wave responses of the impact event. To maintain calculation accuracy to the greatest extent possible and reduce the time consumption as much as

possible, a hybrid mesh technology is used in the model by applying refined mesh to the primary yarns and coarse mesh to the secondary yarns. Typically, the FE fabric model involves 154,620 eight-node solid brick elements. The typical calculation time in current research is 96h on average using an Inter xeon® 12 core CPU.

The damage progression is modeled using the general erosion criteria for solid elements. when the Lagrange processor is used within ANSYS®-Autodyn, an erosion material model can be used which enables the removal of highly distorted material elements from the computational domain to prevent excessive numerical complications. In this study, a maximum principal strain failure criterion is used for element erosion: that is, when $\varepsilon \geq \varepsilon_f$, the element is failure and removed from the calculation, where ε_f demonstrate the strain at yarn's failure. The determination of the value of ε_f will be discussed in subsequent text.

4.4.2 Dynamic mechanical properties of Twaron® fiber

4.4.2.1 Constitutive model

Twaron® fiber has a proven sensitivity to strain rate based on many experiments [26-28]. As with most polymers, Twaron® is viscoelastic, a significant property during impact problems. The present tests reaffirmed this characteristic because the results showed that the breaking load and fiber modulus as well as breaking elongation increased with strain rate even when the variation in the strain rate is not extreme.

A semi-empirical approach of a three-element system of two Hookean springs and a Newtonian dashpot, which represent elastic, solid and fluid-like behaviors, was

adopted to model the viscoelastic behavior of Twaron® by C.T. Lim et al. [29]. They reported that the model provided a reasonable representation of the deformation micro-mechanisms in Twaron fibers. The model can be seen in Fig.4-9. The stress–stain response of a three-element viscoelastic model can be described by:

$$\left(1+\frac{K_2}{K_1}\right)\sigma+\left(\frac{\mu}{K_2}\right)\dot{\sigma}=K_2\varepsilon+\mu\dot{\varepsilon} \quad (1)$$

where σ, ε and $\dot{\varepsilon}$ are the stress, strain and strain rate, respectively. For initial conditions of σ=0, ε=0and $\dot{\varepsilon}$=0, the explicit expressions of stress as a function of strain and strain rate are obtained as:

$$\sigma=\frac{k_1k_2}{k_1+k_2}\varepsilon-\frac{{k_1}^2\mu}{(k_1+k_2)^2}\dot{\varepsilon}\left(e^{-\left[{(K_1+K_2)}/{\mu}\right]\varepsilon/\dot{\varepsilon}}-1\right) \quad (2)$$

and

$$\frac{d\sigma}{d\varepsilon}=\frac{k_1k_2}{k_1+k_2}+\frac{{k_1}^2}{k_1+k_2}\left(e^{-\left[{(K_1+K_2)}/{\mu}\right]\varepsilon/\dot{\varepsilon}}\right) \quad (3)$$

It is apparent from Eq. (3) that stiffness of Twaron® is a function of strain rate with parameters K_1, K_2 and μ. V.B.C. Tan et al. [30] obtained the dynamic mechanical parameters of Twaron® CT716 by conducing dynamic tests in a split Hopkinson pressure bar setup. When the aforementioned three-element model was also implemented, by taking values of K_1=116.67 GPa, K_2=203.3 GPa, μ=4.35Mpa.s, it was found that the results obtained correlate reasonably well with the dynamic properties of Twaron® obtained experimentally. These mechanical parameters of Twaron® CT716 are considered to be the same as CT612 because they are manufactured with the same fiber type of Twaron 2040.

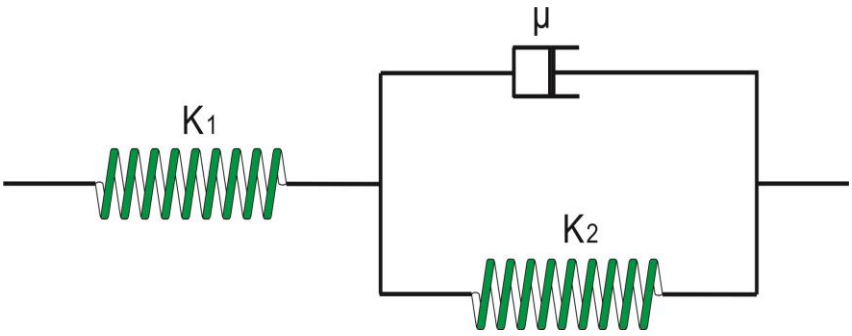

Fig. 4-9. Three-element spring-dashpot model

To represent strain rate dependent elastic behavior, the constitutive model is incorporated in the current FE yarns model and the material model is implemented in terms of a history dependent stiffness given by

$$k = k_\infty + (k_0 - k_\infty)e^{-\alpha t} \quad (4)$$

where k_∞, k_0 and α is the long-term stiffness, instantaneous stiffness and the decay constant respectively. The parameters in above equations can be related by

$$k_\infty = \frac{k_1 k_2}{k_1 + k_2}\ ,\ k_0 = k_1\ ,\ \alpha = \frac{k_1 + k_2}{\mu} \quad (5)$$

In FE analysis, stiffness K of an element can be represented by Young's modulus E, then we have

$$E_\infty = \frac{E_1 E_2}{E_1 + E_2}\ E_0 = E_1\ \alpha = \frac{E_1 + E_2}{\mu} \quad (6)$$

In ANSYS®-AUTODYN, viscoelastic behavior is introduced via an instantaneous shear modulus G_0 and a viscoelastic decay constant β, according to the well-known relationships between shear modulus G and Young's modulus E shown in Eq. (7), we can obtain the model parameters though the Eq. (8) shown below.

$$G = \frac{E}{2(1+\nu)} \quad (7)$$

$$G_\infty = \frac{G_1 G_2}{G_1+G_2} \quad G_0 = G_1 \quad \beta = \frac{G_1+G_2}{\mu} \tag{8}$$

4.4.2.2 Failure strain

As observed in the impact experiments that there is an increase in the failure strain of Twaron® as the strain rate increases, therefore, dynamic parameters must be assigned to the model when simulating different impact energies applied. According to experiment results, V.B.C. Tan et al. [30] also put forward linear prediction equation between failure stain and stain rate for Twaron®, Therefore, as long as the strain rate of drop weight impact is known, the value of failure strain can be obtained by referring to the equation. Thus, the question arises of how to measure the strain rates during drop weight impact events at different impact velocities.

During the impact scenario in present study, a method of approximately calculating the stain rate is proposed. To simplify the impact problem, the fabric is depicted as a single yarn. A hemisphere-head impactor impacts a single yarn of $2L_0$ in length, which has its two ends fixed with an impact velocity of V_0 at T=0. Suppose a very small amount of time Δt passes. (The time is long enough for the yarn to decrimp and become completely stretched but not long enough for the impactor to penetrate the yarn.) The impactor travels distance D and its velocity is reduced to V_1 while the yarn is stretched and deformed. The velocity of the impactor is assumed to decreases linearly with time. Details are depicted in Fig.4-10. R, C and $\dot{\varepsilon}$ denote the radius of the impactor's hemisphere-head, the fabric's decrimp rate and the stain rate, respectively. We then have following equations.

$$L = L_0(1 + C) = L_1 + L_2, \quad (9)$$

$$L_2 = \theta\pi R/180, \quad (10)$$

$$\theta = \tan^{-1} D/L_0, \quad (11)$$

$$\varepsilon = (\frac{D}{\sin\theta} - L)/L, \quad (12)$$

$$\Delta t = 2D/(V_0 + V_1), \quad (13)$$

$$\dot{\varepsilon}=\varepsilon/\Delta t. \quad (14)$$

To be able to compare this with the experiment, the aforementioned parameters are drawn based on three experimental impact energy scenarios. The Twaron® CT612 fabric's decrimp rate is calculated to be 0.78% based on our previous tensile test, V_1 is considered to be the impactor's velocity at the fabric's moment of failure, and the strain rate is calculated to be 22.8 s^{-1}, 18.2 s^{-1} and 15.4 s^{-1} for the impact energies of 30 J, 20 J and 15 J, respectively. Furthermore, the linear fitting equation (R^2 = 0.997) of strain rate $\dot{\varepsilon}$ and initial impact velocity V_0 during a low-speed drop weight impact can be described by

$$\dot{\varepsilon} = 1.725{V_0}^2 + 8.214 \quad (15)$$

Therefore, by following V.B.C. Tan's prediction data, the values of ε_f are calculated to be 0.0325, 0.0314 and 0.0308 for the impact energies of 30 J, 20 J and 15 J, respectively.

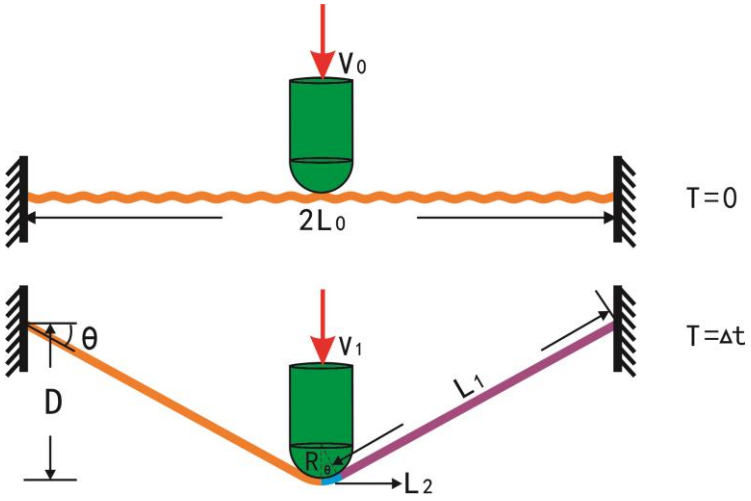

Fig. 4-10. Schematic of a single yarn during a drop weight impact event

4.5 Numerical simulation results and discussion

4.5.1 Validation of the numerical results

In Figs. 4-11, 4-12 and 4-13, the *F–d* curve, *V–t* curve and energy absorption obtained in the experiment and numerical simulation at three impact energies are compared. It can be concluded from the figures that remarkably close agreement is obtained between the simulations and experiments at various impact scenarios. The obvious discrepancies are as follow. In the *F–d* curves, the contact forces increase smoothly in the experimental results while there are slight fluctuations continuously in the simulation results; in the *V–t* curves, the maximum velocities and residual velocities of the impactor in the experiments are slightly smaller than what is demonstrated in the simulations; and the energy absorption in the experiments is slightly higher than that in the simulations of the energy absorption comparison figures.

The discrepancies between the numerical simulation and experimental results can be interpreted as follows: the fabric circumference is perfectly fixed in the simulation

process, but a perfect fit cannot be attained in the actual experiment. In addition, yarns outside the circular target area are also more or less involved in the impact process in the experimental conditions. Therefore, first, owing to the perfectly fixed boundary and small specimen radius in the simulation, the transverse wave produced by the impact continuously bounces back from the fixed boundary to the center of the impact, resulting in slight fluctuation in the contact force. In the experiment, however, the transverse wave is partly absorbed by the clamp setup. Second, because some yarns outside the circular target area are involved in the impact process during the experiment, the energy absorption capacity of the fabric is improved to some extent, thus reducing the residual velocity accordingly. As a result, the impactor's maximum velocity in the simulation is slightly higher during front section of impact event than that in the experiment. However, from an overall point of view, the numerical results show negligible discrepancies with experiment results.

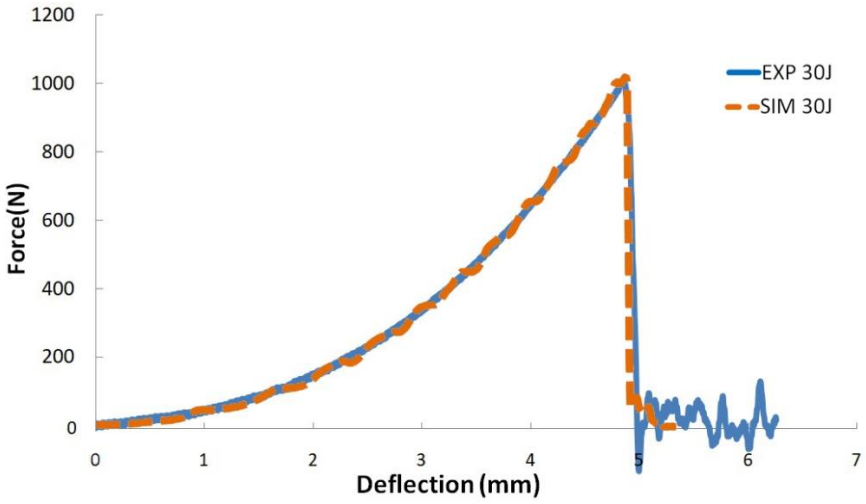

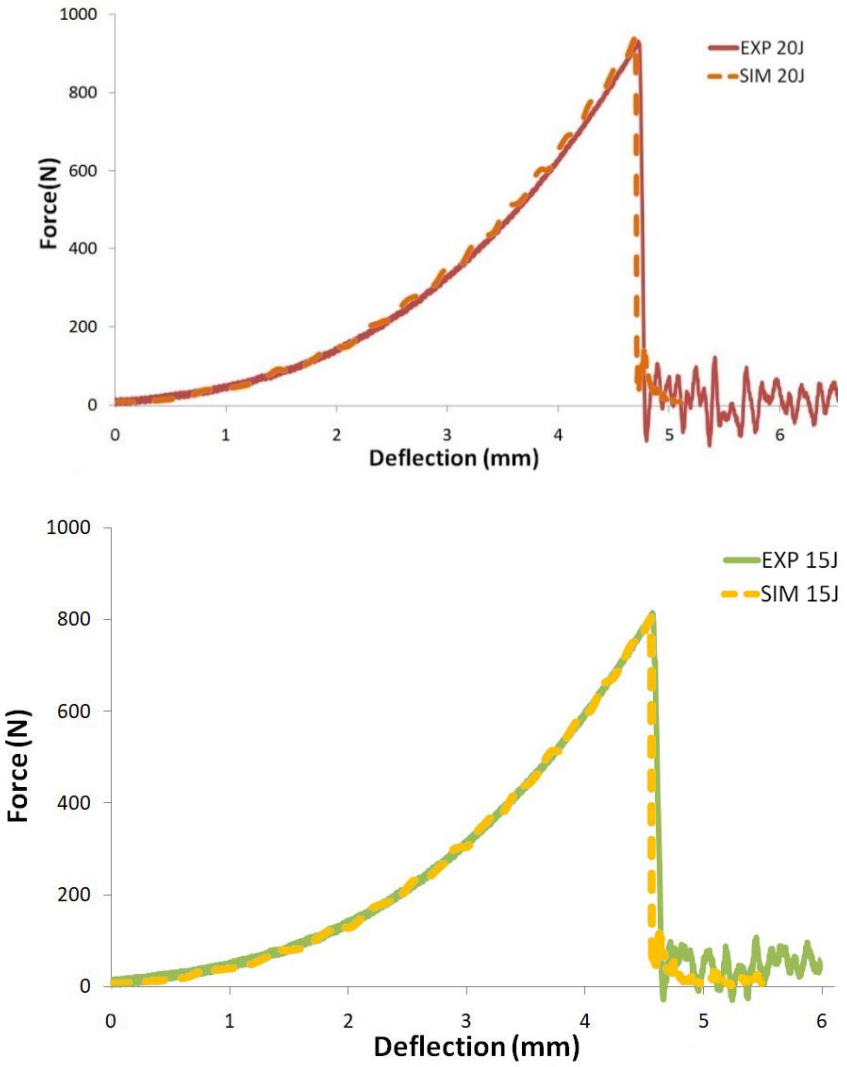

Fig. 4-11. Comparison of numerical and experimental *F-d* results at various impact energies

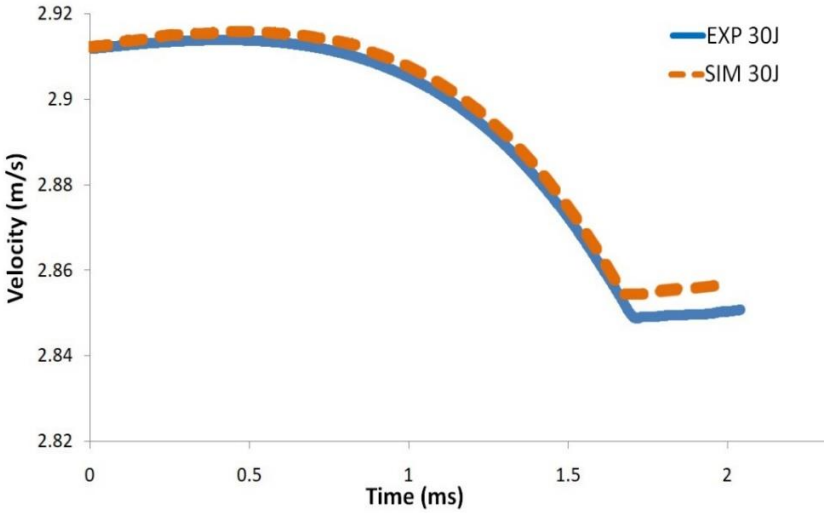

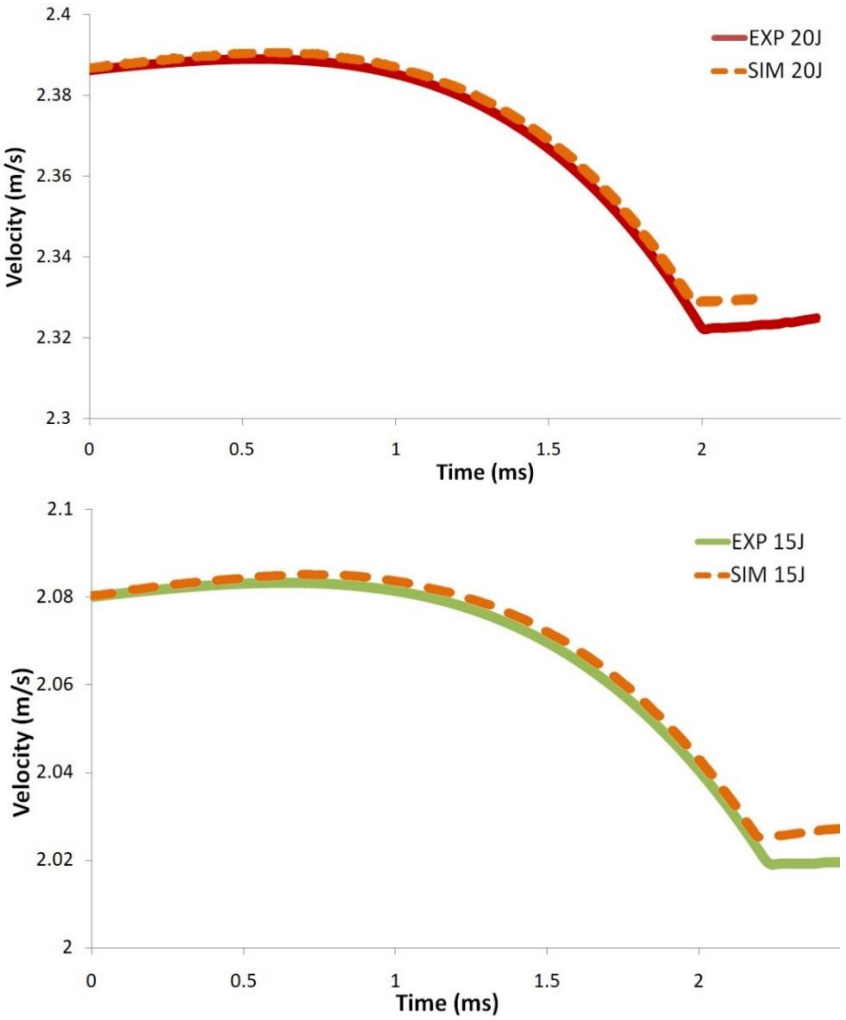

Fig. 4-12. Comparison of numerical and experimental *V-t* results at various impact energies

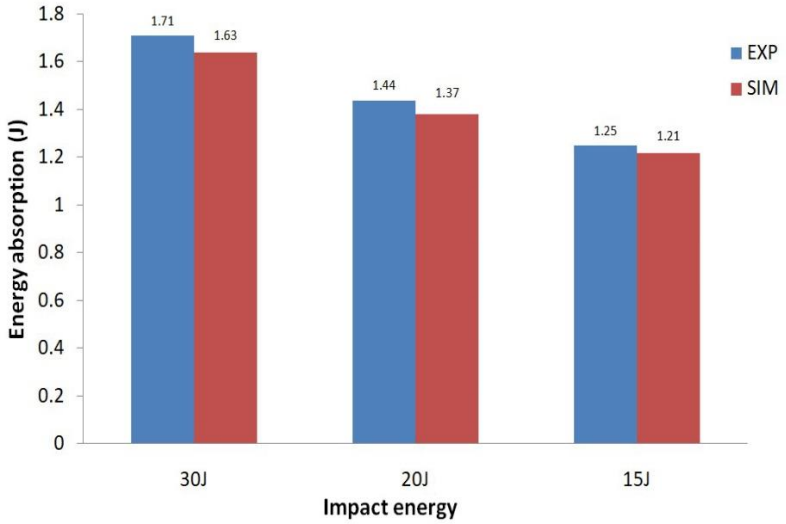

Fig. 4-13. Comparison of numerical and experimental energy absorption at different impact energies

4.5.2 Further numerical investigation

4.5.2.1 Stress distribution

The impact response of the fabric is dominated by the propagation of two types of waves. The transverse wave causes the fabric's deflection in the primary yarns and the longitudinal wave generates stress waves in the material that propagate at the sound speed of the material down the axis of the yarns. As reported by many researchers like McCrackin FL et al. [31], the longitudinal stress wave speed on a free yarn c depends on both the yarn's tensile elastic modulus E and the volumetric density ρ, according to the following expression:

$$c = (E/\rho)^{1/2}. \quad (16)$$

Roylance et al. [32] determined the yarn strain at the impact point in the case of a transverse impact on a very long straight yarn, ε, as a function of the yarn's tensile elastic modulus E, volumetric density ρ, and the impact velocity V based on:

$$2\varepsilon\sqrt{\varepsilon(\varepsilon+1)}\text{-}\varepsilon^2 = \frac{\rho V^2}{E}, \quad (17)$$

The transverse wave which propagates away from the impact point at a relatively lower speed and the speed u is given by:

$$u = c\sqrt{\varepsilon/1+\varepsilon}\ . \quad (18)$$

Ahead of the transverse wave front but behind the longitudinal wave front, yarn material moves longitudinally toward the impact point while behind the transverse wave front, yarn material moves transversely in the impact direction. And the

transverse deflection proceeds until the stress at the impact point reaches a breaking stress.

Theoretically, the longitudinal stress wave speed of a Twaron® straight yarn (when assumed to be linearly elastic material with Yang's modulus 75Gpa) c is calculated to be 7216.9m/s approximately. On the other hand, according to Eqs (17) and (18), transverse wave speed u is directly affected by impact velocity, and it is calculated to be 36.6m/s approximately in 30-J impact scenario in theory. Due to the fact that the time for the longitudinal wave to propagate from the center of the specimen to the boundary is very short (about a few microseconds) in comparison to the response of milliseconds, for a low-velocity impact event, variation in stress distribution is mainly affected by transverse wave.

Fig.4-14 shows the variation in the Von-Mises stress distribution contours of fabrics undergoing different impact energies at 0.5 ms, 0.8 ms, 1.2 ms and 1.5 ms. The primary yarns appear darker because of the application of finer mesh. The figures clearly demonstrate the variation process of stress distribution. In the initial stage of impact, the overall stress is at a low level due to yarns' decrimp effect. When the longitudinal wave reaches the clamped boundary, it is reflected back and the strain magnitude will be doubled, and the stress first begins to propagate in the two central primary yarns which are perpendicular to each other, then gradually spreads to all primary yarns as the contact area of fabric-impactor increases. As the impact continued, interaction between yarns at crossovers causes secondary yarns to involve moving transversely, during this stage the stress propagates to all the secondary yarns.

The magnitude gradient of stress also simultaneously appears according to the propagation sequence. In the meantime, during the impact process, owing to the influence of the transverse wave, transverse deflection with a square base occurs. Accordingly, a square stressed area, with its two diagonals coinciding with the warp and weft directions, also propagates to become larger and larger until it overlaps with the aforementioned stressed area. Because of the relatively lower speed of the transverse wave, the propagation speed of the square stressed area is also lower. Fig.4-14 also shows that under the same impact moment before fabric's failure, a wider stressed area and a greater maximum stress can be found in the higher impact energy event. This coincides with the results of the *F-t* and *E-t* diagrams. In addition, Fig.4-15 reveals variation in the Von-Mises stress distribution contours of the fabric at different impact energies during impactor deflections of 2 mm, 3 mm and 4 mm. Local parts are magnified for a clearer view because the differences are not obvious. Similarly, it shows that under the same deflection before fabric failure, a wider stressed area and larger maximum stress can be found in the higher impact energy event. This also coincides with the results of the *F-d* and *E-d* diagrams.

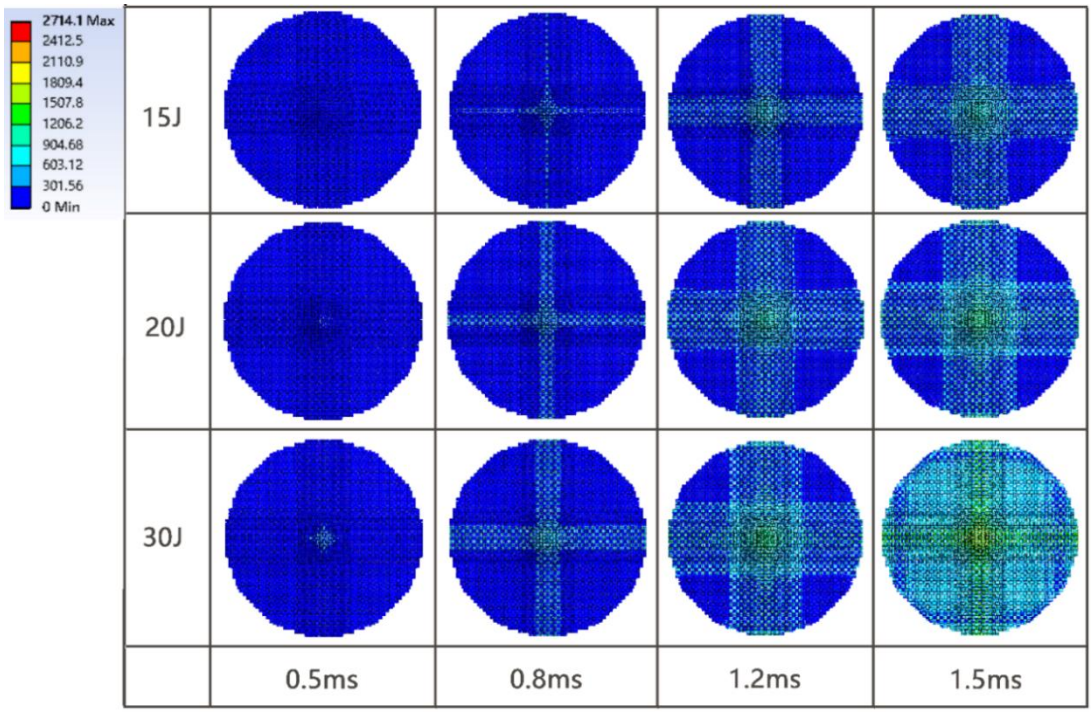

Fig. 4-14. Variation in the Von-Mises stress distribution contours at different moments

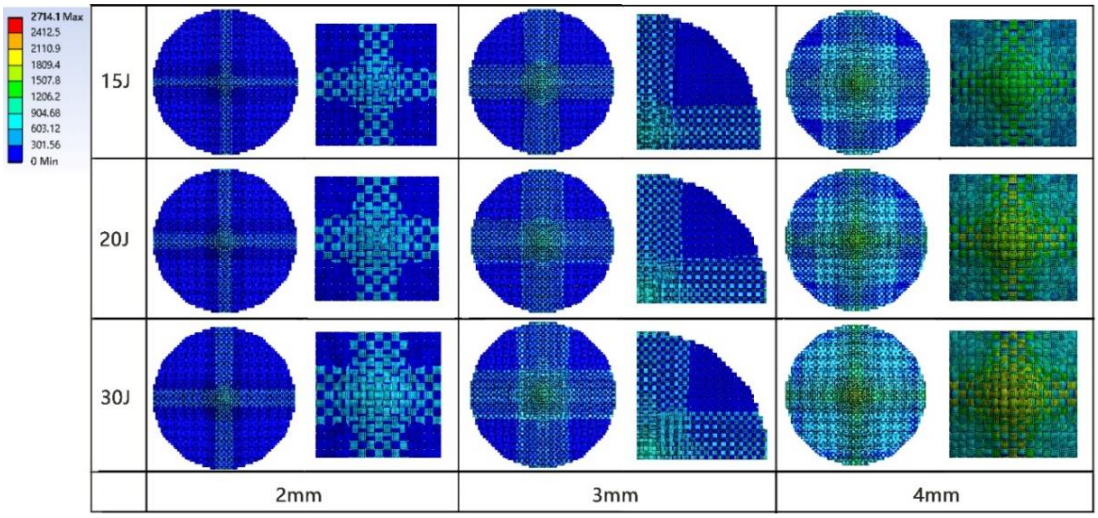

Fig. 4-15. Variation in the Von-Mises stress distribution contours at different deflections

4.5.2.2 Further investigation of energy absorption mechanism

Different for ballistic impacts, the total energy of the drop weight impact system continues to increase due to the effect of gravity, which cannot be neglected and is thus taken into consideration in the current research. Because the velocity of the

impactor first increases then decreases during the impact event, before reaching maximum velocity, the impactor's kinetic energy loss (ΔE_P) is negative. At this stage, gravitational potential energy (E_G) plays a major role in the energy absorption. When the velocity of the impactor begins to decline, kinetic energy loss become the main source of the fabric's energy absorption gradually.

As in the numerical simulation process, the elements erode and are removed from the calculation while reaching their failure criteria, and this causes the energy loss of the impact system after the fabric's failure. The energy absorption is only investigated from the beginning of the impact to the moment of fabric's failure. Until the fabric's failure, the total energy absorption, which comprises lost projectile kinetic energy and the impactor's gravitational potential energy, is absorbed by the fabric through the mechanisms of yarn strain energy (E_S), yarn kinetic energy (E_K) and frictional sliding dissipated energy (E_F). If the impactor's mass, standard earth gravity, impactor's deflection, initial velocity, and residual velocity are denoted by m, g, d, v_i and v_r respectively, then we have following equations:

$$E_G = mgd \tag{20}$$

$$\Delta E_P = \frac{1}{2}mv_i^2 - \frac{1}{2}mv_r^2 \tag{21}$$

$$\Delta E_P + E_G = E_S + E_K + E_F \tag{22}$$

The energy transfer as a function of time during the 30-J impact just before the fabric's moment of failure is depicted in Fig.4-16. It is obvious that when the fabric experiences a drop weight impact, the yarn strain energy demonstrates an absolutely

dominant energy absorption mechanism. The strain energy accounts for 96.1% of the total absorbed energy on average. The frictional sliding dissipated energy accounts for 3.7% and the yarn kinetic energy only accounts for 0.2% of the total absorbed energy on average. Fig.4-17 shows a schematic of the fabric's kinetic energy variation history at various impact energy scenarios. Owing to the influence of the transverse wave bouncing back from the clamped boundary, the kinetic energy of yarn fluctuates at very low levels until the moment of failure. It then rises dramatically as a result of the sharp fall of the yarn strain energy. Greater impact energy results in more significant kinetic energy fluctuation. The energy absorption of primary yarns is also investigated in current research. Fig.4-18 shows the average energy absorption ratios of primary yarns in kinetic energy, strain energy and frictional sliding dissipated energy under various impact energy events. The primary yarns play an important role in energy absorption during the impact process because all energy absorption ratios are higher than 75% under various impact energies. There is no obvious effect of impact energy on the energy absorption ratios of the primary yarns.

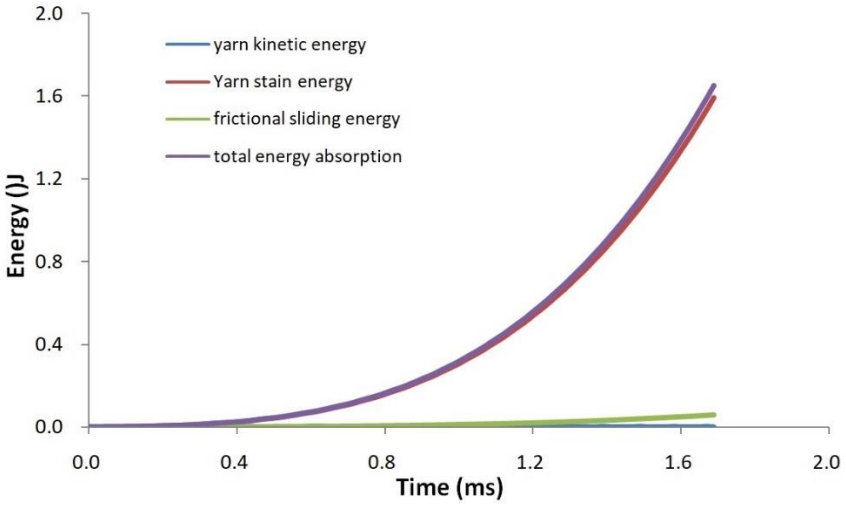

Fig. 4-16. Energy transfer as a function of time in the 30-J impact

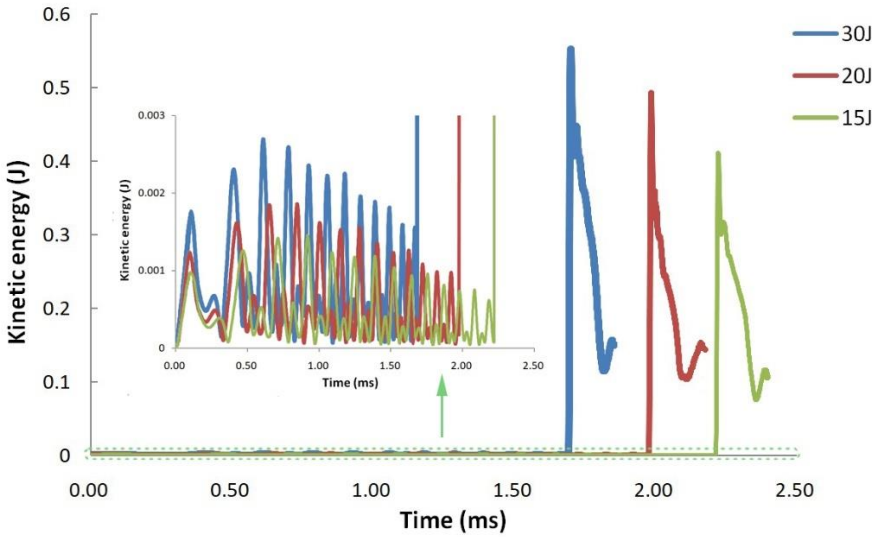

Fig.4-17. Schematic of the fabric's kinetic energy variation history in various impact energy scenarios

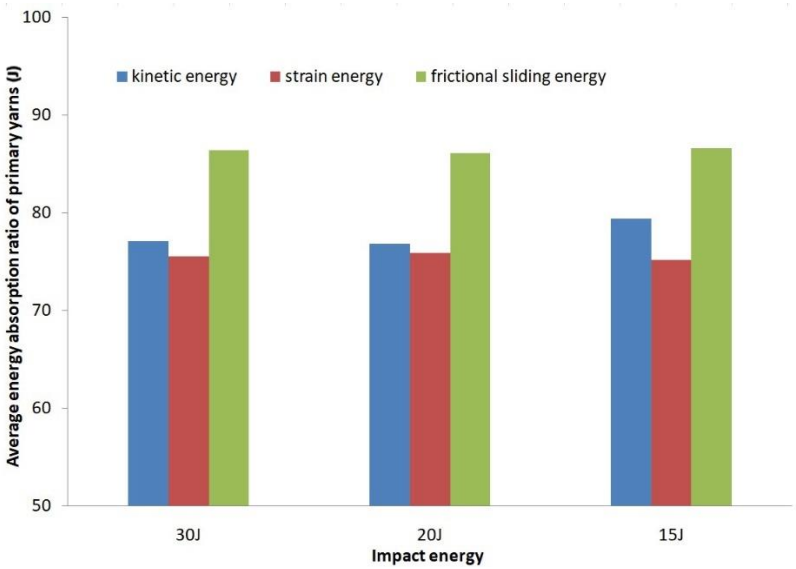

Fig. 4-18. Average energy absorption ratio of primary yarns in various impact energy scenarios

4.5.2.3 Influence of specimen shape and size

To determine whether there is an influence of specimen shape and size, two groups of specimens are compared in the present research. Four models of Twaron® woven fabric are prepared, a square model of 70 mm × 70 mm and three circular models with diameters of 54.5 mm (small), 70 mm (medium) and 84.5 mm (large). An impact energy of 30-J was implemented while all boundary conditions and parameters are

maintained at the aforementioned. The impact results are shown in Tables4-2 and 4-3, where V_R is the residual velocity; F_M is the maximum contact force; E is the energy absorbed by yarn, and T and D are the contact duration and deflection when the impactor reaches maximum contact force.

From Table 4-2 we can see that the impact results show hardly any difference in residual velocity and energy absorption between the two specimen shapes while an obvious difference in impactor's deflection occurs. Although the two specimens have primary yarns of the same size, the square specimen has a larger area than the circular specimen. In other words, the square specimen has a longer average distance from impact center to the fixed end. For this reason, the square specimen has a longer contact duration than the circular specimen, which results in a longer contact time and greater deflection. A longer contact duration contributes to improving the energy absorption ability, however smaller contact force will in turn reduces the energy absorption ability for square specimen, and finally the impact of two specimen shapes results in almost the same level of energy absorption and residual velocity.

As shown in Table4-3, because larger specimens have longer primary yarns, the tendency for larger specimens to have stronger impact resistance is clearly demonstrated. Larger specimens show not only better contact duration but also greater contact force; both of which contribute to improving the energy absorption ability and leading to lowering the impactor's residual velocity. However, results from specimens larger or smaller than what were tested in the present study still need further investigation.

Table 4-2. Results comparison of two shapes of specimens at a 30-J impact

V_R(m/s)		F_M(N)		E(J)		T(ms)		D(mm)	
circular	square	circular	square	circular	square	circular	square	circular	square
2.858	2.858	1018.5	1024.7	1.641	1.646	1.68	1.73	4.87	4.98

Table 4-3. Results comparison of three diameters of circular specimens at a 30-J impact

V_R(m/s)			F_M(N)			E(J)			T(ms)			D(mm)		
S	M	L	S	M	L	S	M	L	S	M	L	S	M	L
2.873	2.858	2.847	940.2	1018.5	1051.4	1.181	1.641	1.930	1.22	1.68	2.07	3.53	4.87	6.02

4.6 Conclusions

In this chapter, a low-velocity drop weight impact experiment on a single layer plain-woven Twaron® CT612 at impact energies of 15, 20 and 30 J was carried out using a 9250HV drop weight impact tester. In addition, the commercial code ANSYS®-AUTODYN was employed for impact simulation on a physically based impact model which was designed and created according to the fabric's geometry parameters and experimental set-up. This paper suggests the following findings:

- The Specially treated specimens were proved successfully designed by experiment results to deal with the inability of boundaries to be perfectly fixed in the equipment because of the flexibility of fabric.

- *F-t, F-d, V-t, D-t, E-d* curves of low-velocity impact on Twaron® fabric at impact energies of 15, 20 and 30 J were depicted firstly in this paper. Experimental results confirmed that the mechanical properties of Twaron® fabric were obviously influenced by strain rate.

- A method of approximately calculating the stain rate for Low-velocity drop weight impact were proposed, based on the method, the values of failure strain ε_f

are obtained.

- Dynamic mechanical parameters of Twaron® yarn was analyzed with three-element spring-dashpot model to describe the rate-sensitive Twaron® material. Furthermore, standard earth gravity is applied to the impact model to reflect the impact process realistically. Remarkably agreement was found between FE simulation results with experiments at various impact scenarios.

- Von-Mises stress distribution contours of the fabric experiencing different impact energies during the dynamic impact process are depicted and clarified. Results showed no matter under the same impact moment or under the same deflection before fabric failure, a wider stressed area and a greater maximum stress can be found in the higher impact energy event.

- The energy absorption mechanisms analysis indicated that yarn strain energy demonstrated an absolute dominant energy absorption mechanism when the fabric experiences a drop weight impact, and the analysis results show there was no obvious effect of impact energy on the energy absorption ratios in various impact energy scenarios.

- The influence of specimen shape and size were also numerically investigated systemically with a reasonable result. The size of primary yarns evidently affected the energy absorption ability of the fabric during impact event. These results indicated that the present experimental set-up and the developed fabric geometry model were effective for investigating many more mechanical problems

in textile fabrics and/or flexible material structures.

References

[1] Mulat Alubel Abtew, François Boussu, Pascal Bruniaux, Carmen Loghin, Irina Cristian. Ballistic impact mechanisms – A review on textiles and fibre-reinforced composites impact responses. Composite Structures 223 (2019) 110966.

[2] T.G. Montgomery, P.L. Grady, C. Tomasino. The Effects of Projectile Geometry on the Performance of Ballistic Fabrics. Text Res J, 52 (1982), pp. 442-450.

[3] B.J. Briscoe, F. Motamedi. Role of interfacial friction and lubrication in yarn and fabric mechanics. Text Res J, 60 (1990), pp. 697-708.

[4] B.Parga-Landa, F.Hernández-Olivares. An analytical model to predict impact behaviour of soft armours. Int J Impact Eng 1995,16(3):455–466.

[5] V.B.C.Tan, V.P.W.Shim, X.Zeng. Modelling crimp in woven fabrics subjected to ballistic impact. Int J Impact Eng 2005;32(1-4):561–574.

[6] C.Y.Tham, V.B.C.Tan, HP.Lee. Ballistic impact of a KEVLAR® helmet: Experiment and simulations. Int J Impact Eng 2008;35(5):304–318.

[7] DejuZhu, AdityaVaidya, BarzinMobasher, Subramaniam D.Rajan. Finite element modeling of ballistic impact on multi-layer Kevlar 49 fabrics. Compos Part B Eng. 2014(56):254-262.

[8] Piotr Kędzierski, Arkadiusz Popławski, Roman Gieleta, Andrzej Morka, Grzegorz Sławiński. Experimental and numerical investigation of fabric impact behavior. Compos Part B Eng. 2015(69):452-459.

[9] Karahan M, Jabbar A, Karahan N. Ballistic impact behavior of the aramid and

ultra-high molecular weight polyethylene composites. J Reinf Plast Compos 2015;34(1):37–48.

[10] Mudric T, Giacomuzzo C, Francesconi A, Galvanetto U. Experimental investigation of the ballistic response of composite panels coupled with a self-healing polymeric layer. J Aerosp Eng 2016;29(6):04016047.

[11] Almohandes AA, Abdel-Kader MS, Eleiche AM. Experimental investigation of the ballistic resistance of steel-fiberglass reinforced polyester laminated plates. Compos Part B Eng 1996;27(5):447–58.

[12] Yungwirth CJ, Radford DD, Aronson M, Wadley HNG. Experiment assessment of the ballistic response of composite pyramidal lattice truss structures. Compos Part B Eng. 2008; 39(3):556–69.

[13] Mudric T, Giacomuzzo C, Francesconi A, Galvanetto U. Experimental investigation of the ballistic response of composite panels coupled with a self-healing polymeric layer. J Aerosp Eng 2016; 29(6):04016047.

[14] Hassanpour Roudbeneh F, Liaghat G, Sabouri H, Hadavinia H. Experimental investigation of impact loading on honeycomb sandwich panels filled with foam. Int J Crashworthiness 2018;8265:1–12.

[15] Parga-Landa B, Hernández-Olivares F. An analytical model to predict impact behaviour of soft armours. Int J Impact Eng 1995;16(3):455–66.

[16] Naik NK, Shrirao P, Reddy BCK. Ballistic impact behaviour of woven fabric composites: formulation. Int J Impact Eng 2006; 32(9):1521–52.

[17] Yanfei Yang，Xiaogang Chen.Study of energy absorption and failure modes of

constituent layers in body armour panels. Compos Part B Eng. 2016; 98(1):250–259.

[18] Xiaogang Chen, YiZhou, GarryWells. Numerical and experimental investigations into ballistic performance of hybrid fabric panels. Compos Part B Eng. 2014; 58(3):35–42.

[19] YingWang, Xiaogang Chen, Robert Young, Ian Kinloch. A numerical and experimental analysis of the influence of crimp on ballistic impact response of woven fabrics. Composite Structures. 140(2016)44-52.

[20] Emre Palta, Howie Fang. On a multi-scale finite element model for evaluating ballistic performance of multi-ply woven fabrics. Composite Structures.207(2019)488-580.

[21] V.P.W Shim, Y.B. Guo, V.B.C.Tan. Response of woven and laminated high-strength fabric to oblique impact. Int J Impact Eng.48(2012)87-97.

[22] Y.Duan, M.Keefe, T.A.Bogetti, B.A.Cheeseman. Modeling the role of friction during ballistic impact of a high-strength plain-weave fabric. Composite Structures. 2016.68(3)331-337.

[23] Cuong Ha-Minh, Abdellatif Imad, François Boussu, Toufik Kanit, David Crépin.Numerical study on the effects of yarn mechanical transverse properties on the ballistic impact behaviour of textile fabric. The Journal of Strain Analysis for Engineering Design.2012.47(7)524-534.

[24] Canyi Huang, Lina Cui, Hong Xia, Yiping Qiu, Qing-Qing Ni. Influence of crimp and inter-yarn friction on the mechanical properties of woven fabric under uniaxial/biaxial tensile loading. FIBRES & TEXTILES in Eastern Europe 2020; 28,

6(144).

[25] Yanfei Yang, Xiaogang Chen, Investigation on energy absorption efficiency of each layer in ballistic amour panel for applications in hybrid design. Composite Structure. 164(2017)1-9.

[26] Yang Wang, Yuanming Xia. The effects of strain rate on the mechanical behaviour of kevlar fibre bundles:an experimental and theoretical study. Composites Part A .29A (1998) 1411–1415.

[27] V.P.W. Shim*, C.T. Lim, K.J. Foo. Dynamic mechanical properties of fabric armour. Int J Impact Eng 25 (2001) 1-15.

[28] Lvtao Zhu, Ifra Marriam, Fujun Xu. Experimental and theoretical study on the strain rate dependence of the mechanical properties of Twaron fiber tows with different fiber fineness. Textile Research Journal 2019, 89(12) 2395–2405.

[29] C.T. Lim, V.P.W. Shim, Y.H. Ng. Finite-element modeling of the ballistic impact of fabric armor. Int J Impact Eng 28 (2003) 13–31.

[30] V.B.C. Tan , X.S. Zeng, V.P.W. Shim. Characterization and constitutive modeling of aramid fibers at high strain rates. Int J Impact Eng 35 (2008) 1303–1313.

[31] McCrackin FL, Schiefer HF, Smith JC, Stone WK. Stress-strain relationships in yarns subjected to rapid impact loading: part II. Breaking velocities, strain energies, and theory neglecting wave propagation. Text Res J Jun. 1955;25(6):529-34.

[32] Roylance D. Ballistics of transversely impacted fibers. Text Res J Oct.1977;47(10):679-84.

Chapter 5

Hole defect effect on the low-velocity impact behavior of Twaron® woven fabric

Chapter 5

Chapter 5: Hole defect effect on the low-velocity impact behavior of Twaron® woven fabric

5.1 Introduction

Over the past several decades, numerous experiments and theoretical studies have been conducted to understand the impact behavior of these high-performance fabrics [1–5]. Existed studies have been reported that various physical and mechanical properties affect the ballistic impact performance of fabrics, including the woven architecture [6, 7] and physical properties, such as crimp [8, 9], thread and yarn linear density [10], inter- and projectile-yarn friction coefficient [11,12], fabric boundary conditions [13-15], and projectile shape [16, 17]. However, little research exists on low-velocity impact of high-performance fabrics and on the influence of fabric defects on the mechanical properties of high-performance fabrics. Defects such as holes often appear in fabrics, which are the main components of soft body armor, after long-term use or damage. Furthermore, fabric reinforced composites containing holes or cut-outs are often used in structural applications. Hole defects create stress or strain concentrations, which weaken the mechanical properties of fabric-based soft body armor or fabric-reinforced composites to a certain degree [18]. Overall, prediction of effect on the mechanical properties of fabrics caused by hole defects is important for material designers.

As mentioned in previous chapters, numerical methods have become widely used tools for quickly and efficiently exploring new materials, weaves, and architectures

through parametric studies and for identifying and understanding various mechanisms of deformation, failure, and energy dissipation that cannot be easily elucidated through experimental means [19], and while numerical methods are able to provide insight into the nature of impact events.

Hence, in this chapter, we seek to better understand the influence of fabric hole defects on the impact behavior of high-performance Twaron® fabric from three different perspective. First, the influence of the size and location of hole defect on the impact behavior of single-layer Twaron® fabric, the influence of hole defects of different sizes on the impact behavior, and the effects of different locations of hole defects are investigated. In addition, the effects of hole defects on the impact behavior of multilayer armor panels are studied by considering the *F–t* curve, transverse deflection, and energy absorption. Furthermore, the effects of hole defects on the impact behavior of different weaving architectures (i.e., plain, twill, basket, and satin weave) are analyzed considering the *F–d* curve, transverse wave velocity, and energy absorption.

5.2 FE model validation

The impact model of Twaron® woven fabric had been verified in chapter 4 for 15-30J impact scenarios, but we have to point out the impact velocity are quite low(2-3m/s). In order to judging whether it is effective of the model for a wider range of impact velocity, the 9250HV drop weight impact tester is used for further validating. The free-fall drop-dart machine with changeable load cells that have a large measurement

capacity. The impactor's height and weight are adjustable to facilitate the different initial impact velocities. Two sensors for impact loading and acceleration are installed on the impactor with a diameter of 12.7 mm and are used to measure the contact force between the impactor and specimen as well as the acceleration during the low velocity impact. Based on the impact loading *F(t)*, acceleration *α(t)*, and initial velocity v_i, calculating the velocity *v(t)* and deflection *D(t)* of the impactor and the absorbed energy *E(t)* of specimen were possible [20].

$$v(t) = vi + \int_0^T \alpha(t)\, dt \quad (1)$$

$$D(t) = \int_0^T v(t) dt \quad (2)$$

$$E(t) = \int_0^T F(t) v(t) dt \quad (3)$$

The fabric specimens are fabricated using the same method in chapter 4. Impacts of a single layer of Twaron CT® fabric are performed ten times at velocities in the 1–12 m/s range in both experiments and simulations. The results of the fabric's energy absorption and residual velocities of the projectile from the experimental tests and FE simulations are compared. Fig. 5-1(a) and (b) show the correlation between the FE predictions and experimental results, where the gradients of the regression line are 0.9542 and 1.0015, respectively, which indicates good validity of the model.

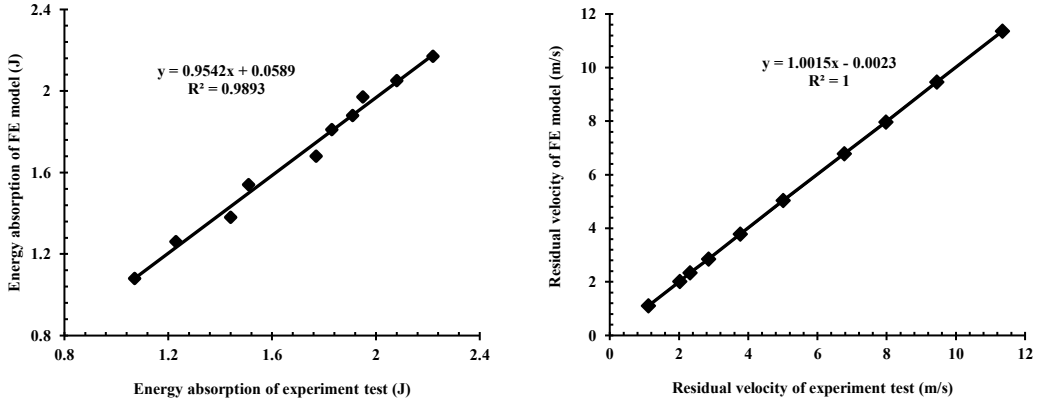

(a) (b)

Fig.5-1. Comparison of FE and experiment results: (a) Energy absorption and (b) Residual velocities.

5.3 Hole defect effect on single layer fabric

The process for the drop weight impact experiments in this study is as follows. The impactor is freely dropped from a designated height and its velocity increased to the intended impact velocity as it reached the fabric. At that moment, the fabric deforms and exerts an impact resistance force on the impactor. The impact resistance force increases before eventually reaching a peak when the yarns in the fabric reached their failure stress and starts to break. Then, the fabric rapidly reaches complete failure. At the moment of failure, the resistance force sharply decreases. Thereafter, only a small amount of frictional force remains preventing the impactor from reaching its residual velocity and the impact event ends. Hole defects clearly lower the fabric's impact resistance ability. To find out how and to what extent hole defects affect the impact resistance, impact tests of the drop weight impactor at the specimen's center with an impact velocity of 8 m/s are implemented for all FE impact scenarios. Important indices reflecting the impact resistance ability, such as the maximum contact force during the entire impact event, the impactor's deflection at the fabric's time of failure,

fabric's impact duration time before failure, and total energy absorption are determined from FE simulation results. Among these, the total energy absorption includes the loss of projectile kinetic energy and the impactor's gravitational potential energy. These factors can be calculated from the measured strike and exit velocity of the impactor and the deflection of the impactor at the point of exit using Equation (4).

$$E_T = MGD + {}^1\!/_2\, M(v_i{}^2 - v_r{}^2) \quad (4)$$

where E_T is the energy absorption by the panel; G is standard earth gravity. M is the mass of the impactor; v_i and v_r are the strike and exit velocity, respectively; and D is the deflection of the impactor at the time at which the exit velocity is achieved.

5.3.1 Influence of hole defect size

To study the influence of hole defects on the impact behavior of single layer fabric, four different models of Twaron® fabric are created for comparison. The model denoted as P0 has no hole, and models denoted as P1, P3, and P5 are fabrics with hole defects at the sample center with sizes of 1 × 1, 3 × 3, and 5 × 5 yarn interweaving points, respectively; the side length of the holes were, respectively, 7.8%, 23.6%, and 39.4% that of the impactor's diameter. Fig. 5-2 shows a schematic fabric model of P3. Fig. 5-3 compares the impact results of the different fabric models. Hole defects of greater size had a significantly greater effect on the impact resistance ability of the fabric. The maximum contact force of the fabric P0 without holes is as high as 1635.3 N, but this parameter is reduced to 75.9%, 49.3%, and 19.9% for the impact of fabrics P1, P3, and P5, respectively. Simultaneously, between fabrics P0 and P5, the

deflection of the impactor at failure decreases from 6.98 to 6.39 mm and the fabric impact duration time decreases from 0.876 to 0.800 ms. In addition, the energy absorption for P0 was 2.06 J, which decreases to 76.2%, 35.9%, and 11.9% for fabrics P1, P3, and P5, respectively. Larger hole defects involve more primary yarns, which play a major role in the impact resistance breakage; hence, the large holes resulted in a sharp decline in the impact resistance performance of the fabric. We conclude that fabric specimens with better impact resistance performance, in other words, greater energy absorption ability, will always have a greater maximum contact force, longer impact duration time, and greater impactor deflection.

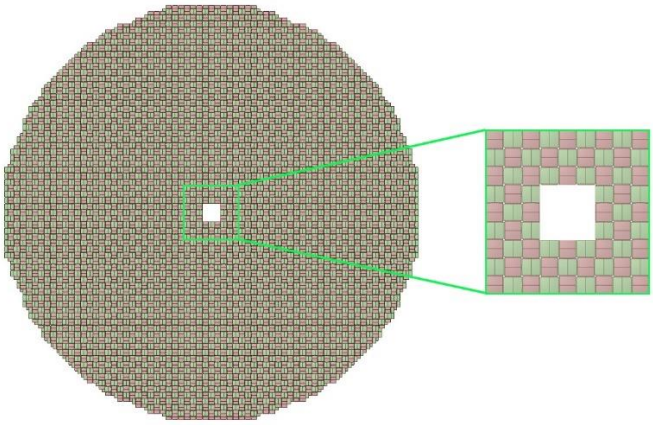

Fig. 5-2. Schematic of the P3 fabric model.

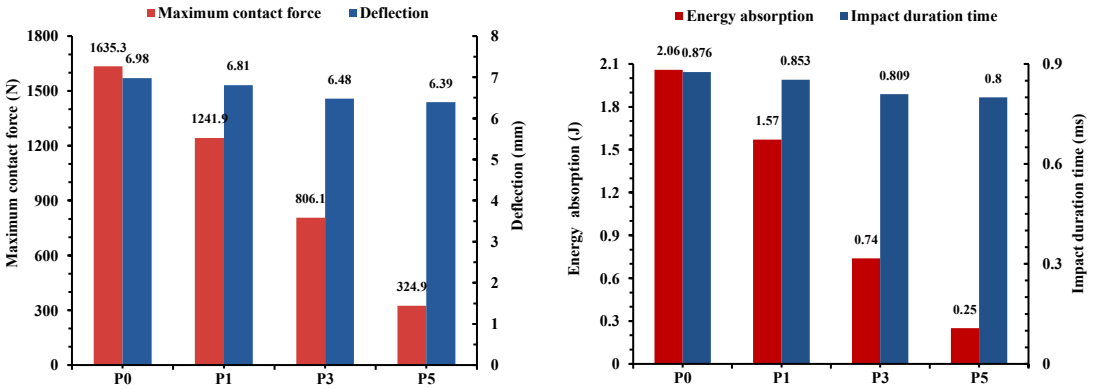

Fig. 5-3. Comparison of the impact results of fabrics with different hole defect sizes: (a) maximum contact force and impactor deflection and (b) energy absorption and impact duration time.

5.3.2 Influence of the hole defect location

In addition, we consider the effect of the relative position of the hole and the impact center on the impact performance of the fabric. A unified hole size of 3 × 3 yarn interweaving points is used in all models; each model had a single hole defect at a different location, as shown in Fig.5-4. The model P3 has a hole at the fabric center, and models H1, H2, and H3 have hole defects arranged in line with the central primary yarn, whereas the models S1, S2, and S3 have the central points of their hole defects arranged equidistantly in a line 45° to the central primary yarn. Due to the round shape of the models, the central points of the hole defects in models H2 and S2 are located at the midpoint between the impact point and fixed boundary.

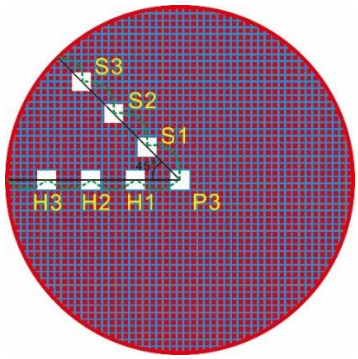

Fig.5-4. Schematic of the location of hole defects in each model.

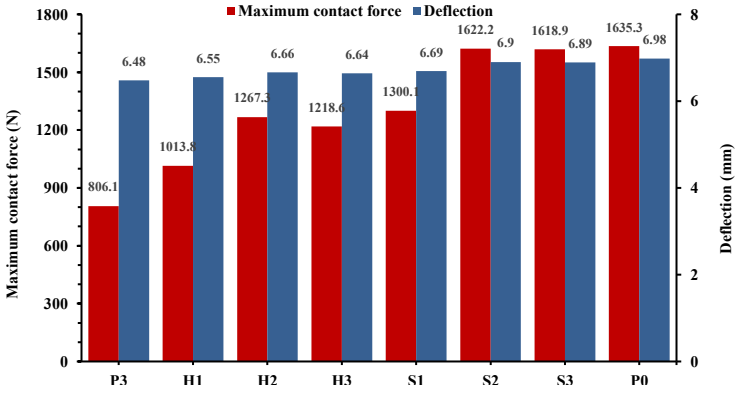

(a)

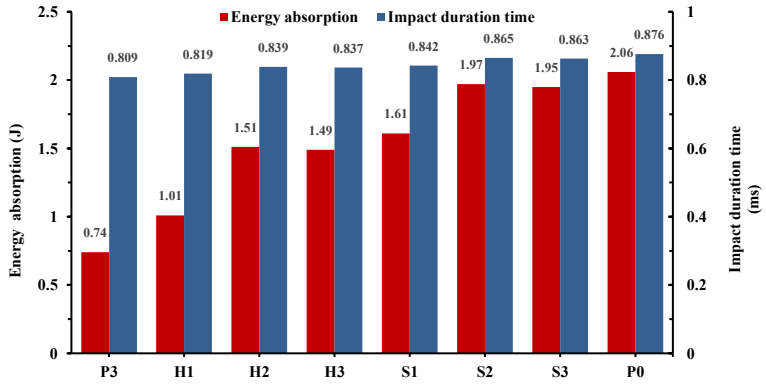

(b)

Fig. 5-5. Comparison of impact results of fabrics with different hole defect locations: (a) maximum contact force and impactor deflection and (b) energy absorption and impact duration time before failure.

Fig. 5-5 compares the impact results of fabric models with different hole defect locations. Excluding the fabric model P0 without a hole, model S2 has the best impact resistance performance among all the other models. Moreover, model P3 has the poorest performance because the hole defect is located at the model center, which is also the impact point. For models H1, H2, and H3, the impact scenarios resulted in lower energy absorption compared to models S1, S2, and S3, because the hole defects are located in these models' primary yarns, which contributed the most to energy absorption during impact events. To determine how impact performance changed with distance from the impact center to the center of the hole defect, P3, H1, H2, and H3 were combined into one group and P3, S1, S2, and S3 are combined into another group for further analysis. The energy absorption values of P3, H1, H2, and H3 are, respectively, 35.9%, 49.2%, 73.1%, and 72.5% of the absorption energy of the model P0 without holes; the maximum contact force values are, respectively, 49.3%, 62.0%, 77.5%, and 76.9% that of model P0. The energy absorption values of P3, S1, S2, and S3 were 35.9%, 78.2%, 95.6%, and 94.8% that of model P0, and the maximum

contact forces are 49.3%, 79.5%, 99.2%, and 99.0%, respectively. The impact duration time and deflection followed the same trend for both groups. A comparison of the results of the two groups indicates that as the distance between the impact point and the hole defect increased, the midpoint between the impact point and fixed boundary act as a demarcation point. The energy absorption ability of the fabric first considerably increases and then remains almost stable except for a slight drop. In general, when a fabric with a hole defect is subjected to a drop weight impact, the impact resistance ability is the weakest when the impact point is located at the hole defect. The hole defect of model S2 had the least effect on the impact resistance performance of the fabric. In fact, the influence of the hole defect at the location in model S2 on the impact performance of the fabric was quite limited.

5.4. Hole defect effect on multi-layer fabric armor panels

High-performance fabrics are frequently assembled into multilayers to improve the energy absorption properties of body armor or composites. In this study, we stack models of P0 and P3 into 2-, 3-, and 4-layer fabric armor panels for further investigation. Specifications of the specimens are listed in Table5-1. The difference in the area density of the panels with and without holes was small; hence, they are considered to be the same.

Table 5-1. Specifications of specimens

Material	The number of layers	Thickness(mm)	Area Density(g/m^2)
Twaron® plain weave (with and without holes)	1	0.2	124.6
	2	0.4	249.2
	3	0.6	373.8
	4	0.8	498.4

5.4.1 Effect on *F–t* curves

Fig.5-6 shows the impact comparison results of *F–t* curves of different stacking layers of P0 and P3. In the impact scenarios without holes, except for a slight fluctuation caused by the stress wave, the contact force in each type of panel basically steadily increases before its peak and then sharply decreases over a very short time after reaching the peak value. The peak force appears at the moment when the specimen began to fracture in the impact scenarios without holes, and a sharp decrease in the contact force of the multilayer specimens suggests an almost uninterrupted perforation between the layers. For the case of models with holes, the contact force has a more complex tendency for the multilayer cases as irregular peak fluctuations appeared. The labels marked A–D on the impact *F–t* curves of the 4-layered panel of the scenario with holes in Fig. 5-6 indicate the failure times of layers from first to last. Furthermore, a schematic diagram of the impact times A–D for each layer as the impact progressed is shown in Fig.5-7, and the failure mode of each layer had clear intervals between the perforation of the layers.

In addition, the peak forces reached for the 2-, 3-, and 4-layers in systems without a hole are 1.57, 2.18, and 2.94 times that of the single layer scenario. In the models with holes, these values are 1.79, 2.44, and 3.05 times that of the single layer scenario, respectively. Evidently the impact resistance ability of multi-layers cannot reach the superposition of the impact resistance ability of a single layer regardless of holeless and with-hole case. And this phenomenon is more obvious in holeless case. In considering the different numbers of layers in the armor panel, hole defects have less

effect on the contact force as the number of layers increased, because the contact force ratio of the cases with and without holes are 43.2%, 43.9%, 47.6%, and 49.3% for 1-, 2-, 3-, and 4-layer panels, respectively.

Furthermore, although the total time of the impact process (i.e., from the initial moment to the time when the impactor reached its minimum velocity) increases as the number of layers increased, the same trend shows that the impact time to reach the peak contact force become slightly shorter in the multilayer scenarios with and without holes. However, the difference of perforation mode is notable between scenarios with and without holes. For the case of impact on specimens without a hole when the contact force reached its peak at the moment when the first layer of the specimen started to fracture. Conversely, for cases with a hole, the peak force is reached at the moment after the fracture of the penultimate layer but before the fracture of the back layer. Further supporting data is provided in Fig.5-8, which shows the fracture time of each individual layer and the peak force time in the 4-layer panel scenarios with and without holes. The time between the front and back layer fracture for the case without holes is 0.007ms and 0.155 ms for the case with holes; hence, the uninterrupted and interval perforation characteristics of the two different panels are, respectively, confirmed.

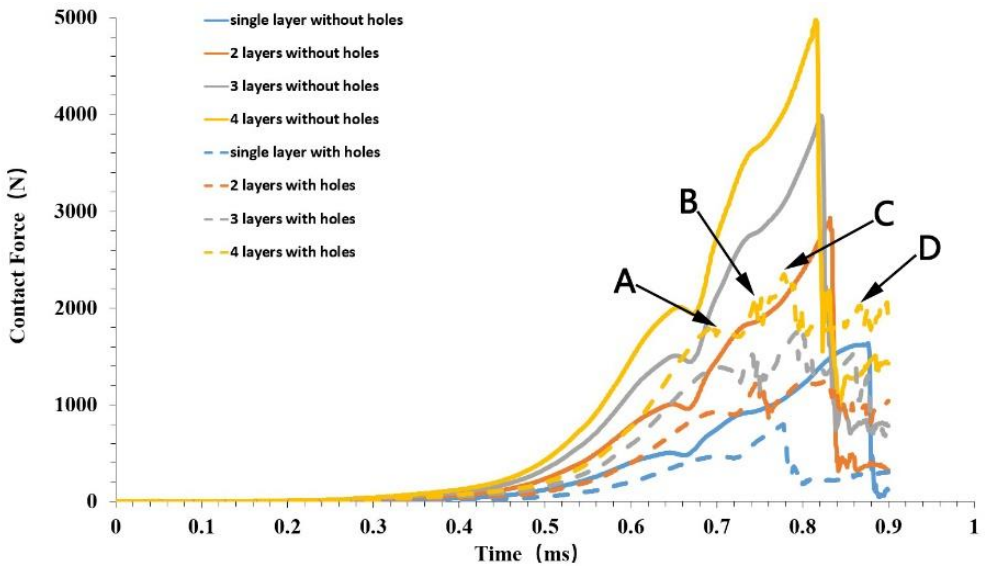

Fig. 5-6. Comparison of the impact *F–t* curves of each type of panel for scenarios with and without holes.

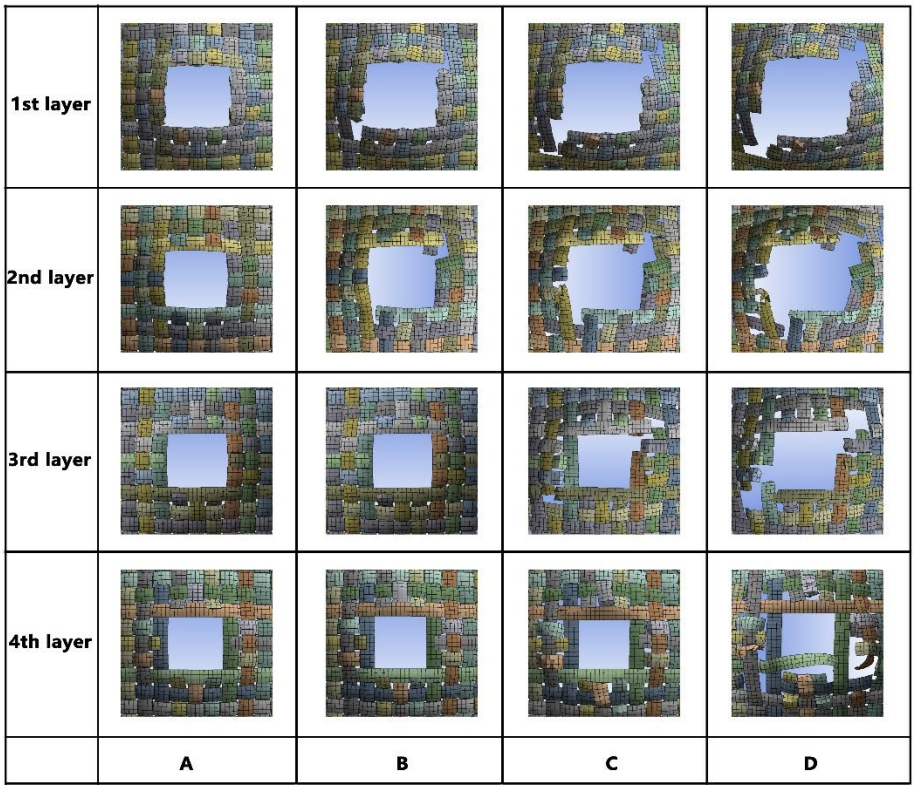

Fig.5-7. Schematic of each layer in the 4-layered panel with a hole subjected to an impact at times A–D.

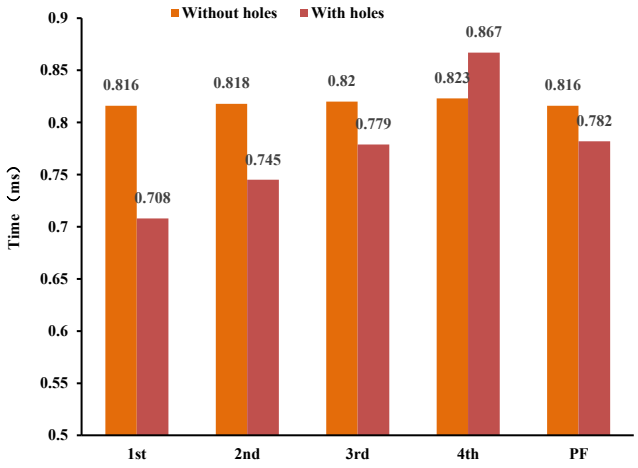

Fig. 5-8. Fracture time of each layer and peak force time for the 4-layered panel in scenarios with and without holes.

5.4.2 Effect on transverse deflection

In the present study, we mainly consider low-velocity perforation impacts. For high-velocity ballistic impact events, sufficient time is not present for obvious transverse deflection propagation to take place. However, for low-velocity impact events, sufficient time is present for transverse deflections to propagate and reach the fabric edges, resulting in creasing and stretching over a wider region [21]. In other words, low-velocity impacts tend to extend and break the fabric rather than shear yarns, which are observed for high-velocity events. In a multilayer panel perforation impact event, primary yarns of each layer are stretched to a large extent and the fabric layer reached the maximum transverse deflection and failure. In this study, the maximum transverse deflection of the front layer at the corresponding fracture time for each layered panel for scenarios with and without holes are quantified by FE simulations to better compare the two scenarios; the third primary yarn (i.e., two yarns spacing from the center primary yarn) is chosen as an object, and the results are shown in Fig.5-9. The maximum deflection for the scenario with holes for each type

of panel is clearly smaller than that without holes. Since hole defects are located in the central primary yarns, the third primary yarn plays the role of the first stressed yarn, which leads to a greater stress concentration, resulting in earlier fracture than that for the scenario without holes. Fig. 5-9 also indicates that for the multilayer panel scenarios with and without holes, transverse deflection of the front layers is constrained by the back layers, and the constraining effect became more notable as the number of layers increases. This result is demonstrated in Fig.5-10, which shows that the fracture time of the front layer decreases as the number of layers increases for the multilayer panel, regardless of the presence or absence of holes. Furthermore, to compare the constraining effect on the two scenarios, the constraining effect index γ, defined by equation (5), is established, where n is the number of layers in the multilayer panel, d_i is the maximum deflection of the *ith* layer in the panel, and d_0 is the maximum deflection of a single layer panel. A smaller γ value indicates a more severe constraining effect for the multilayer panel:

$$\gamma = \frac{\sum_{i=0}^{n} d_i}{n d_0} \tag{5}$$

These data are compared in Fig.5-11, which shows that the constraining effect becomes more severe for a greater number of layers for both scenarios. For the impact scenario with holes, the constraining effect is less severe than that without holes for all multilayer panel cases.

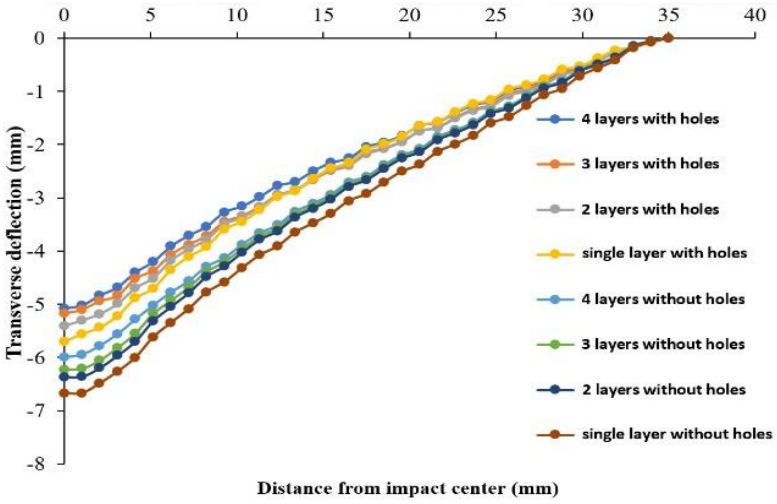

Fig. 5-9. Maximum transverse deflection of the front layer before fracture for each type of panel in scenarios with and without holes

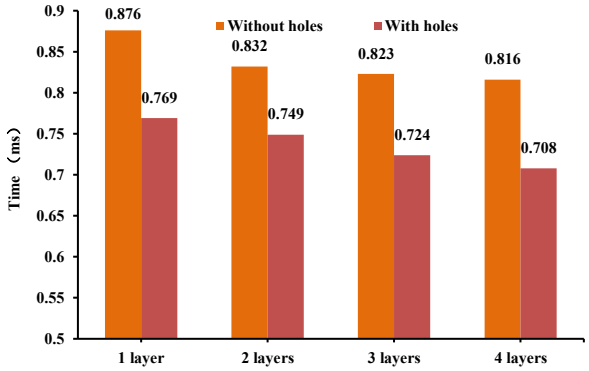

Fig. 5-10. Fracture time of front layer in each type of panel in scenarios with and without hole

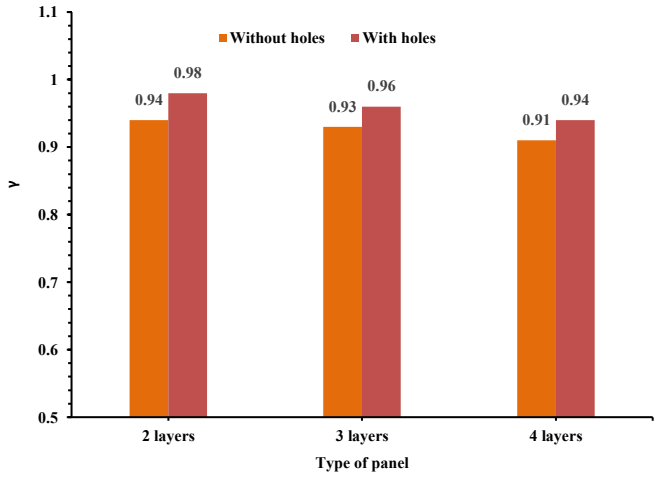

Fig. 5-11. Comparison of γ of each multilayer panel for scenarios with and without holes.

5.4.3 Effect on total energy absorption

In this study, the total energy absorption E_T and the specific energy absorption (*SEA*) are calculated to examine the energy absorption of the panels with different amounts of material. *SEA* is normalized by dividing the total energy absorption by the corresponding areal densities of the panel, as indicated in Equation (6):

$$SEA = {}^{E_T}/_{A_d} \quad (6)$$

where A_d is the areal density (g/cm^2). These results are plotted in Fig.5-12. The results for scenarios with and without holes both show an increase in the total energy absorption as the number of layers increased in the armor panel, whereas *SEA* decreases when more fabric layers are present in the panel. Notably, for the scenario without holes, *SEA* decreases to 93.8%, 91.4%, and 90.2% the values of the single layer case for 2-, 3-, and 4-layer panels, respectively; for the scenario with holes, the *SEA* decreases to 95.5%, 93.9%, and 93.2%, respectively. This decrease is more severe for the scenario without holes than that with holes. Furthermore, the energy absorption ratios of the scenarios with and without holes are 54.1%, 55%, 55.6%, and 55.9% for 1-, 2-, 3-, and 4-layer panels, respectively. These data demonstrate that the difference in the energy absorption of the two scenarios narrowed as the number of layers in the armor panel was increased.

In addition, for the multilayer panel, because the same fabric layers contributed to different amounts of energy absorption when placed at different positions, the energy absorption efficiency *R* is used for further investigations and is defined by Equation [22]:

$$R = {}^{E_{ith}}/_{E_S} \times 100\% \quad (7)$$

where R is the energy absorption efficiency, E_{ith} is the energy absorption of the *ith* layer in a panel, and E_s is the energy absorption of a single fabric layer.

Fig.5-13 shows the impact energy absorption efficiency of each layer in the multilayer panels for scenarios with and without holes. These results indicate that regardless of the presence of a hole, the constraining effects on the front layers by the back layers became more notable for armor panels containing more fabric layers. Compared to the scenario without holes, the energy absorption for the scenario with holes is more dispersed over the layers, the front layer is more severely constrained for each type of panel, and the back layer had a higher energy absorption rate.

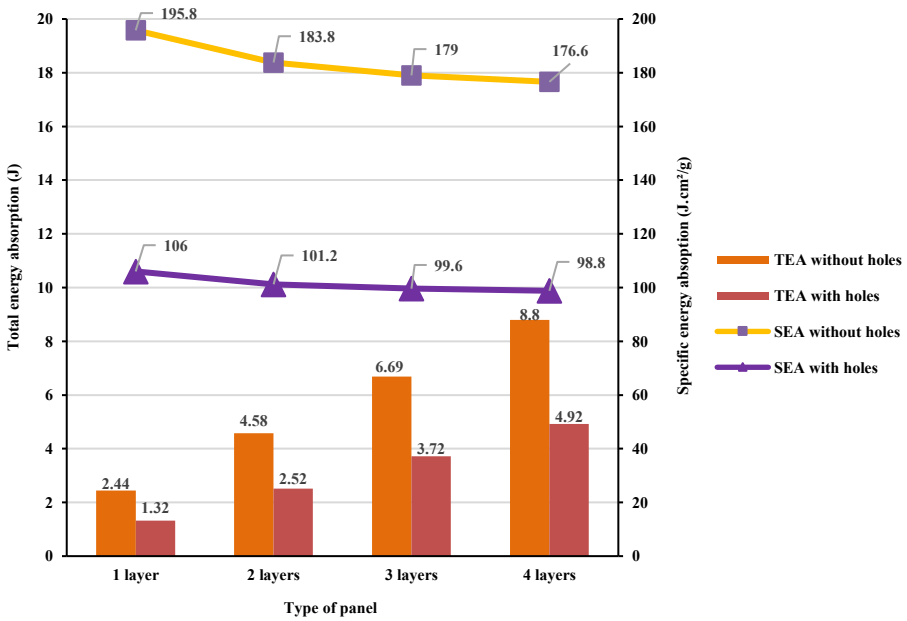

Fig. 5-12. Total energy absorption and specific energy absorption for each type of panel.

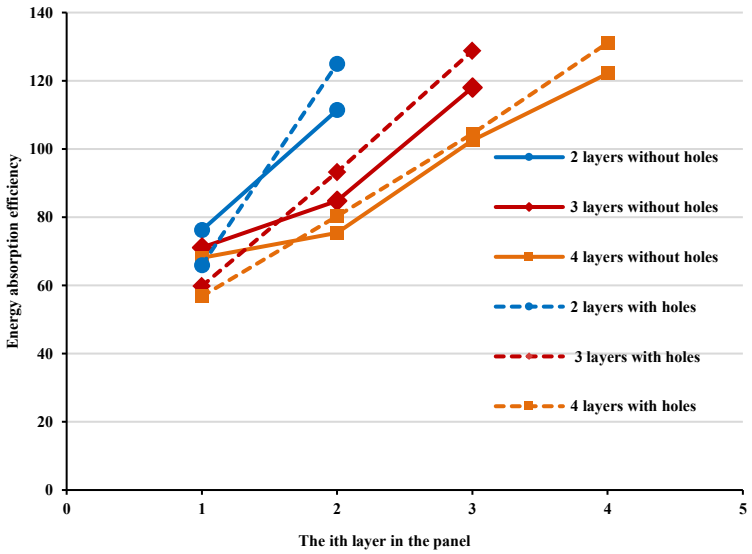

Fig. 5-13. Energy absorption efficiency of each layer in each type of panel.

5.5 Hole defect effect on different weaving architectures

Studies on the effects of holes on the impact behavior of fabrics with different weaving architectures are also performed for fabrics with plain, 4-harness satin, 2/2 basket, and 2/2 twill weaves, as shown in Fig.5-14. All the specimens with holes have the same configuration as the plain-woven model P3. The geometric parameters of various fabrics are kept consistent as much as possible to allow a comparison of only the effects of the architecture factor. In this study, the yarns in all architectures have the same cross-section and yarn spacing; the fabrics are constructed with identical thickness, length, and width, and the difference of their area density is almost negligible. The differences in the yarn interlacing pathway cause a higher yarn crimp rate for the plain weave than for the other three weaves. As shown in Fig.5-14, the yarns in the satin weave have the longest continuous float length, the basket weave and twill weave have the same length (second only to the satin weave), and the yarns in the plain weave have the shortest continuous float length. These geometric

properties are listed in Table 5-2.

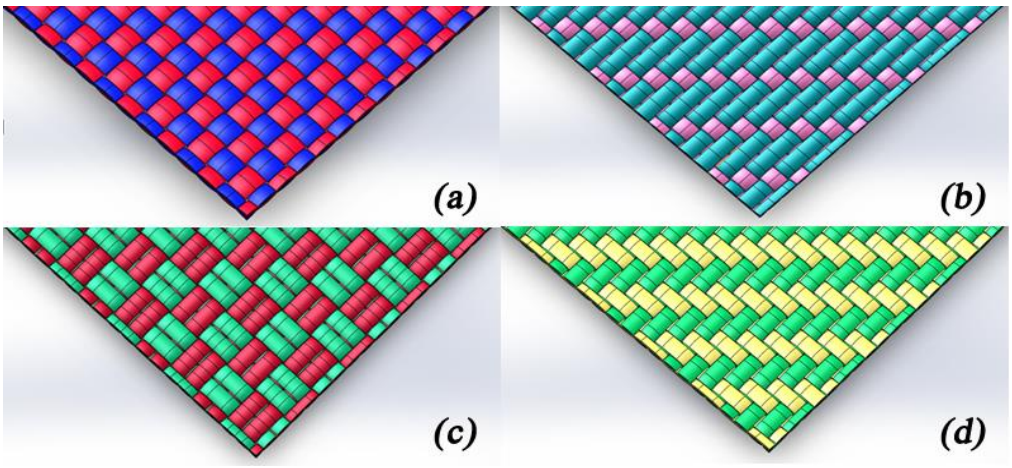

Fig. 5-14. Schematic of different fabric models: (a) plain woven; (b) 4-harness satin; (c) 2/2 basket; and (d) 2/2 twill.

Table 5-2. Geometry properties of different fabric architecture

Fabric	Size (mm)	Yarn width(mm)	Yarn thickness(mm)	Yarn spacing (mm)	Fabric thickness(mm)	Area density (g/m^2)	Crimp rate (%)
Plain	60×60	0.902	0.1	0.909	0.2	124.591	0.66
4-harness satin	60×60	0.902	0.1	0.909	0.2	124.584	0.33
2/2 basket	60×60	0.902	0.1	0.909	0.2	124.587	0.33
2/2 twill	60×60	0.902	0.1	0.909	0.2	124.581	0.33

5.5.1 Effects on *F–d* curve

Contact force is the most important indicator reflecting a fabric's impact resistance and is still one of the main factors to be studied. The *F–d* curve shown in Fig.5-15 suggests that for scenarios with and without holes, the plain weave fabric always have the highest maximum contact force. The maximum contact forces reach by the basket and twill weaves are very close; however, the basket weave is a little higher and second only to the plain weave fabric. The satin weave has the smallest maximum contact force. Conversely, the satin weave reacts most rapidly on impact because the

contact force is always the greatest among all the fabrics over the same time before failure in both scenarios, whereas the plain weave reacts the slowest on impact. In addition, the deflection of the impactor at the time of fabric failure follows the same trend: the plain weave fabric has the greatest deflection for both impact scenarios, followed by the basket weave, twill weave, and satin weave. Notably, the basket and twill weaves have very similar *F–d* curves for both scenarios, especially before the fabric's failure. Moreover, the twill weave specimen with a hole has better after-failure duration ability than the other three fabrics, as indicated by the largest difference between the failure time and complete failure time among all the scenarios with holes.

In general, hole defects drastically reduce the maximum contact force and simultaneously shorten the impact deflection at failure to a certain degree. The maximum contact force in the plain weave fabric with a hole is 49.3% that of the scenario without holes. The relative differences are 45.8% for the basket weave, 48.3% for the twill weave, and 45.6% for the satin weave. The impactor deflection at the time of failure for the scenario of the plain weave fabric with holes decreases to be 92.8% that without holes. The relative differences are 94.1% for the basket weave, 94.5% for the twill weave, and 89.7% for the satin weave. Overall, the satin weave is most notably affected, whereas the plain weave is least affected by hole defects in the contact force during impact event. In terms of impactor deflection at the time of failure, the satin weave is most notably affected, and the twill weave is least affected by hole defects.

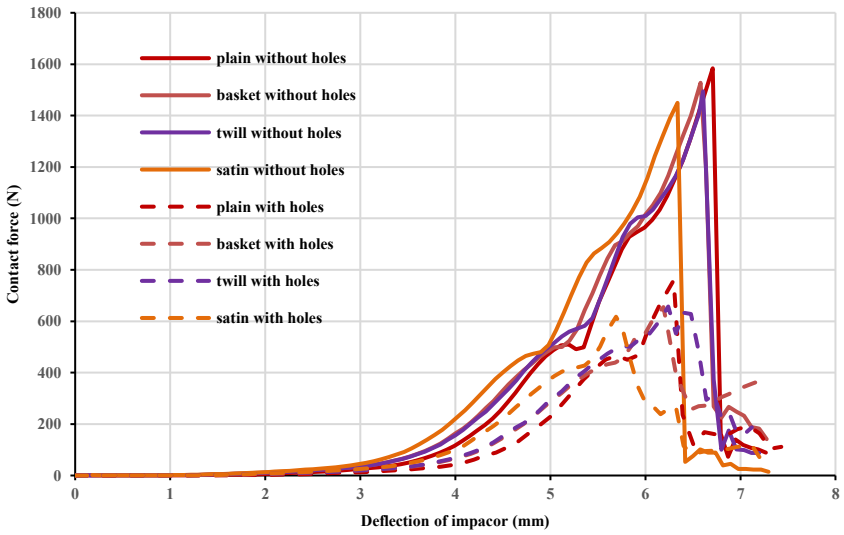

Fig.5-15. Comparison of the impact *F–d* curves of each fabric for scenarios with and without holes

5.5.2 Effects on transverse wave velocity

When an impactor impacts a fabric, two stress waves, namely longitudinal and transverse waves, are produced. The longitudinal stress wave propagates at the speed of sound of the material along the axis of the yarns, whereas the transverse wave propagation depends upon the impact velocity of the impactor and the material type [23]. The longitudinal wave velocity of a straight yarn depends on the yarn's longitudinal Young's modulus and volume density and is calculated to be greater than 7000 m/s for the Twaron® fabric. For a low-velocity impact event, within a very short instant, the stress wave propagates to a considerable distance from the impact center, while the stress applied in yarns remains quite small. Therefore, we infer that the influence of the woven architecture and hole defects is minimal on the longitudinal wave velocity; hence, in this study, we focus on the transverse wave velocity only because it is significantly slower than the longitudinal wave velocity.

When an impactor impacts a fabric, the transverse wave propagation results in transverse deflection in the primary yarns and causes the fabric to form a deformation zone, which becomes greater in size as the impact event progresses. Fig.5-16 shows a cross-sectional image of the side view deformation zone for each fabric at 0.3 ms for the scenarios with and without holes. A wider deformation zone simultaneously appears, indicating that a faster transverse wave velocity is archived during the impact event. Hence, the transverse wave velocity decreases in the following order: satin > basket > twill > plain in the absence of a hole. Furthermore, the hole defect reduces the transverse wave velocity for all fabrics because a narrower deformation zone appeared at the same observation time. Notably, the transverse velocity of the twill weave surpasses basket weave and results in the transverse wave velocity decreases in the following order: satin > twill > basket > plain for the scenario without hole. Ordinarily, the velocity of the transverse wave propagation is calculated from the distance traveled by the stress wave from the impact point to the locations where the magnitude of the deflection becomes zero and the associated time [24]. Similar methods are applied in the present study by capturing the transverse displacement and associated time from the probed node located 20 mm away from the impact center of all fabrics for both scenarios. Fig.5-17 shows the time histories of the transverse displacement of the probed node; arrows indicate the arrival time of transverse waves of plain and satin weaves for the scenario without holes. In addition, the transverse wave velocities of all fabrics for both scenarios are calculated and shown in Fig.5-18. These results are consistent with the conclusions obtained in Fig.5-15; the satin weave

has the fastest transverse wave velocity for both scenarios, whereas the plain weave has the lowest. This fast wave transfer is attributed to the longest continuous float length in yarns, in other words, the smallest number of cross-over points in satin weave, and inversely, plain weave had the most number. Furthermore, under the influence of hole defects, the transverse wave velocity decreases to 69.1%, 77.9%, 70.2%, and 72.6% the values of the plain, twill, basket, and satin weaves in the scenario without holes, respectively. The plain weave fabric is most affected in terms of transverse wave velocity, followed by the basket and satin weaves. The twill weave is the least affected by the hole defect.

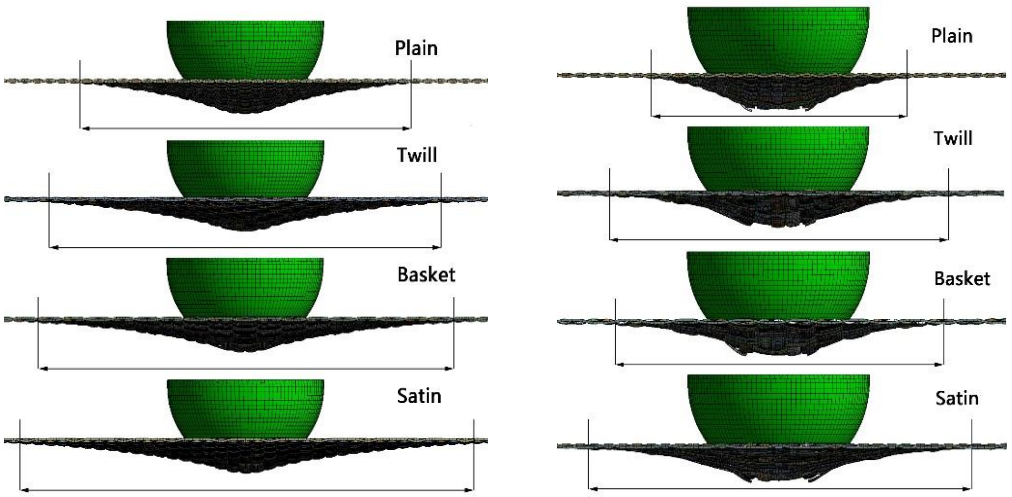

(a) (b)

Fig.5-16. Side view of impact deformation zone at 0.3 ms for different fabrics: (a) without hole; (b) with hole.

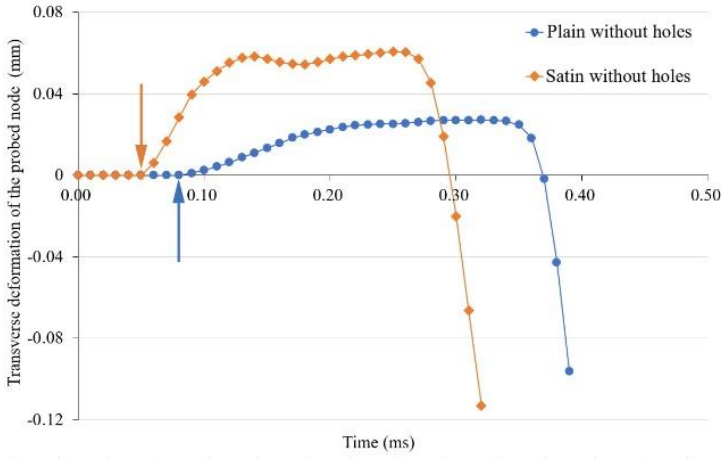

Fig.5-17. Time histories of transverse displacement of the probed node.

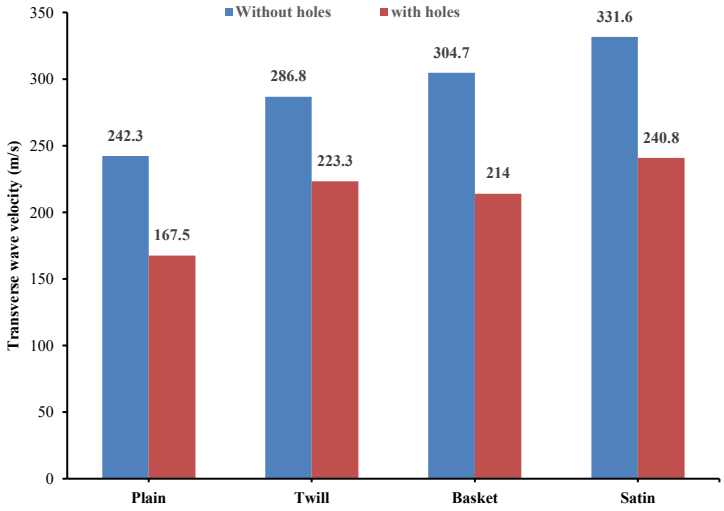

Fig.5-18 Transverse wave velocity of different fabrics

5.5.3 Effects on total energy absorption

Many studies have confirmed that plain weaves outperform other fabric weaves in terms of energy absorption under high-velocity ballistic impact events [7, 25]. Because of the low-velocity nature of the impact events in this study (Fig.5-19), the plain weave similarly has the apparent highest energy absorption capability under both scenarios although the plain weave has a higher crimp rate than other weaves (the higher crimp rate counteracts the energy absorption owing to the decrease of the yarn's tensile modulus and it was discussed in chapter 3). This result is attributable to

the plain weave having the most firmly interlaced architecture. Furthermore, the transverse wave velocity in the satin weave is the fastest and that of the plain weave is slowest for both scenarios. The faster wave velocity implies that stress transferred more rapidly through the longitudinal direction to the boundaries. This weave architecture evidently results in the fastest reaction to impact. However, this architecture does not result in a greater energy absorption ability, but rather it performs poorest in terms of energy absorption in both scenarios. This is because the satin weave is not as firmly interlaced as the twill, basket, or plain weave. Hence, greater allowable movement is present between the yarns in the satin weave, making it easier for the impactor to push the primary yarns away and enabling easier and quicker penetration of the fabric. In addition, the basket and twill weaves have a higher number of cross-over points than the satin weave but fewer than the plain weave. These two architectures have very similar behaviors during the impact progress and have similar *F–d* curves, transverse waves, and total energy absorption, particularly for the case without a hole. Moreover, since it has the highest number of cross-over points, the plain weave can absorb a greater amount of energy despite having a slower reaction to the impact than the other three weaves.

As demonstrated in Fig.5-19, for the scenario without holes, the energy absorption capacity decreased in the following order: plain > basket > twill > satin; for the scenario with holes, the better after-failure duration ability of the twill weave afforded it better performance than the basket weave, while the rankings of two other weaves remained unchanged. By quantifying the effects of hole defects on each fabric, the

total energy absorption in the plain weave in the scenario with holes decreased to 64.1% that of the scenario without holes, and it reduces to 67.5% in the twill weave, 58.1% in the basket weave, and 57.6% in the satin weave. The satin weave is the most affected, followed by the basket weave and plain weave. The twill weave is least affected by the hole defects in terms of energy absorption.

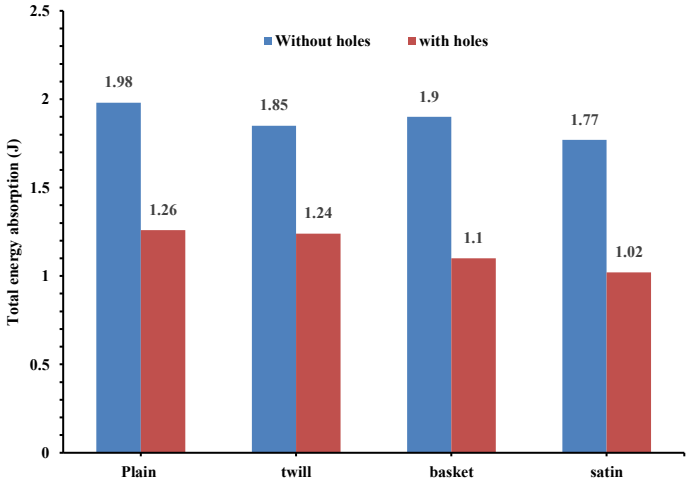

Fig. 5-19. Total energy absorption of each fabric in both scenarios.

5.6. Conclusions

On the basis of a low-velocity drop weight impact model, which was validated by experiments, models of Twaron® single layer fabric with and without holes for multilayer fabrics (2-, 3-, and 4-layer) and different woven architectures (pain weave, 2/2 twill weave, 2/2 basket weave, and 4 harness satin weave) were created to investigate the effects of hole defects on the impact behavior of soft body armor in this chapter. We obtained the following findings:

- The numerical results of the low-velocity impact agreed well with the experimental results, suggesting that it is valid to use the proposed model to investigate the following problems.

- The size and position of the hole defects affected the impact resistance ability. The impact resistance ability was lower for larger hole defects than for the smaller hole defects. The fabric model P5 had only 11.9% the energy absorption of the model P0 without holes. The impact resistance ability was the weakest when the hole defect was located at the impact center, and the hole defect of model S2 had the least effect on the impact resistance performance of the fabric.

- Uninterrupted perforation and interval perforation characteristics were found as the impact progressed for panels without and with holes, respectively. A greater number of layers in the multilayer armor panel negated the influence of the hole defects in terms of the impact contact force, and less severe constraining effect was present on the front layer of the panel. Compared to the scenario without holes, the energy absorption for the scenario with holes was more dispersed over the layers. The front layer was more severely constrained for each type of panel, whereas the back layer had a higher energy absorption rate.

- The plain weave fabric similarly had the apparent highest energy absorption capability among all weave architectures in impact scenarios with and without holes. Basket and twill weaves demonstrated very similar behavior in terms of impact progress, especially for the scenario without holes. The satin weave was most affected, whereas the plain weave was least affected by hole defects in terms of contact force during impact events. Moreover, the satin weave was the most affected and the twill weave was the least affected by hole defects in terms of impactor deflection at the time of failure and energy absorption. In addition, plain

weave fabric is the most affected and twill weave is the least affected by hole defects in transverse wave velocity.

References

[1] Wilde AF. Photographic investigation of high-speed missile impact upon nylon fabric. Part II: retarding force on missile and transverse critical velocity. Text Research Journal 1974; 44(10):772–8.

[2] Field JE, Sun Q. A high speed photographic study of impact on fibers and woven fabrics. Proceedings of the 19th international congress on high-speed photography and photonics; 1990. p. 703–12.

[3] Shim VPW, Tan VBC, Tay TE. Modeling deformation and damage characteristics of woven fabric under small projectile impact. Int J Impact Eng 1995;16(4):585–605.

[4] Gu BH. Analytical modeling for the ballistic perforation of planar plain-woven fabric target by projectile. Compos Part B-Eng 2003;34(4):361–71.

[5] Zhou Y, Chen X, Wells G. Influence of yarn gripping on the ballistic performance of woven fabrics from ultra-high molecular weight polyethylene fibre. Compos Part B Eng Jun. 2014; 62:198-204.

[6] P Tran, T Ngo, EC Yang, P Mendis and W Humphries. Effects of architecture on ballistic resistance of textile fabrics: Numerical study. Int. J. Damage Mech. 2014, 23: 359.

[7] Cheng-Chou Yang, Tuan Ngo, Phuong Tran. Influences of weaving architectures

on the impact resistance of multi-layer fabrics. Materials and Design 85 (2015) 282–295.

[8] Ying Wang, Xiaogang Chen, Robert Young, Ian Kinloch. A numerical and experimental analysis of the influence of crimp on ballistic impact response of woven fabric. Composite Structure. 140(2016)44-52.

[9] V.B.C. Tan, V.P.W. Shim, X. Zeng. Modelling crimp in woven fabrics subjected to ballistic impact. Int J Impact Eng, 32 (2005), pp. 561-574.

[10] Tuan-Long Chu, Cuong Ha-Minh, Abdellatif Imad. A numerical investigation of the influence of yarn mechanical and physical properties on the ballistic impact behavior of a Kevlar KM2 ® woven fabric. Composites Part B 95 (2016) 144-154.

[11] Yanyan Chua, Shengnan Min, Xiaogang Chen. Numerical study of inter-yarn friction on the failure of fabrics upon ballistic impacts. Materials and Design 115 (2017) 299–316.

[12] Gaurav Nilakantan, John W. Gillespie Jr. Ballistic impact modeling of woven fabrics considering yarn strength, friction, projectile impact location, and fabric boundary condition effects. Composite Structures 94 (2012) 3624–3634.

[13]Ying Wang, Xiaogang Chen, Robert Young, Ian Kinloch.Finite element analysis o f effect of inter-yarn friction on ballistic impactresponse of woven fabrics.Composite Structures 135 (2016) 8–16.

[14]Yanyan Chu, Shengnan Min, Xiaogang Chen.Numerical study of inter-yarn frictio

n on the failure of fabrics upon ballistic impacts. Materials and Design 115 (2017) 299–316.

[15] Y. Duan, M. Keefe , T.A. Bogetti , B. Powers. Finite element modeling of transverse impact on a ballistic fabric. Int. J. Mechanical Sciences 48 (2006) 33–43.

[16] Gaurav Nilakantan, Eric D.Wetzel, Travis A.Bogetti, John W. Gillespie Jr. Finite element analysis of projectile size and shape effects on the probabilistic penetration response of high strength fabrics. Composite Structures ,94(2012): 1846-1854.

[17] H. Talebi, S.V. Wong, A.M.S. Hamouda. Finite element evaluation of projectile nose angle effects in ballistic perforation of high strength fabric. Composite Structures.87 (2009) 314–320.

[18] Surya D. Pandita, Kazuaki Nishiyabu, Ignaas Verpoest. Strain concentrations in woven fabric composites with holes. Composite Structures 59 (2003) 361–368

[19] Gaurav Nilakantan, Steven Nutt. Effects of ply orientation and material on the ballistic impact behavior of multilayer plain-weave aramid fabric targets. Defence Technology 14 (2018) 165-178.

[20] Hairong Miao, Zhenyu Wu, Zhiping Ying, Xudong Hu. The numerical and experimental investigation on low-velocity impact response of composite panels: Effect of fabric architecture. Composite Structures 227 (2019) 111343.

[21] S. Gogineni, X. -L. Gao, N. V. David, J. Q. Zheng. Ballistic Impact of Twaron CT709® Plain Weave Fabrics. Mechanics of Advanced Materials and Structures, 19:6,

441-452.

[22] Yanfei Yang, Xiaogang Chen. Study of energy absorption and failure modes of constituent layers in body armour panels. Composites Part B 98 (2016) 250-259.

[23] Cunniff PM. An analysis of the system effects in woven fabrics under ballistic impact. Textile Res J 1992; 62:495–509.

[24] Ying Wang, Xiaogang Chen, Robert Young, Ian Kinloch. A numerical and experimental analysis of the influence of crimp on ballistic impact response of woven fabrics. Composite Structures 140 (2016) 44–52.

[25] P Tran, T Ngo, EC Yang, P Mendis, W Humphries Effects of architecture on ballistic resistance of textile fabrics: Numerical study. International Journal of Damage Mechanics 2014, 23(3) 359–376.

Chapter 6

General Conclusions

Chapter 6

Chapter 6: General Conclusions

This dissertation carried out study on the mechanical behavior of woven fabric material in terms of static tensile and dynamic low-velocity impact by combining experimental and numerical methods. The mechanism performance and behavior of woven fabric that have not been explored before were deeply investigated and analyzed in this dissertation, such as mechanism of the effect of crimp and inter-yarn friction on fabric's tensile performance, low-velocity impact behaviors of high-performance woven fabric.

In Chapter 1, an overview of characteristic of woven fabric and high-performance Twaron® fiber, current research status of static as well as dynamic mechanical behavior in terms of experiment and numerical methods have been presented.

In Chapter 2, existed modelling techniques are compared and discussed, 3D solid element yarn-level method is implemented and geometric fabric model which is physically based on Twaron® fabric is introduced and the woven fabric model is created.

In chapter 3, we investigated how, and to what extent, crimp and inter-yarn friction of woven fabric influence its tensile performance during tensile processes. A finite element woven fabric tensile model which was validated by experiment results was applied to tensile simulation. The results revealed that, regardless of the case of a single yarn or fabric, the greater the crimp, the easier it is to stretch the yarn or fabric, which has a smaller equivalent modulus in both uniaxial and biaxial tensile scenarios.

In addition, the contact stresses result in a group of nodal points chosen in the model showed that under biaxial tension, more protruding deformation causes more contact pressure, producing a larger friction force. At the same crimp, a larger friction force leads to larger internal stress in the yarns, which makes them more difficult to stretch, resulting in a larger equivalent modulus than during uniaxial tension. Finally, there was an obvious tendency for the equivalent moduli of the UCPWs to increase as the frictional coefficient increased in both the uniaxial and biaxial tensile tests.

In chapter 4, low-velocity drop weight impact experiment on a single layer plain-woven Twaron® CT612 at impact energies of 15, 20 and 30 J was carried out using a 9250HV drop weight impact tester. Commercial code ANSYS® is employed for impact simulation on a physically based impact model. Dynamic mechanical parameters of Twaron® yarn was analyzed with three-element spring-dashpot model to describe the rate-sensitive Twaron® material. Remarkably agreement was found between FE simulation results with experiments at various impact scenarios. In addition, Von-Mises stress distribution contours of the fabric experiencing different impact energies were depicted and the results show no matter under the same impact moment or under the same deflection before fabric failure, a wider stressed area and a greater maximum stress can be found in the higher impact energy event. Furthermore, The energy absorption mechanisms analysis indicates that yarn strain energy demonstrates an absolute dominant energy absorption mechanism when the fabric experiences a drop weight impact, and the analysis results show there is no obvious effect of impact energy on the energy absorption ratios in various impact energy

scenarios. Finally, the influence of specimen shape and size were also numerically investigated. The size of primary yarns evidently affected the energy absorption ability of the fabric during impact event.

In chapter 5, based on the low-velocity drop weight impact model, which was validated by experiments, models of Twaron® single layer fabric with and without holes for multilayer fabrics (2-, 3-, and 4-layer) and different woven architectures (pain weave, 2/2 twill weave, 2/2 basket weave, and 4 harness satin weave) were created to investigate the effects of hole defects on the impact behavior of soft body armor. Results showed the size and position of the hole defects affected the impact resistance ability. The impact resistance ability was lower for larger hole defects than for the smaller hole defects. The fabric model P5 had only 11.9% the energy absorption of the model P0 without holes. The impact resistance ability was the weakest when the hole defect was located at the impact center, and the hole defect of model S2 had the least effect on the impact resistance performance of the fabric. In addition, uninterrupted perforation and interval perforation characteristics were found as the impact progressed for panels without and with holes, respectively. A greater number of layers in the multilayer armor panel negated the influence of the hole defects in terms of the impact contact force, and less severe constraining effect was present on the front layer of the panel. Compared to the scenario without holes, the energy absorption for the scenario with holes was more dispersed over the layers. The front layer was more severely constrained for each type of panel, whereas the back layer had a higher energy absorption rate. Finally, the plain weave fabric similarly had

the apparent highest energy absorption capability among all weave architectures in impact scenarios with and without holes. Basket and twill weaves demonstrated very similar behavior in terms of impact progress, especially for the scenario without holes. The satin weave was most affected, whereas the plain weave was least affected by hole defects in terms of contact force during impact events. Moreover, the satin weave was the most affected and the twill weave was the least affected by hole defects in terms of impactor deflection at the time of failure and energy absorption. In addition, plain weave fabric is the most affected and twill weave is the least affected by hole defects in transverse wave velocity.

These results indicate that the present experimental set-up and the developed fabric geometry model are effective for investigating many more mechanical problems in textile fabrics and/or flexible material structures.

List of publication

1. **Canyi Huang**, Lina Cui, Hong Xia, Yiping Qiu, Qing-Qing Ni. Influence of Crimp and Inter-yarn Friction on the Mechanical Properties of Woven Fabric under Uniaxial/Biaxial Tensile Loading. *FIBRES & TEXTILES in Eastern Europe*. (Published in 2020.11)

2. **Canyi Huang**, Lina Cui, Yajun Liu, Hong Xia, Yiping Qiu, Qing-Qing Ni. Low-velocity drop weight impact behavior of Twaron® fabric investigated using experimental and numerical simulations. *International Journal of Impact Engineering.* (Published in 2021.3)

3. **Canyi Huang**, Lina Cui, Hong Xia, Yiping Qiu, Qing-Qing Ni. A numerical study on the influence of hole defects on impact behavior of Twaron ® fabric subjected to low-velocity impacts. *Journal of Engineered Fibers and Fabrics*. (Published in 2021.5)

Scientific Presentation

Canyi Huang, Yajun Liu, Hong Xia, Qing-qing Ni. FE investigation of the influence of crimp and inter-yarn friction on the mechanical properties of plain weave fabric under uniaxial/biaxial tensile loading. 日本繊維学会. 秋季研究発表会, 上田, 2009.11

Acknowledgement

First of all, I would like to express my sincere gratitude to my supervisor Prof. Qing-Qing Ni, for his valuable instruction and important suggestion, as well as enduring patience, fruitful encouragement and large support thorough my doctoral career in Shinshu University.

I am also grateful to Dr. Hong Xia and Prof. Toshiaki Natsuki in the same group as my continuous guidance and advice to this work. Their advice, insightful comments and suggestions provided significant support on this work.

I would like to express my gratitude to Pro. Yiping Qiu and Pro Fujun XU in Donghua University for providing me important experiment materials for my research.

I also want to forward my gratitude to various people, Mr. kobayashi, Mr. hayashi and Mr.ichikawa for their valuable technical support and extensive guidance of experimental equipments on this work.

Special thanks also to all my friends, especially my research group members. (Mr. Liu Yajun, Ms. Chen Si, Mr. Chen Hairong, MS. Yu Juhong, Mr. Yan Yongjie, Mr. Guan Xiaoyu, Mr. Hong Jun, Mr. Jing Yinan, Mr. Li Chongchao), I am very lucky to meet them during PhD career in Japan, Without yours help and support, the life in Japan will full of vapidity, and I cannot complete my PhD.

Finally, I dedicate this work to my beloved families, for their understanding and support through the duration of my study.